國立臺灣大學電機資訊學院光電工程學研究所

碩士論文

Graduate Institute of Electro-Optical Engineering
College of Electrical Engineering & Computer Science
National Taiwan University

Master Thesis

斜向入射電子束蒸鍍法製作超低折射率奈米孔洞薄膜以及其在布拉格反射鏡和抗反射薄膜上的應用

Fabrication of Ultra-Low-Refractive-Index Nanoporous Thin Film by E-Beam Oblique-Angle Deposition and The Applications for Distributed Bragg Reflector (DBR)/ Anti-Reflection (AR) Thin Films

劉俊廷

Jun-Ting Liu

指導教授：李允立 博士

Advisor: Yun-Li Li, Ph. D

中華民國 97 年 6 月

June, 2008

國立臺灣大學碩士學位論文
口試委員會審定書

斜向入射電子束蒸鍍法製作超低折射率奈米孔洞薄膜
以及其在布拉格反射鏡和抗反射薄膜上的應用

Fabrication of Ultra-Low-Refractive-Index Nanoporous Thin Film by E-Beam Oblique-Angle Deposition and The Applications for Distributed Bragg Reflector (DBR)/ Anti-Reflection (AR) Thin Films

本論文係劉俊廷（R95941076）在國立臺灣大學光電工程學研究所完成之碩士學位論文，於民國 97 年 06 月 16 日承下列考試委員審查通過及口試及格，特此證明

口試委員：李元玉 （簽名）

（指導教授）

曾雪峰　　黃鼎偉

所長 黃升龍 （簽名）

致謝

本研究成果得以順利完成，首先感謝指導教授李允立博士的細心指導與諄諄教誨，使得我獲益良多，在此至上我衷心的敬意與感激。此外亦感謝我的口試委員曾雪峰教授以及黃鼎偉教授對於本論文的指導，使得本論文的內容更為完善並提供更多未來研究方向與想法。

誠摯的感謝台大化學系梁文傑教授和趙學長，高分所陳文章教授和郭學長，化工所王大銘教授，光電所陳奕君教授以及光電所的邱天隆學長在量測光譜儀上面無私的協助。並感謝國家奈米元件中心 TFSEM 委託操作的黃秀俐小姐在最需要的時候無條件的加班幫忙完成實驗所需的資料。感謝台大金工廠廖師傅在實驗器具製作上的幫忙。以及光電所許多實驗設備的協助，尤其是林清富教授實驗室負責管理的電子束蒸鍍系統，對於本論文的完成有相當大的幫助。

感謝實驗室已經畢業的凱文、蘇逸學長和博士班的隨贏、逸儒、志凌、冠詠學長和惠心、玫丹學姊在實驗上面的解惑和指示；鈞傑、心煜、育弘和閔馨在實驗室上面的互相討論；執中、劭宇和宗彧在實驗上面的協助，更特別感謝敬堯實驗上面的大力幫忙。

最後要感謝父母從小對我付出的心力與支持，提供我在物質與精神上不予匱乏的生活環境，令我在研究的領域上得以盡心盡力無後顧之憂。最後還要感謝曾經協助過我的更多人，感謝大家。

摘要

折射率是光學元件中最重要的光學性質。對於許多光學元件來說如望遠鏡和眼鏡，還有光學鍍膜如布拉格反射鏡和抗反射薄膜，折射率匹配的設計主宰了整個光學應用的表現。事實上對於光學元件中，某些特定折射率數值的需求是常被需要的。但是等效折射率數值常被用來彌補這個需求的空缺。斜向入射電子束蒸鍍法可以用來製造可調變折射率和超低折射率的奈米孔洞薄膜。我的實驗中奈米孔洞的薄膜是利用二氧化矽，二氧化鈦和矽蒸鍍源蒸鍍而成，並分別討論他們的奈米孔洞結構，折射率的變化，奈米孔洞結構的薄膜厚度減少量和空洞佔奈米孔洞薄膜的比率。其中我們做出最低的折射率是折射率等於 1.08 的奈米孔洞薄膜。

在奈米孔洞薄膜的應用上面，已經利用只有二氧化鈦的材料製作出單對和雙對在矽基板的布拉格反射鏡並且將反射率提高至 74%。而在載玻片上面製作的單層抗反射層也將反射率從原先中心波長的 7%下降至 0.1%。四層的漸近折射率抗反射層在矽基板也使反射率降至小於 5%的區域從 527 奈米到 1279 奈米，反射率小於 1 % 的區域從 618 奈米到 972 奈米，這個抗反射層提供了廣波段的抗反射頻譜圖。

奈米孔洞氧化的現象在之前也被討論過，我的實驗主要針對因為不同蒸鍍的角度對於不同氧化程度的量測，而奈米孔洞氧化現象對於抗反射鍍膜上面的影響也被證實，這裡並且提供一個簡單的方法去避免這種氧化問題。

Abstract

The refractive index is the most important property for optical devices. For optical devices, i.e. telescopes and eyeglasses, optical coatings, i.e. Distributed Bragg Reflector (DBR) and Anti-Reflection (AR) coating, the designs of the refractive index matches are dominating the performance of those optical applications. In reality, some desires of specific refractive index values are often needed for specific optical device designs. However, the effective refractive index can be used to redeem these refractive indices desires. E-beam oblique-angle deposition is a technique to fabricate the tunable and ultra-low-refractive-index nanoporous thin films. In my experiments, the nanoporous thin films deposited by SiO_2, TiO_2 and Si evaporation sources are discussed with the structure analysis, refractive indices change, reduction thickness and porosity of nanoporous thin films. The lowest refractive index of these nanoporous thin film is as low as 1.08.

In my application experiments, the single and double pair DBRs on silicon substrate deposited by only TiO_2 evaporation source were successfully fabricated and enhancing the reflectivity above 74%. The reflectivity at central wavelength of single layer AR coating on glass slider substrate is eliminated from R= 7% to R=0.1%. The gradient-index 4-layer modified quintic AR coating on silicon substrate also diminish the reflectivity R< 5% from 527 nm to 1279 nm and

reflectivity R< 1% from 618 nm to 972 nm. It provides a broad-band very low reflection region.

Oxidation phenomena of silicon nanoporous thin film were discussed before. Discussion for oxidation degree of different nanoporous thin film with different incident flux angles is made in my experiment. Moreover, the effect of degradation of silicon nanoporous thin film for optical AR coating is demonstrated and I provide a simple way to solve this kind of problem.

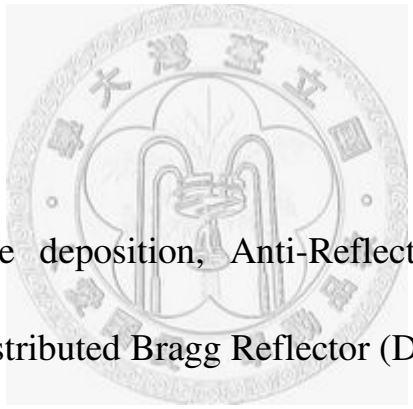

Keywords: oblique-angle deposition, Anti-Reflection (AR) coating, nanoporous thin film, Distributed Bragg Reflector (DBR), oxidation

Contents

List of Acronyms

Distributed Bragg Reflector	DBR
Anti-Reflection	AR
Scanning Electron Microscope	SEM
Light Emitting Diode	LED
Effective Medium Approximations	EMA
Mean Free Path	MFP

Figure list

Table list

Chapter 1 Introduction

1-1 The importance of refractive index for optical devices

Since 1666 the greatest physicist Newton has used prisms to calculate the refractive degree of different color lights, the refractive index thus becomes the most important consideration for optical applications. If we choose the suitable refractive index combinations, these combinations can be used as optical filters, optical reflectors or anti-reflection coatings etc.

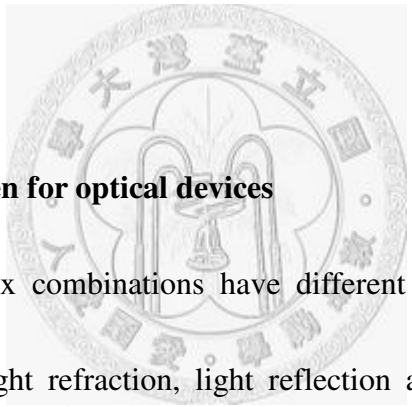

The refractive index chosen for optical devices

Different refractive index combinations have different effects for the light. The different effects include light refraction, light reflection and light transmission etc. Furthermore, interfere is an important effect of refractive index combination for designing many optical devices.

Some optical applications, i.e. anti-reflection coatings are used for elimination of the reflective light from a specific surface. For solar cell, it receives the light of sun and transforms the sunlight into electric energy. In an ideal situation, all the energy of sunlight is received to the solar cell. The primary way is trying to eliminate the reflection of sunlight from solar panel. If the absorbed semiconductor of solar cell

panel is silicon, the refractive index of the absorbed panel is about n=3.8 at red-light range. According to the Snell's law, we have 34% reflection loss of the sunlight, namely, we lost 34% energy just because of the sunlight reflection of the solar cell panel.

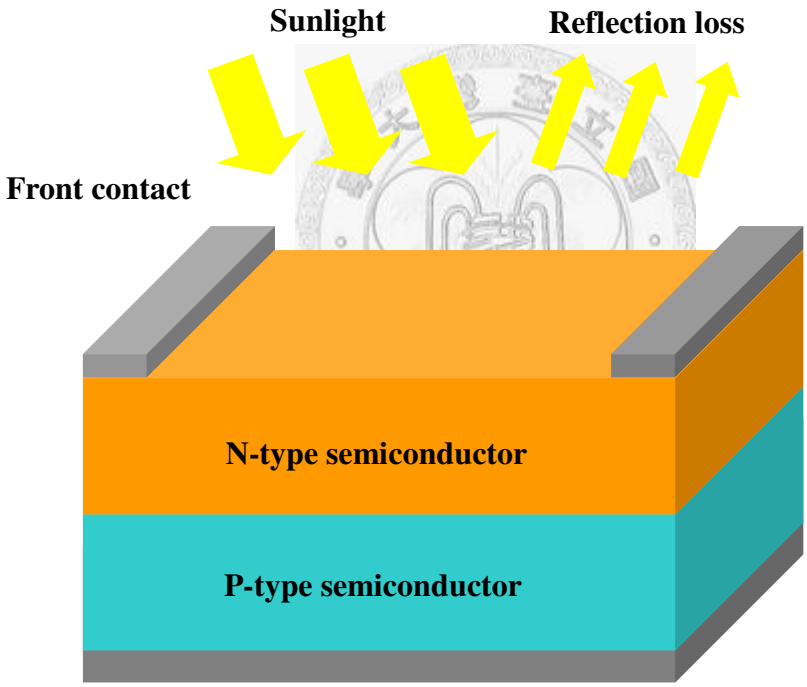

(a)

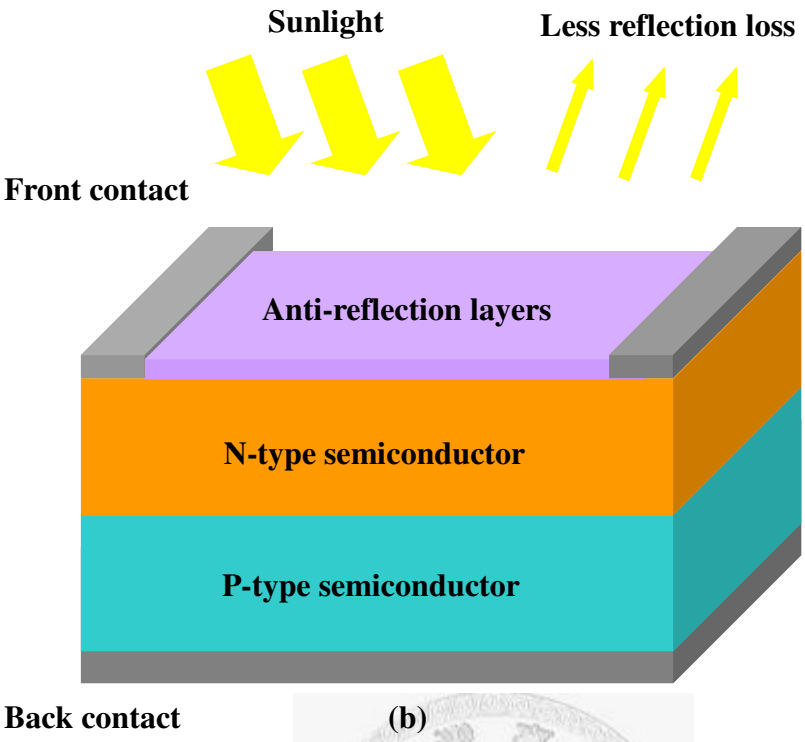

Fig. 1-1 (a) Illustration of solar cell without anti-reflection coating.

(b) Illustration of solar cell with anti-reflection coating.

In Fig. 1-1 (a), it can easily be understand the semiconductor will reflect the sunlight to the air. Unfortunately, the refractive indices of most absorbed semiconductors of solar cell are not small ($n > 2.5$), it's not easily to use the small refractive index ($n < 2.5$) material to avoid this problem. In Fig. 1-1 (b) is the most utility method to solve this problem, namely, to fabricate an anti-reflection layers to eliminate the reflection of the sunlight.

Traditional AR coating and other optical devices

Traditional thin film AR coatings are composed of transparent thin film structures with alternating layers of contrasting refractive indices. Layer thicknesses are chosen to produce destructive interference for the light beams reflected from the interface and constructive interference in the corresponding transmitted light beams. According to the anti-reflection principles, they make the structure's performance change with incident wavelength and incident angle, so that the different reflectivity often appears at different oblique angles. A wavelength range must be specified when designing or ordering such coatings.

Many optical applications can be achieved by thin film coating, including anti-reflection, high reflection, band-pass filtering, color modification and so on. For the particular purposes, refractive index combinations can be used to achieve them. For example, if we want a broadband anti-reflection coating instead of only small wavelength region, we can coat specific different refractive index materials on the optical device in Fig. 1-2. It’s an illustration of anti-reflection (AR) coating on germanium substrate.

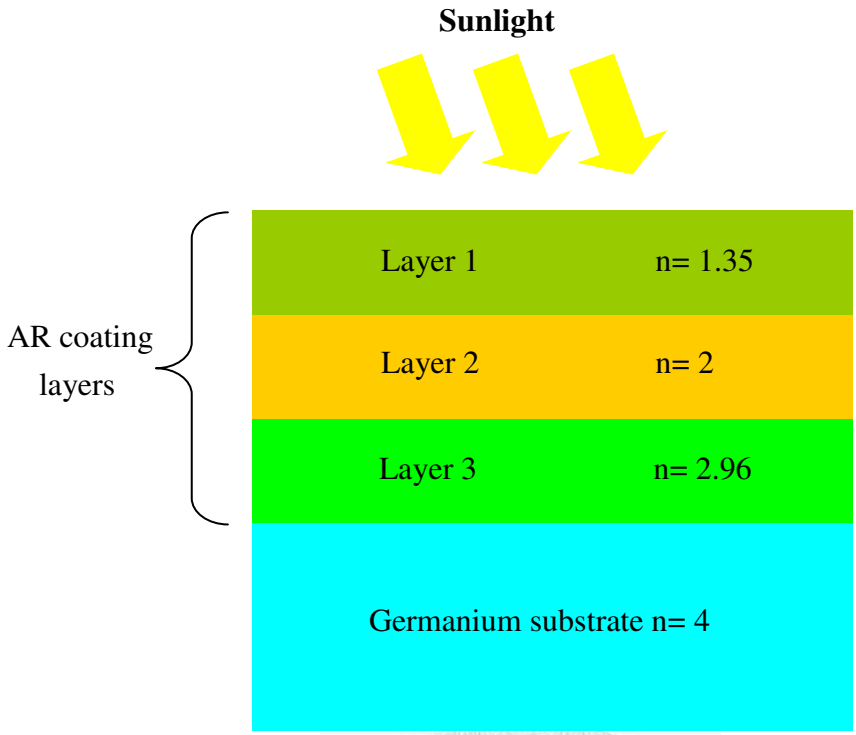

Fig. 1-2 Illustration of a typically 3-layer anti-reflection coating on germanium substrate, but actually, we don't have such nature materials which have n= 2 and n= 2.96 in the world.

This figure shown as above is a typically 3-layer anti-reflection coating, it performs better than only single-layer anti-reflection, which has broader anti-reflection band lower reflectivity than single-layer anti-reflection coating. But we must notice that we don't have such nature materials which have n= 2 and n= 2.96 in the world.

Furthermore, a typical high reflection device, Distributed Bragg Reflector (DBR) is using construction interfere for reflection light beams and destruction interfere for transmission light beams, respectively. The best chosen refractive index materials of high reflection DBR are high contrast refractive index matches, namely, high and low

refractive indices deposition thin film for the periodically reflection layers. But, like anti-reflection coating, there are not such materials for the ideal DBR, because there are no such high refractive index materials or such low refractive index materials. Even, besides the optical property we must consider for an optical device, other properties like electro property and thermo property are what we should consider. It means that we can't arbitrarily use the material if it's not suitable.

Now, we know that refractive index is almost most important property for many optical devices. But there are not all the refractive indices which can satisfy us. Do we have tunable refractive index technique for our new optical devices? Yes, if the structure of this material is nanoporous structure.

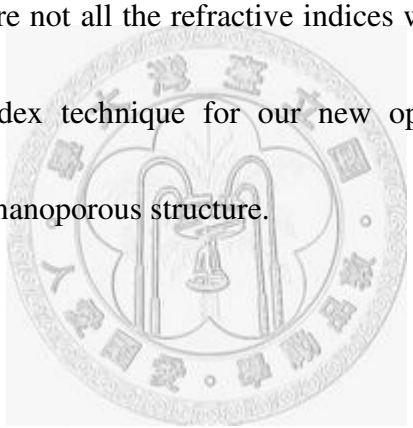

1-2 Effective medium approximations (EMA)

Effective medium approximations [1] are analytical models of mixing macroscopic properties of original medium and imbedded fraction medium. There are many numerous models for description of macroscopic properties.

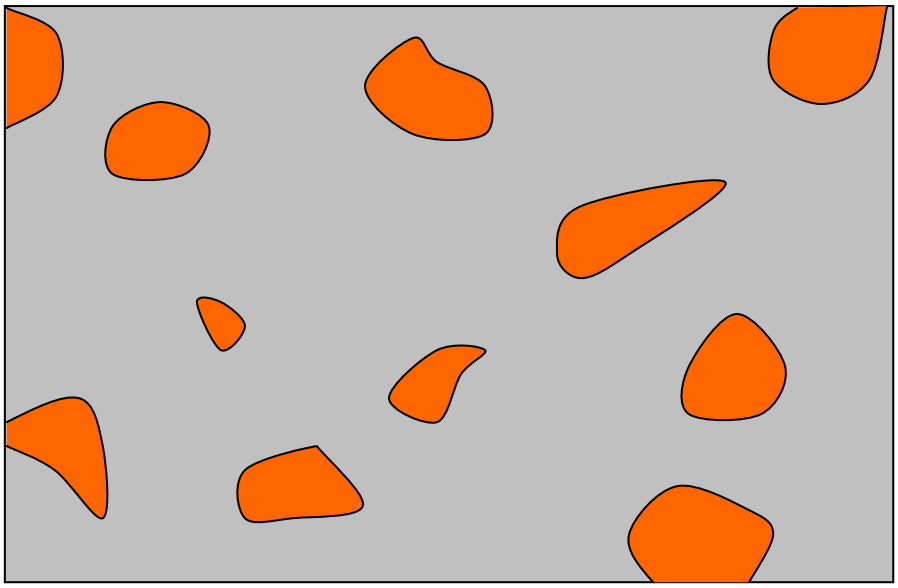

(a) Separated-grain structure

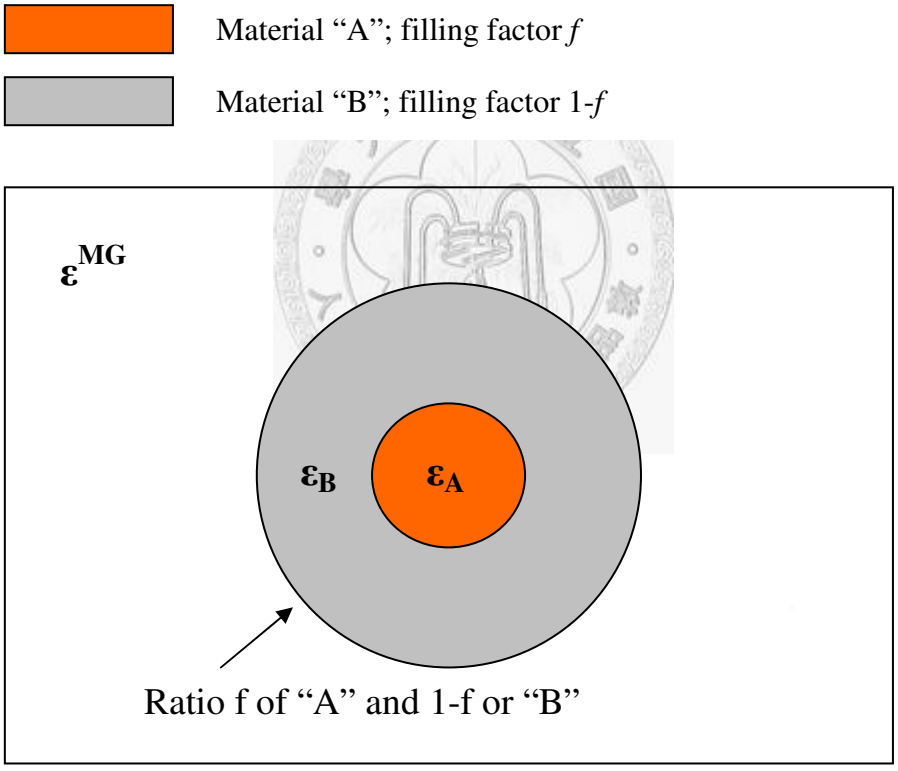

(b) Maxwell Garnett theory model

Fig. 1-3 (a) is the Separated-grain structure, (b) show the corresponding random unit cell model used to explain Maxwell Garnett effective dielectric permeability theory.

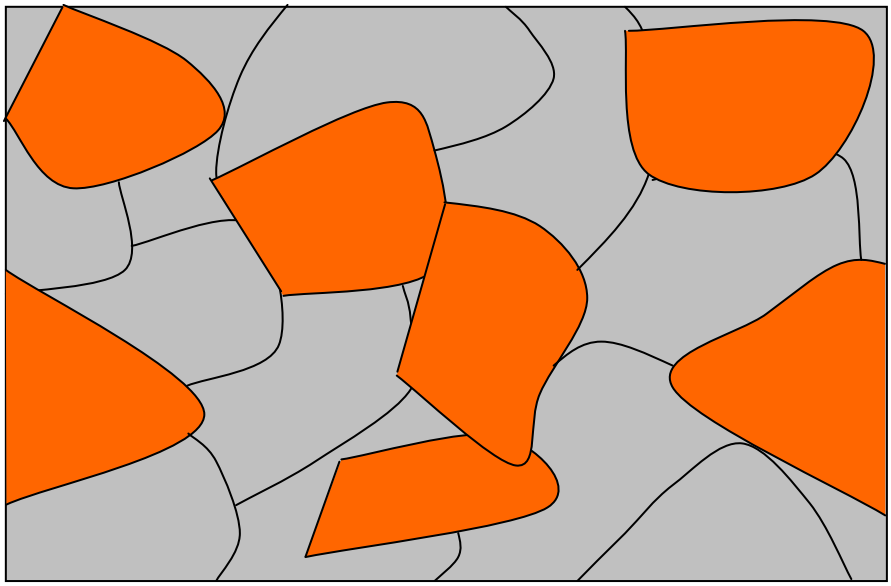

(a) Aggregate structure

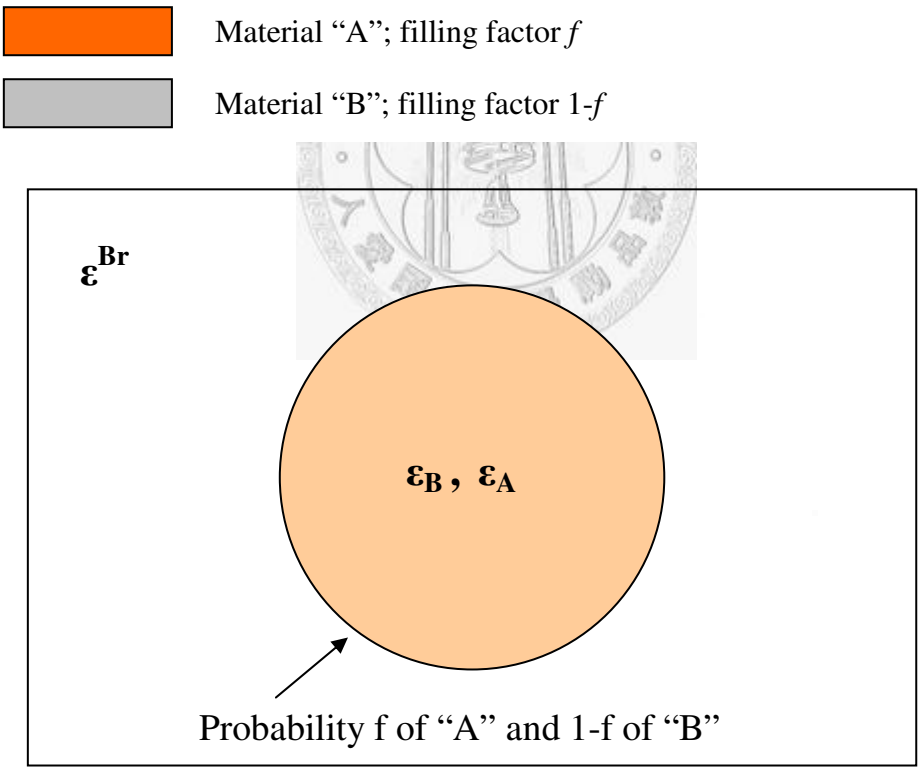

(b) Bruggeman theory model

Fig. 1-4 (c) is aggregate structure, (d) show the corresponding random unit cell model used to explain Bruggeman effective dielectric permeability theory.

Quantitative models for the properties of heterogeneous materials have been discussed since the early 19th century. During the last few decades, the interests in the optical properties of mixtures become particularly popular. The Maxwell Garnett and Bruggeman [2] are the most famous effective models to the phenomenon.

Fig. 1-3 (a) is the separated-grain structure diagram. This diagram depicts particles of material A are dispersed in a continuous host material B. Fig. 1-4 (a) is the aggregate structure in which material A and material B are space-filling random mixture of the two constituents. The volume fraction of material A (namely, the filling factor) is denoted by *f*. Such models can be obtained if we consider a division of the material into cells. Each of the cells is taken to be embedded in an effective medium. The inhomogeneous material can be presumed that it is macroscopic uniformity on a scale comparable with the wavelengths in the material and possesses translational and rotational symmetry, so those random unit cells are spherical.

Those effective medium approximations can analyze effective conductivity, dielectric permeability, etc. In mine experiments, the optical properties will be focused, namely, dielectric permeability, refractive index.

$$\varepsilon^{MG} = \varepsilon_B \frac{\varepsilon_B + 2\varepsilon_B + 2f(\varepsilon_A - \varepsilon_B)}{\varepsilon_A + 2\varepsilon_B - f(\varepsilon_A - \varepsilon_B)} \tag{1-1}$$

$$f\frac{\varepsilon_A-\varepsilon^{Br}}{\varepsilon_A+2\varepsilon^{Br}}+(1-f)\frac{\varepsilon_B-\varepsilon^{Br}}{\varepsilon_B+2\varepsilon^{Br}}=0 \qquad (1\text{-}2)$$

Eq. (1-1), it depicts the effective dielectric permeability in Maxwell Garnett theory model, *f* is the filling factor of the structure. The refractive index n is root square of dielectric permeability *ε*. Eq. (1-2) is the equation in Bruggeman theory model. The *f* is also the filling factor.

Each of the equations of those models has some different presumptions. For generally, the Maxwell Garnett theory can describe phenomenon with small *f* (*f* <0.3) well. Bruggeman can describe phenomenon with large *f*.

In nanoporous structure for optical devices, the filling factor *f* is not usually small. According to the theory of Bruggeman, the thin film with larger filling factor of air has smaller effective refractive index than dense thin film with no air. Many anti-reflection coating is the technique using the effective medium approximation theory. In Fig. 1-5 [3], the AR coating on AIN (n=2.05) substrate with nanoporous thin films fabricated by oblique-angle deposition was presented recently. Different porosity layers contributed to nanoporous thin films with different effective refractive indices. The reflectivity was reduced from 12% to 0.1% at λ= 632 nm. It is believed that the nanoporous thin films with different effective refractive indices can be successfully achieved for many optical applications.

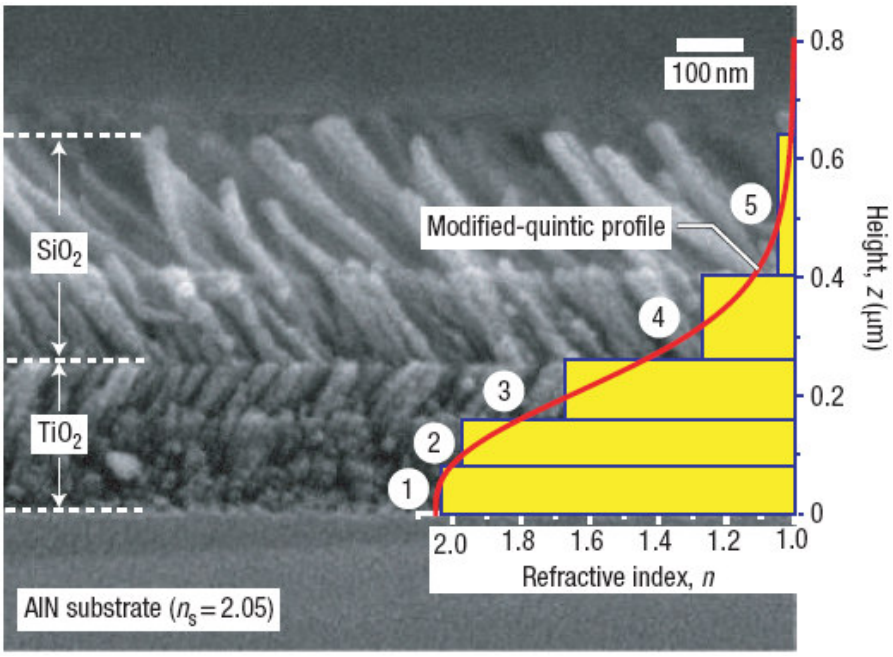

(a)

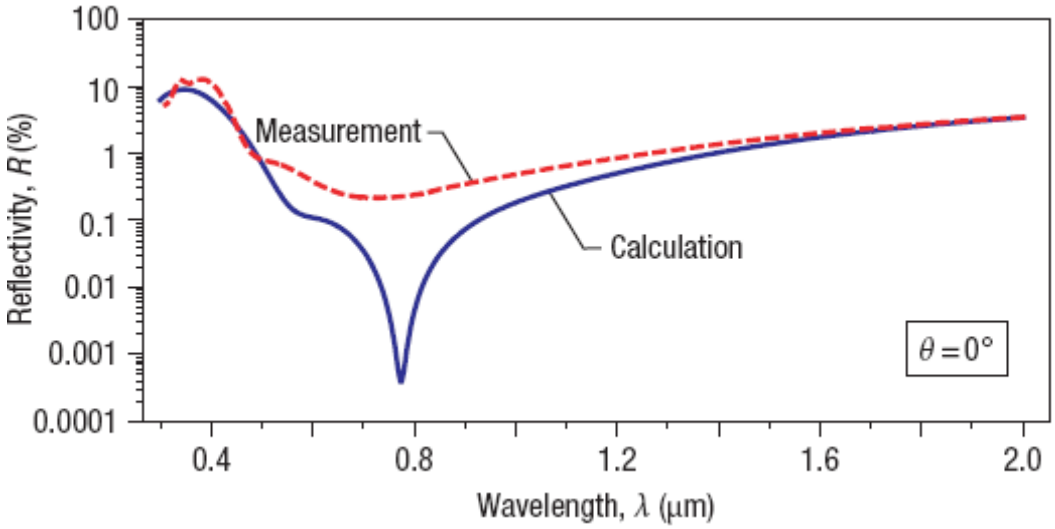

(b)

Fig. 1-5 (a) SEM photos of AR coating on AlN substrate fabricated by oblique-angle deposition.

(b) Reflectivity diagram of AR coating on AlN substrate.

Chapter 2 Fabrication of ultra-low-refractive-index nanoporous thin film

In this chapter, the oblique-angle deposition technique and the electron-beam evaporation system will be introduced. The experiment setup for nanoporous thin film fabrication will be introduced too.

2-1 Theory of nanoprous film by e-beam oblique-angle deposition

Most thin film applications in the microelectronics require dense and durable coatings for optimum performance. However, for some applications such as catalysts or gas sensors, a porous coating is desirable. Those porous films have been fabricated in many ways, but the most common desired feature is a film with a high surface area to volume ratio. The highly oblique incident flux by evaporation [4, 5] has been observed that films produced a high porous ration of bulk.

It has been recognized that thin films grown under conditions of oblique deposition show columnar morphology caused by elongated grains which are tilted away from the substrate and toward the incoming flux.

Shadowing effect of oblique-angle deposition

Now, the two primary mechanisms of oblique-angle deposition will be introduced, the shadowing effect and surface diffusion. In Fig. 2-1, the deposition atoms adhere to the substrate first and the atoms will find a suitable position to deposit, namely, surface diffusion. Higher temperature T makes the atoms diffuse longer distance and narrower shadow region. The continuous incident atoms often deposit near the atom deposited on the substrate before, and form atom clusters. Since the geometric block, it causes a shadow region where no more atoms can deposit. According to this illustration, it's easily believed that the highly incident flux angle α causes the extensive shadow region. The properties of nanoporous film caused by oblique-angle deposition are dominated by the two parameters, temperature T and incident flux angle.

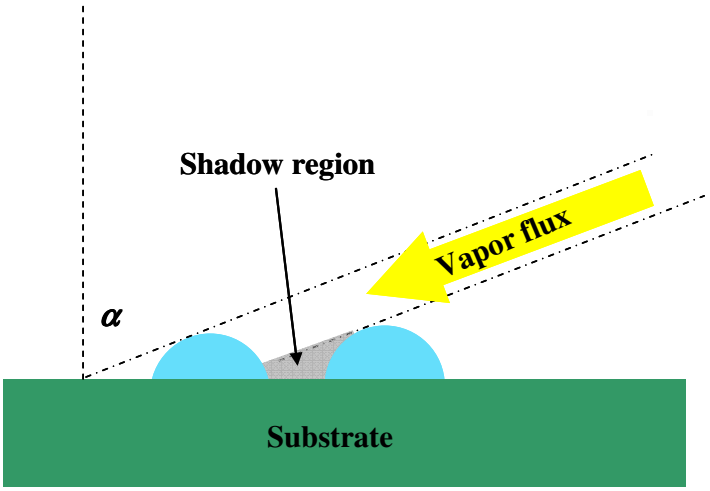

Fig. 2-1 Illustration of shadowing effect. The shadow region is created by screen of the atom cluster.

Experiment documents of the optical anisotropy of such films and modeling of their optical properties [6] has appeared in the literature. If the incident flux remains highly oblique ($\alpha > 80^{\circ}$, where the angle α is the angle subtended by the incoming flux and the outward substrate normal) angle during deposition process, the film will achieve significant porosity. But it must be noticed, for traditional thin film applications such as optical coatings, porosity is to be avoided because the absorption of water and other gases into the film, it leads to degradation of the desired physical and optical properties.

Using this technique, it is possible to manufacture the helix or spiral shape. Currently oblique-angle deposition films are grown by physical vapor deposition (PVD) or by electron beam bombardment.

The reduced effective refractive index of nanoporous film

The continuous incident flux atoms will deposit on the atom clusters instead of the shadow region. After a few time, the structure will become rod-like nanoporous film as shown in Fig. 2-2. To observe the illustration of self-assemble nanoporous film, it shows that the scale of mixing film of void and rod-like materiel is nanoscale structure. The gaps of the rod-like thin film are about 30 nm~50 nm, which is much less than the visible wavelength. In the introduction chapter, the EMA theory has been introduced to

describe the mixing nanoscale thin film. Bruggeman effective medium approximation is suitable to describe this structures, the EMA predicts the approximately linear dependence between the refractive index and the porosity. With the highly oblique incident flux angle, some papers demonstrate the structures have high porosity due to the enhanced shadowing effect and without scattering [7].

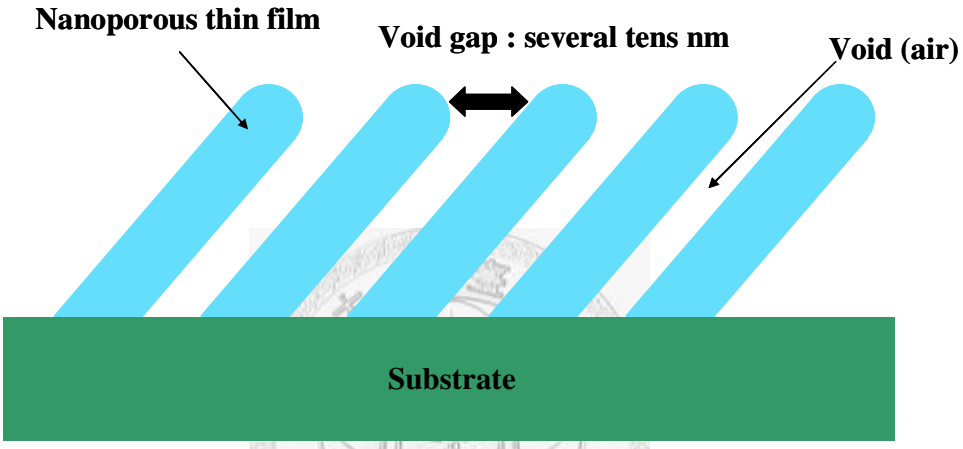

Fig. 2-2 Illustration of nanoporous film, the reduced effective refractive index is due to the mixing of rod-like material and the void and without scattering.

2-2 Experiment setup design

My nanoporous films are fabricated by e-beam evaporation. Thereupon I will describe some details about the e-beam evaporation system and oblique-angle deposition setup.

2-2-1 Introduction to e-beam evaporation system

Electron-beam (e-beam) evaporation is a kind of thermal emission of electrons from a filament (usually tungsten) used to heat source to high temperature. Generally, e-beam is used when required temperatures is too high for thermal evaporation. In Fig. 2-3, the magnetic field caused by deflecting magnet uses to steer beam 270° into deposition source. Sometimes, electrons striking metals can produce X-ray which causes damage to some sample layers on a substrate. An anneal takes care of these problems.

In Fig. 2-3, it shows semicircular symmetry evaporation flux allows multiple wafers to be evaporated simultaneously. To get thin films more uniform, rotating planetary is a helping way. Placing samples far from the source will also help uniformity, but will also lower deposition rate. The deposition rate depends on the position and orientation of the wafer in the chamber. An evaporation rate is the rate at which a material will vaporize (evaporate, change from liquid to vapor) compared to the rate of vaporization of a specific know material. The quantity is a ration, therefore it is unitless. The equation governing evaporation rate is given as follow [8]:

$$R_{evap} = \sqrt{\frac{M}{2\pi kT}} P_e \tag{2-1}$$

Where M is molecular mass, P_e is vapor pressure, k is Boltzman's constant, and T is temperature.

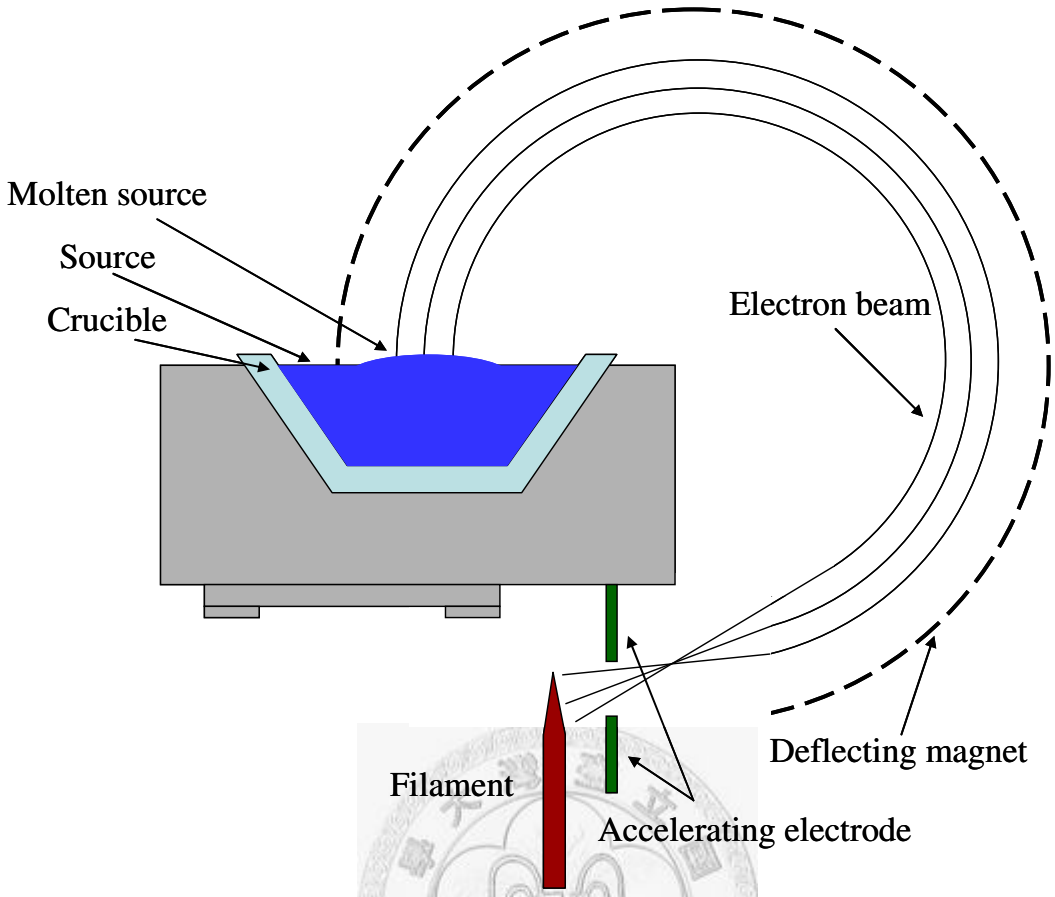

Fig. 2-3 Illustration of e-beam evaporation system.

But the deposition rate is not the evaporation rate. The illustration is shown in Fig. 2-4 and the equation governing deposition rate is given as follow:

$$R_{dep} = \frac{R_{evap}}{\Omega d^2 \rho} \cos \alpha \qquad (2\text{-}2)$$

ρ is the density of the material.

The vapor pressure of a liquid is the pressure exerted by its vapor when the liquid and vapor are in dynamic equilibrium. A substance in an evacuated and closed container will vaporize a finite amount. The pressure in the space upon the substance will increase from zero and eventually stabilize at a constant value, the vapor pressure.

Vapor pressures increase with temperature. The boiling point is the temperature at which the vapor pressure of a liquid equals the external pressure. In general, the higher vapor pressure of a material at a given temperature, the lower the boiling point. In other words, compounds with high vapor pressures form a high concentration of vapor above the liquid.

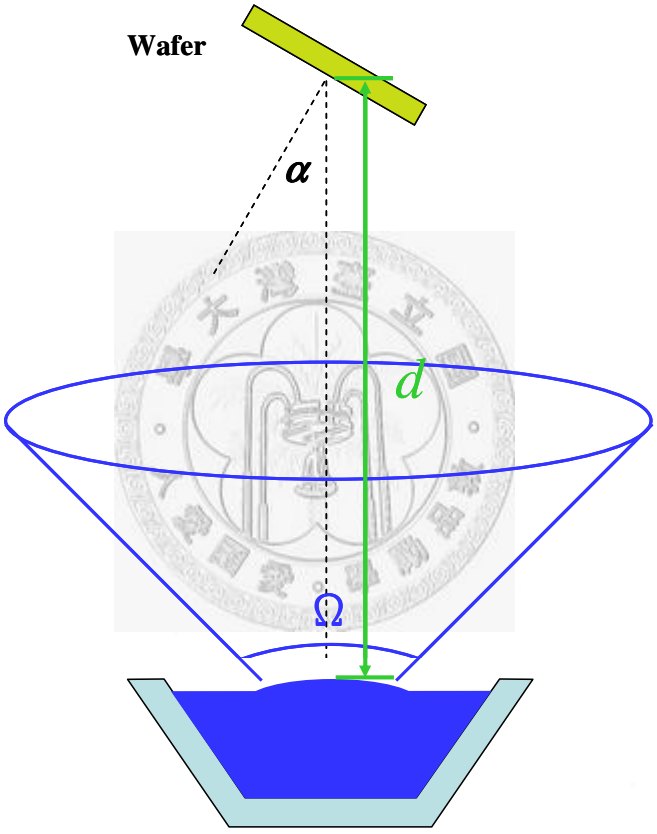

Fig. 2-4 Illustration of deposition relation between material source and distance and orientation of wafer. The deposition rate is dependent on the distance and incident flux angle.

Mean Free Path (MFP), for purposes of evaporation, is the distance a molecule travels in a straight line (in vacuum) before its velocity vector is randomized by a

collision. MFP is $1/(\sqrt{2\pi}nd^2)$, where n is number of moles and d is molecular diameter. This equation represents the average velocity of the molecules times the average time between collisions.

Step coverage

Step coverage describes the conformity of a thin film grown over a feature. The aspect ratio of a step is defined as (step high)/(step width). For a thin film, good step coverage performance is good to form a uniform film. But, not all the thin film need the good step coverage performance, for examples, porous films and films with specific mesas, they need poor step coverage during the deposition process. Fig. 2-5 shows as a description of step coverage. To raise the step coverage performance, it can be improved by planetary with two dimensions of rotation as shown in Fig. 2-5 (b). Besides, by heating the sample substrates to about 60% of the melting temperature, it can promote atom mobility after adhesion. This method improves step coverage by using of surface diffusion. Surface diffusion follows Arrhenius behavior. With a high enough temperature, the diffusion length can be made larger than the feature size as shown in Fig. 2-5 (c).

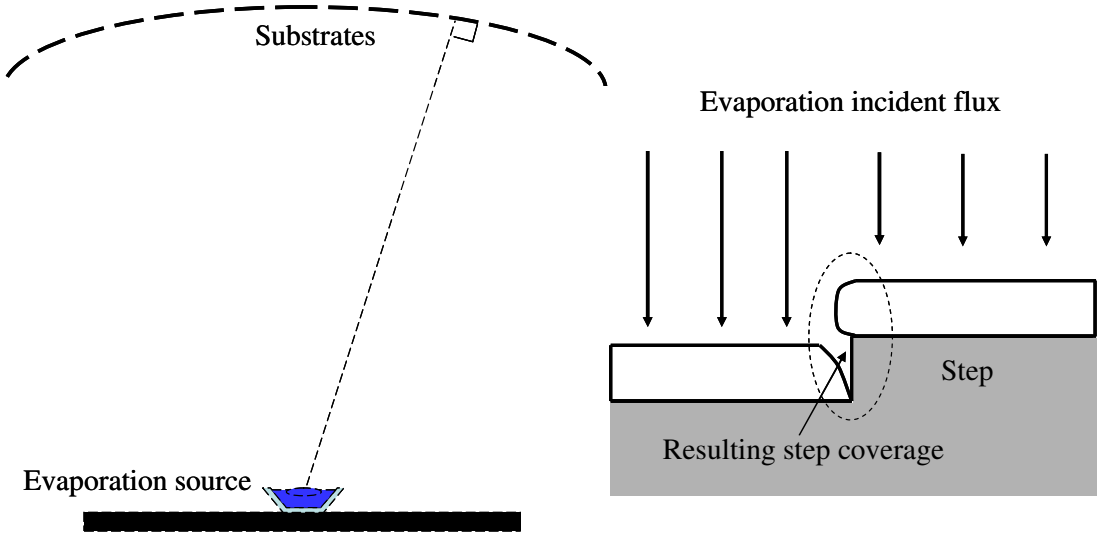
Substrates
Evaporation incident flux
Step
Resulting step coverage
Evaporation source

(a)

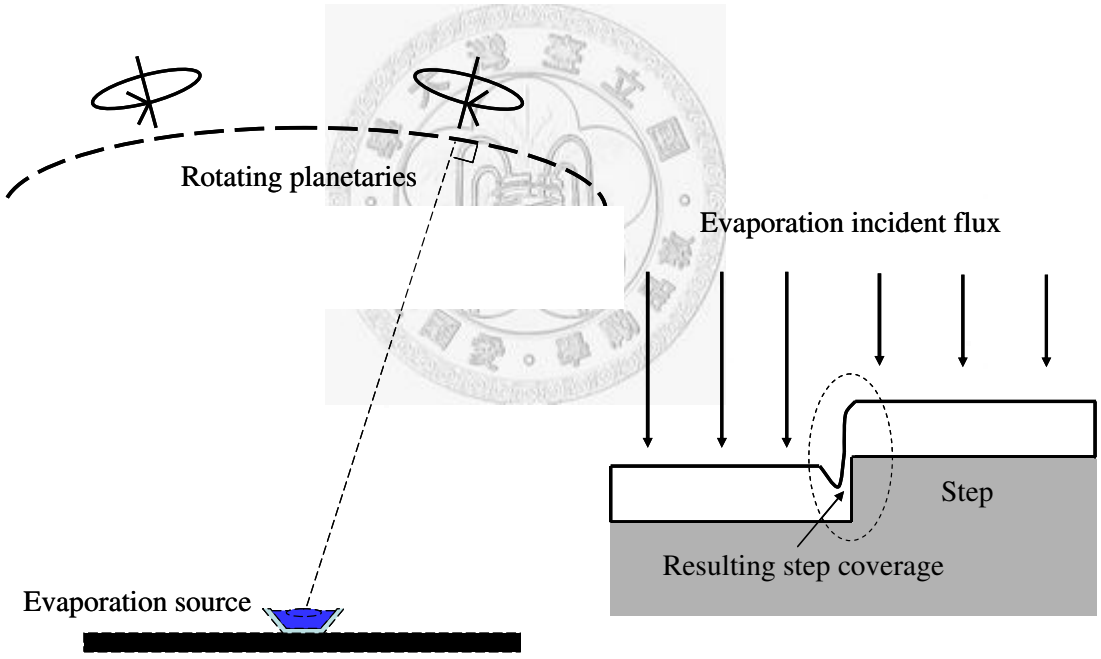
Rotating planetaries
Evaporation incident flux
Step
Resulting step coverage
Evaporation source

(b)

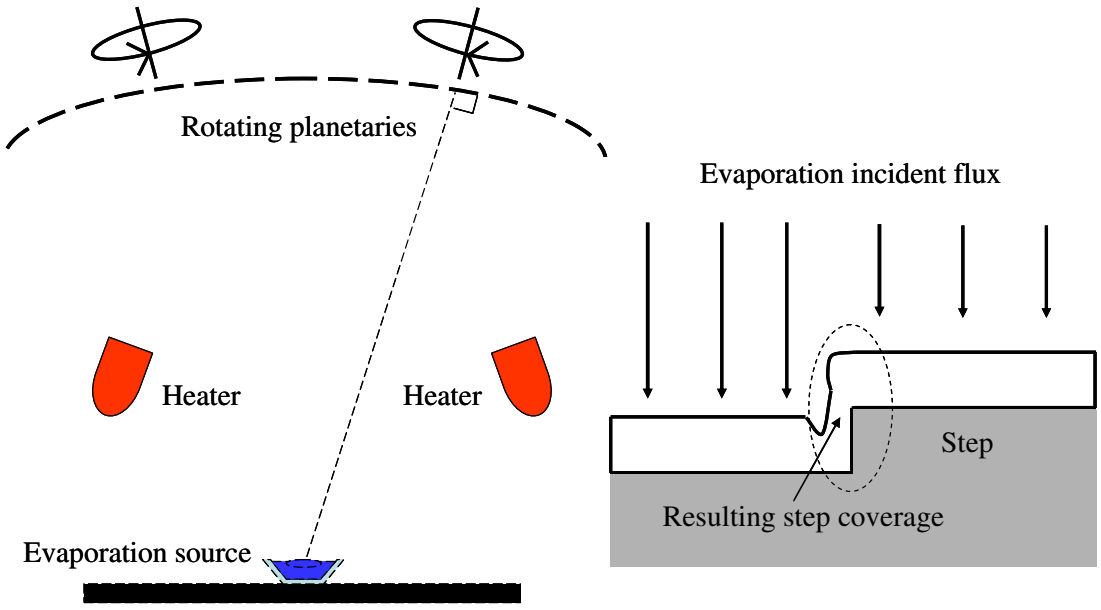

(c)

Fig. 2-5 Source-substrate configurations of e-beam evaporation system.

(a) Step coverage without rotation or heating.

(b) Step coverage with rotation.

(c) Step coverage with rotation and heating.

To get better step coverage, sputter in general has superior step coverage as sputtered atoms have random velocities. For high aspect ratios, CVD process should be considered.

2-2-2 Oblique-angle e-beam deposition setup

My experiment is using e-beam evaporation system to fabricate the nanoporous thin film. The configuration diagram of the oblique-angle deposition setup is shown in Fig.

2-6. Using these implements, fabrication of many different angle samples at a time does work. The distance between substrate and deposition source is about 36cm, according to the Eq. 2-2, for small substrate, the uniform thin film thickness can also be achieved. Moreover, this holder can be used to compare different angles to properties at a time due to the spherical symmetry.

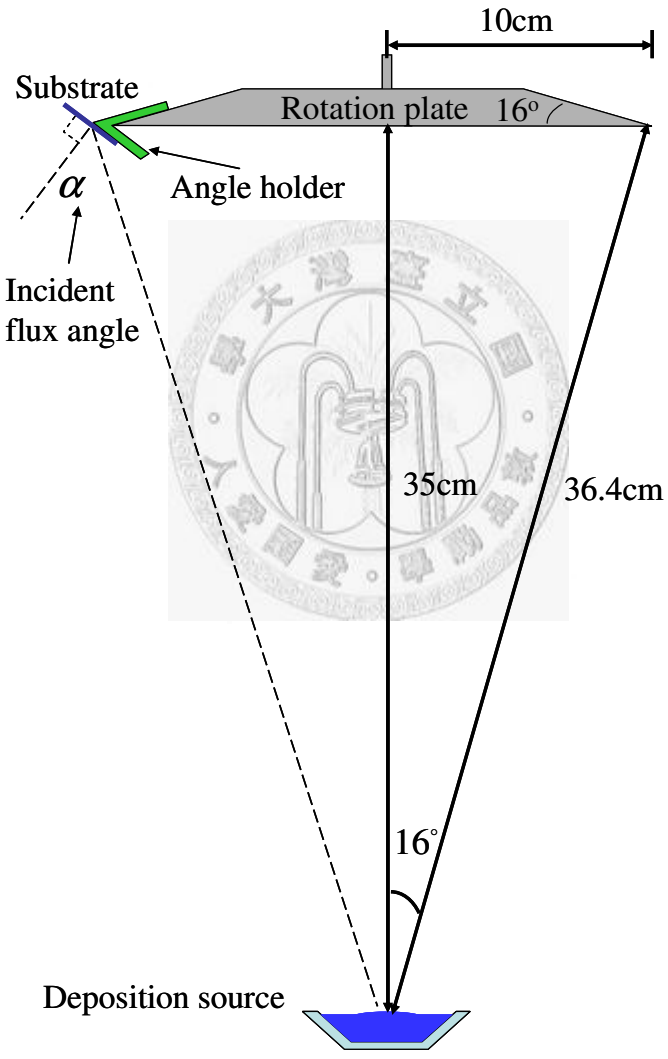

Fig. 2-6 Configuration diagram of angular distribution during oblique-angle deposition.

Chapter 3 Properties of nanoporous thin film

During the oblique-angle deposition process, the deposition rate, the angular distribution of the incident vapor flux, the film and substrate temperature, the energies of the surface–substrate interface, and the partial pressure of residual gases in the deposition chamber will effect the growth of nanoporous thin films. In this work, the nanoporous thin film depending on angular distribution of the incident vapor flux will be discussed. Specifically, optical devices are fabricated with the property of varied angle corresponding to varied refractive indices.

3-1 The nanoporous thin film analysis by Scanning Electron Microscope (SEM)

In this work, SiO_2, TiO_2 and Si thin films are deposited with oblique-angle deposition. The relations between incident flux angles and column angles are analyzed as shown in Fig. 3-1.

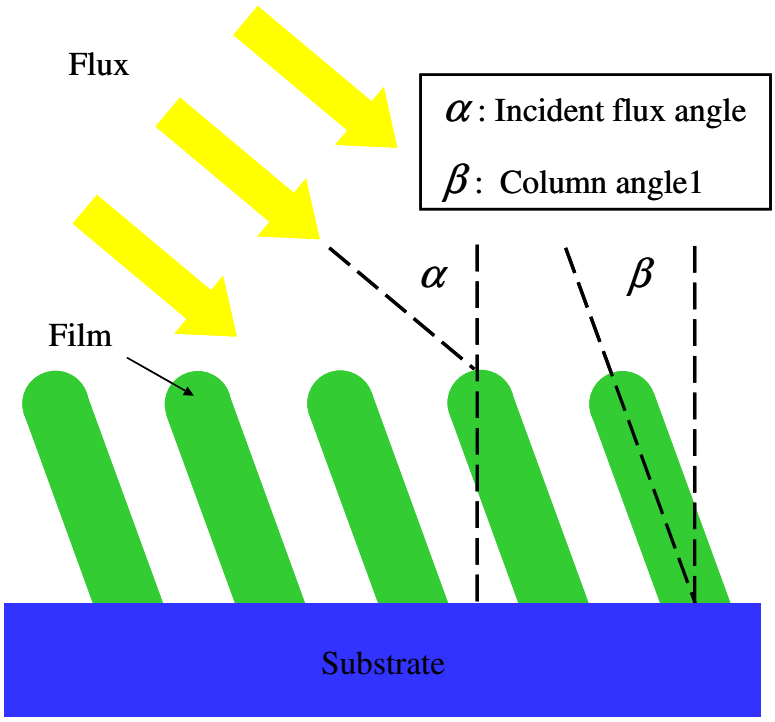

Fig. 3-1 Illustration of nanoporous thin film, α is the incident flux angle, β is the column angle. Several deposition parameters will affect the column angle β.

All the nanoporous films were deposited at the same time. The deposition parameters of three kinds of source are shown in Table 3-1, Table 3-2 and Table 3-3, respectively.

Deposition source	Incident flux angle	Deposition rate	Base pressure	Deposition pressure	Chamber temperature
SiO_2	0^o, 50^o~90^o	0.3 nm/s	1.6×10^{-6} torr	3×10^{-6} ~ 1.5×10^{-6} torr	22^oC ~ 24^oC

Table 3-1 Deposition parameters of SiO_2 nanoporous thin films on Si substrate.

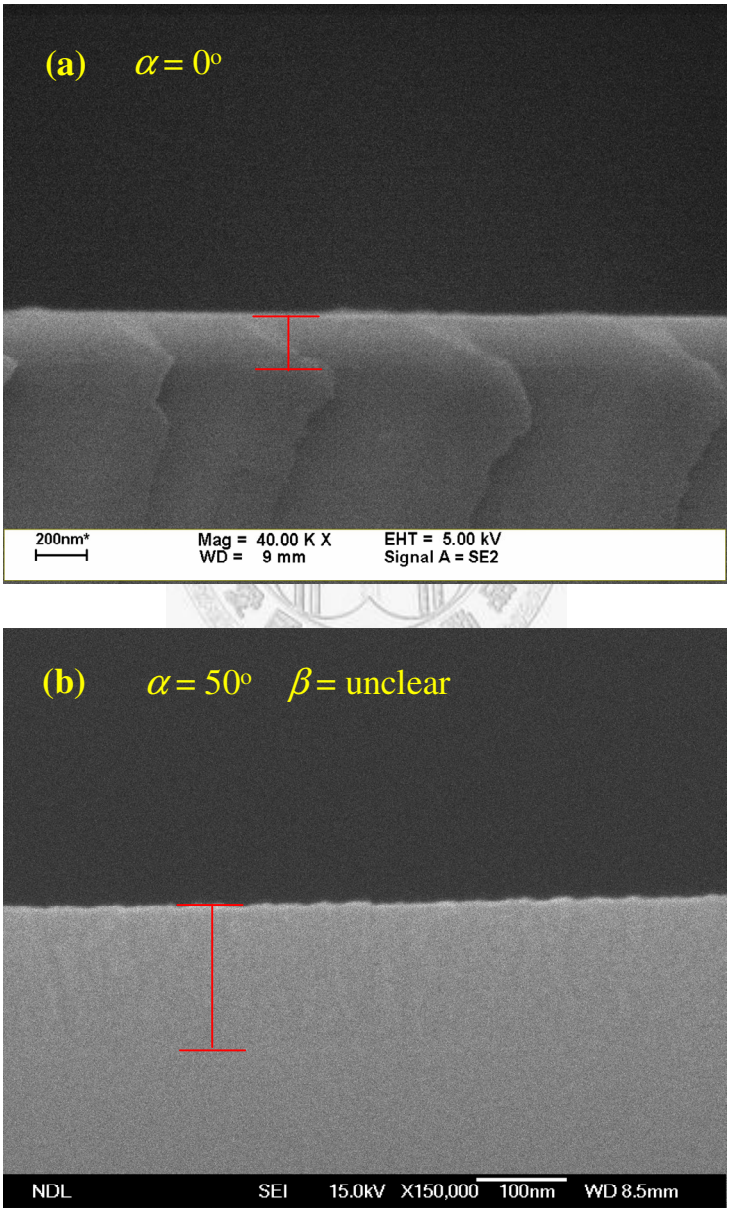

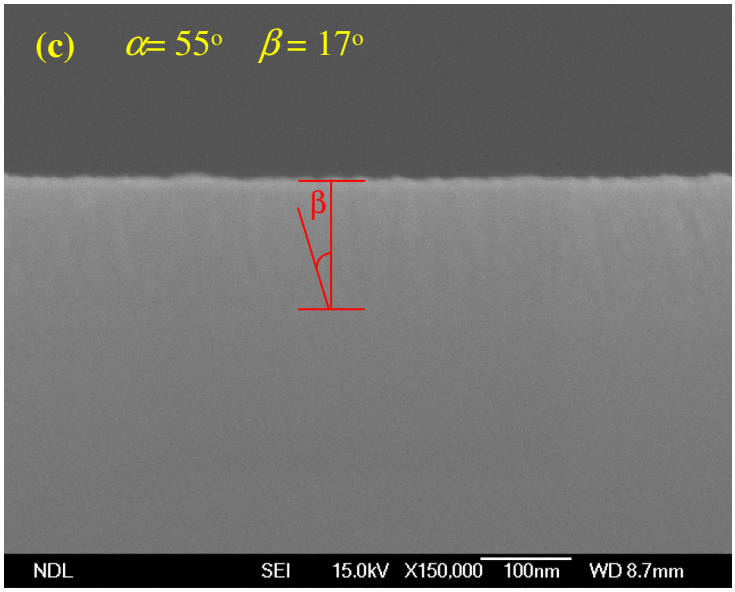
(c) α= 55° β= 17°
β
NDL SEI 15.0kV X150,000 100nm WD 8.7mm

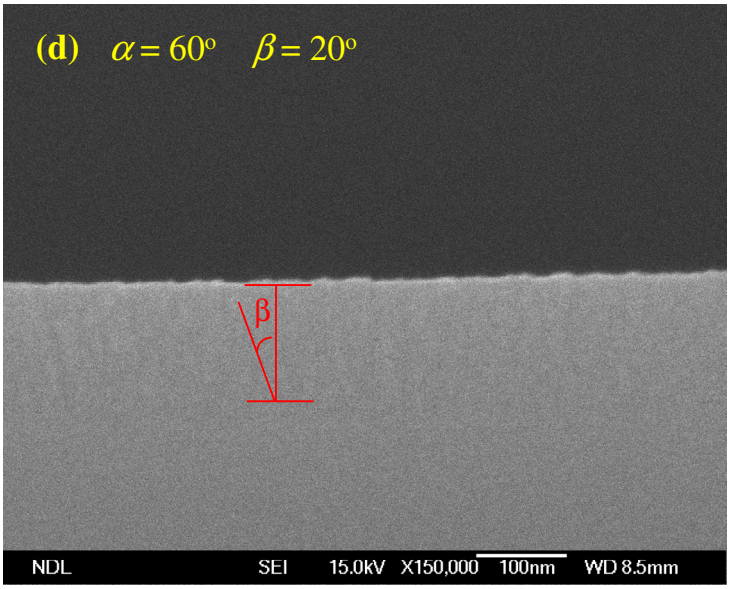
(d) α = 60° β = 20°
β
NDL SEI 15.0kV X150,000 100nm WD 8.5mm

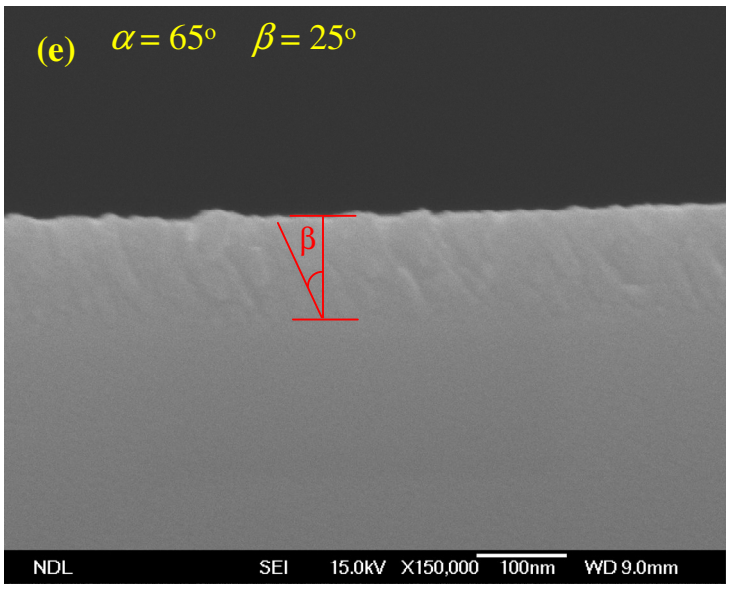
(e) α = 65° β = 25°
β
NDL SEI 15.0kV X150,000 100nm WD 9.0mm

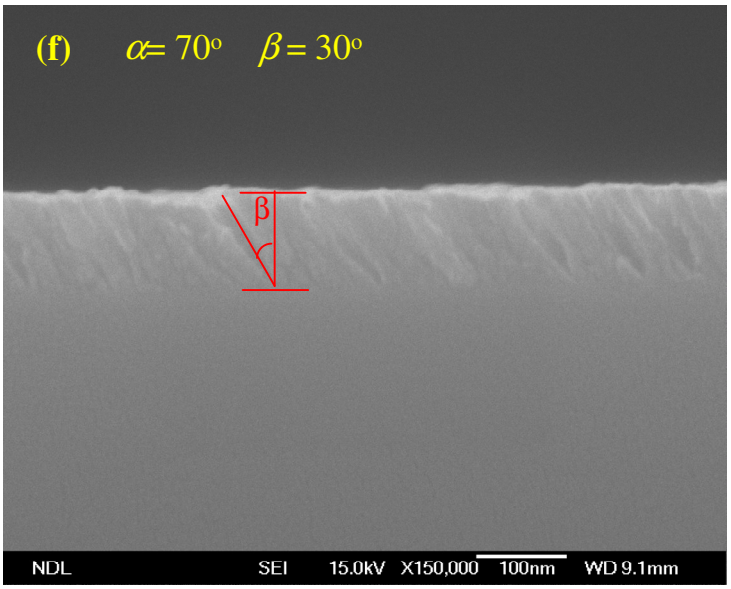
(f) α= 70° β= 30°
β
NDL SEI 15.0kV X150,000 100nm WD 9.1mm

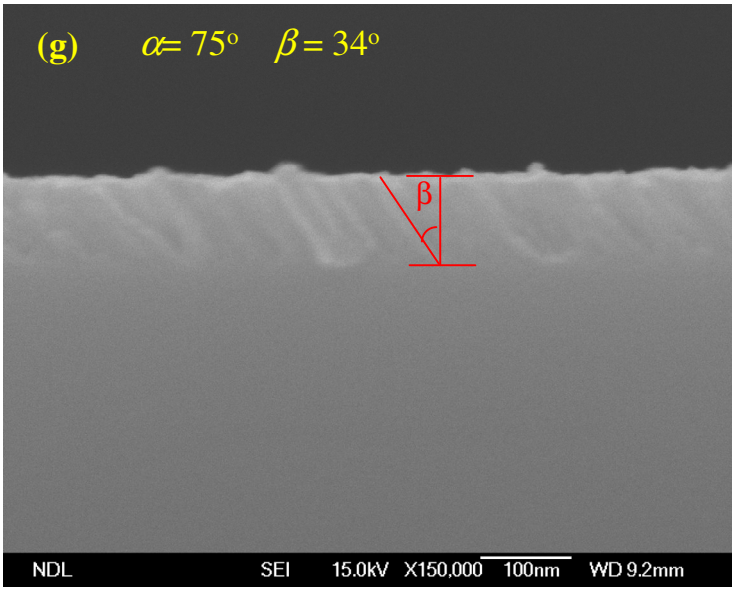
(g) α= 75° β= 34°
β
NDL SEI 15.0kV X150,000 100nm WD 9.2mm

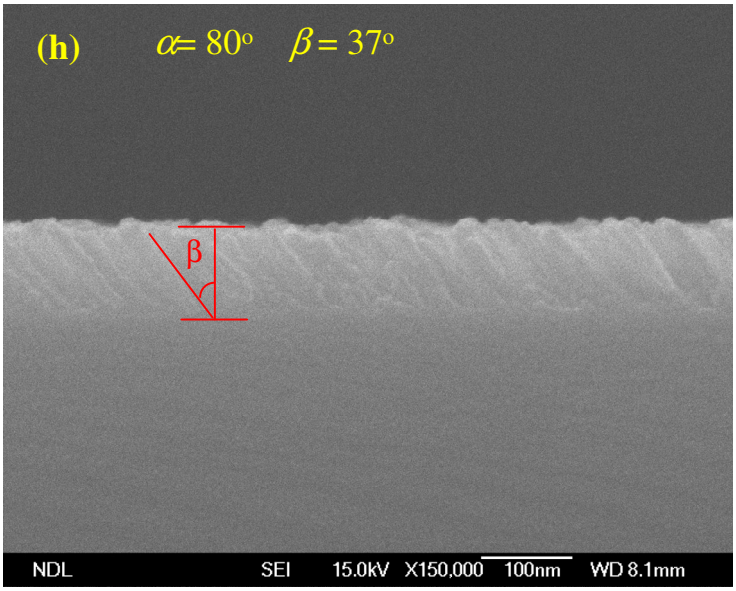
(h) α= 80° β= 37°
β
NDL SEI 15.0kV X150,000 100nm WD 8.1mm

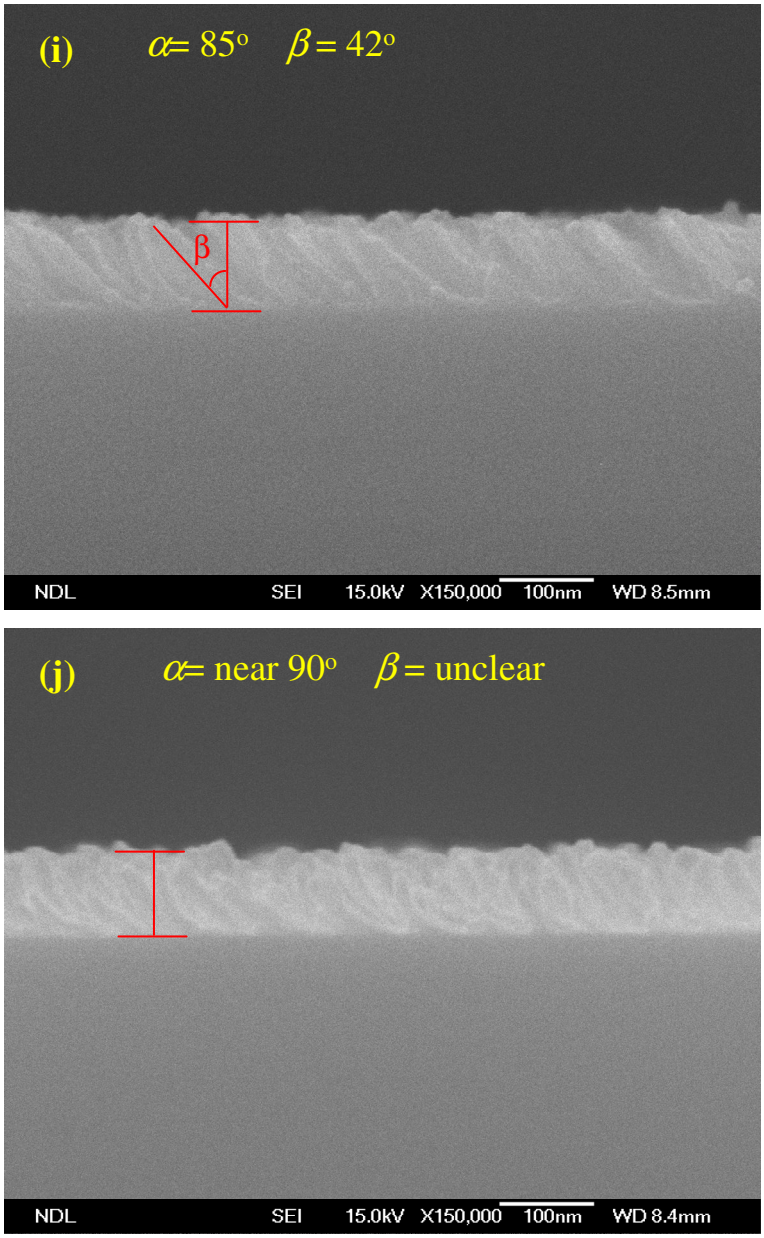

Fig. 3-2 SiO_2 nanoporous thin films on silicon substrate. Higher incident angle, higher porosity and usually higher column angle.

There is no scattering effect due to nanoscale voids in nanoporous thins film are less than 50 nm. The unclear porosity of thin film is due to the little shadowing effect at lower incident flux angle. There are interesting phenomena revealed at the angles of 85^o and near 90^o. The shapes of rods at incident flux angle 85^o of nanoporous thin film

become little bow. When the incident flux angle meets almost 90^{o}, the rods become to disorder, some rods grows with lower column angle, some rods grows with higher column angle but bow to lower column angle. There must be some factors effect the growth angle dominated by surface diffusion and shadowing effect.

Deposition source	Incident flux angle	Deposition rate	Base pressure	Deposition pressure	Chamber temperature
TiO_2	0^o, 50^o~90^o	0.1 nm/s	1.3×10^{-6} torr	7.4×10^{-6} ~ 3.7×10^{-6} torr	23^oC ~ 52^oC

Table 3-2 Deposition parameters of TiO_2 nanoporous thin films on Si substrate.

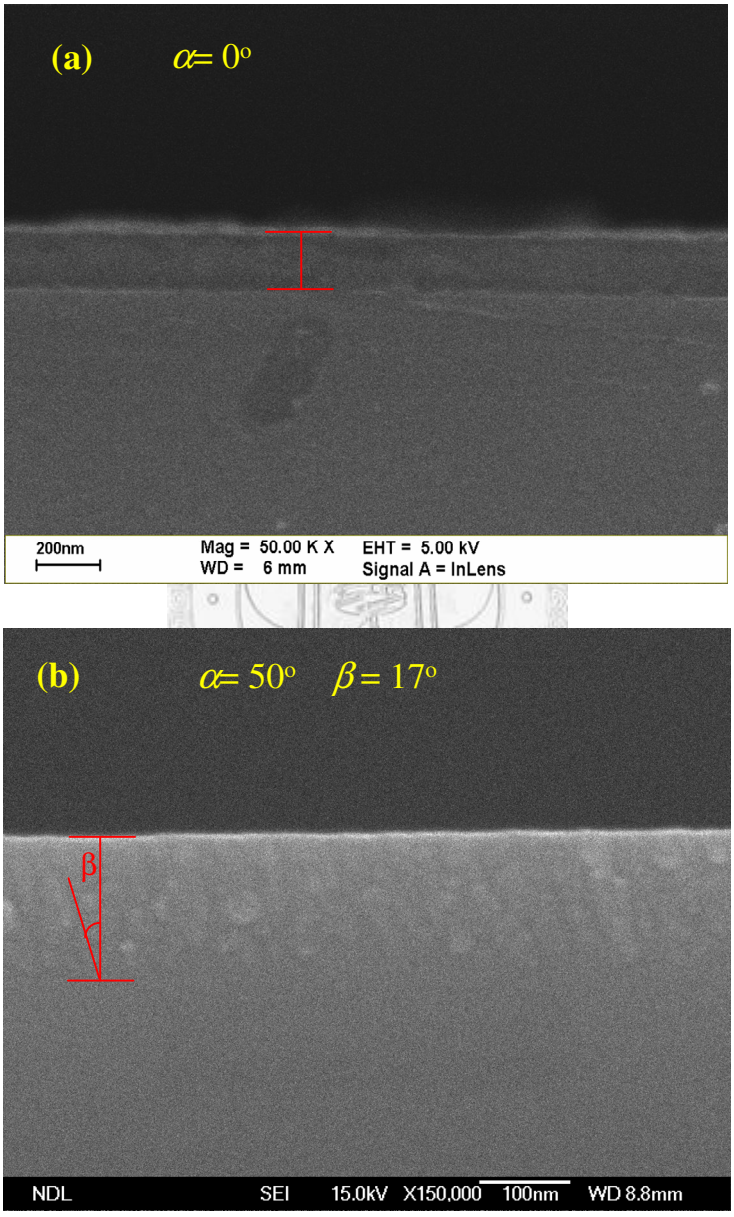

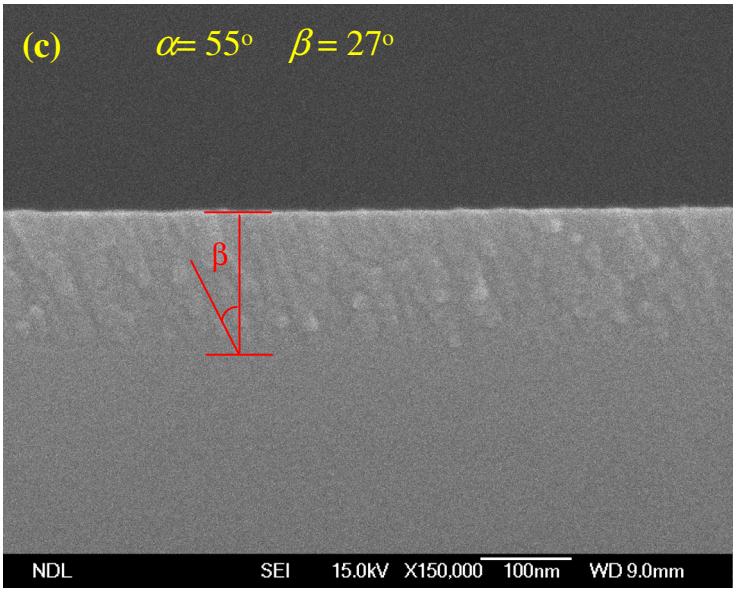
(c) α= 55° β = 27°
β
NDL SEI 15.0kV X150,000 100nm WD 9.0mm

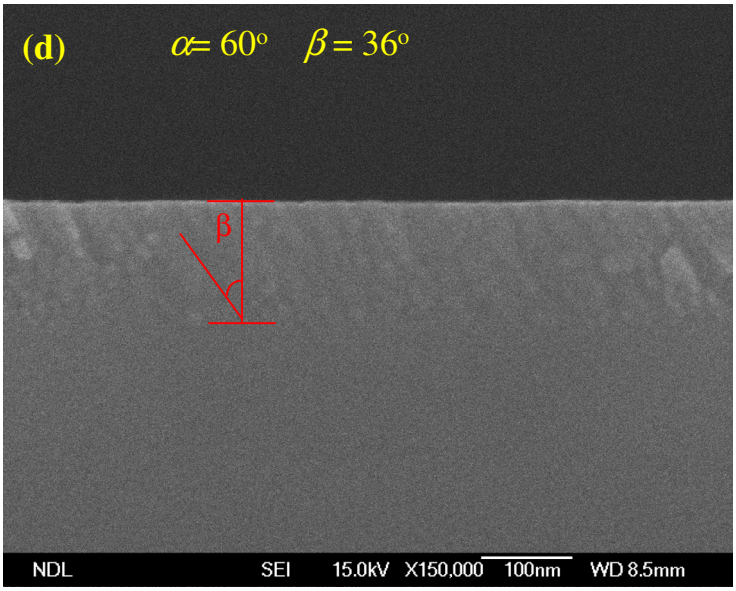
(d) α= 60° β = 36°
β
NDL SEI 15.0kV X150,000 100nm WD 8.5mm

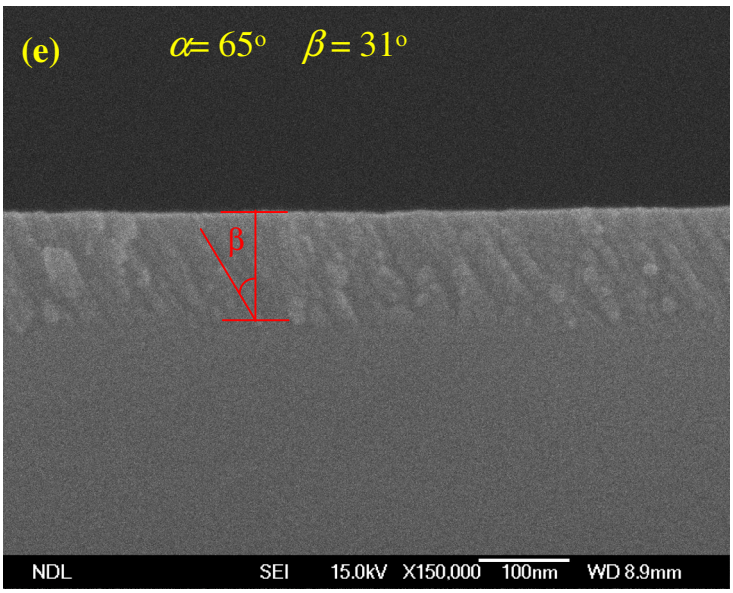
(e) α= 65° β = 31°
β
NDL SEI 15.0kV X150,000 100nm WD 8.9mm

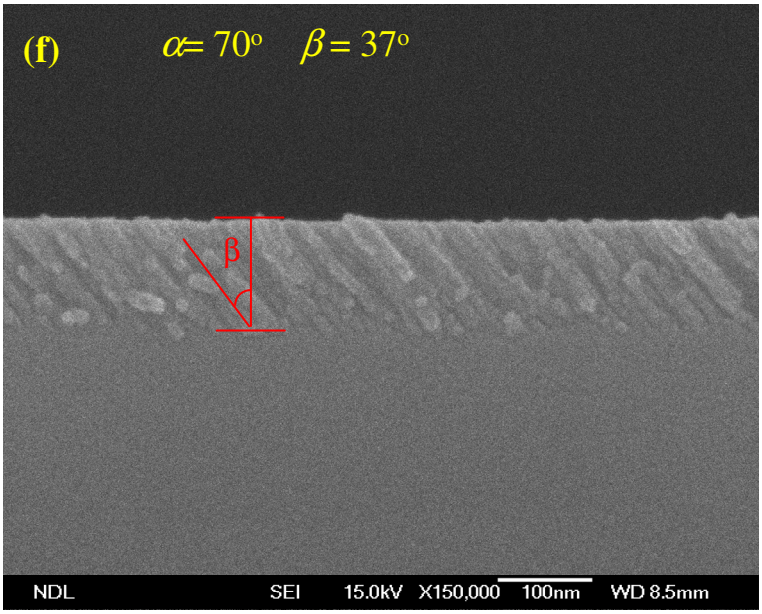
(f)
α= 70°
β = 37°
β
NDL
SEI
15.0kV X150,000
100nm
WD 8.5mm

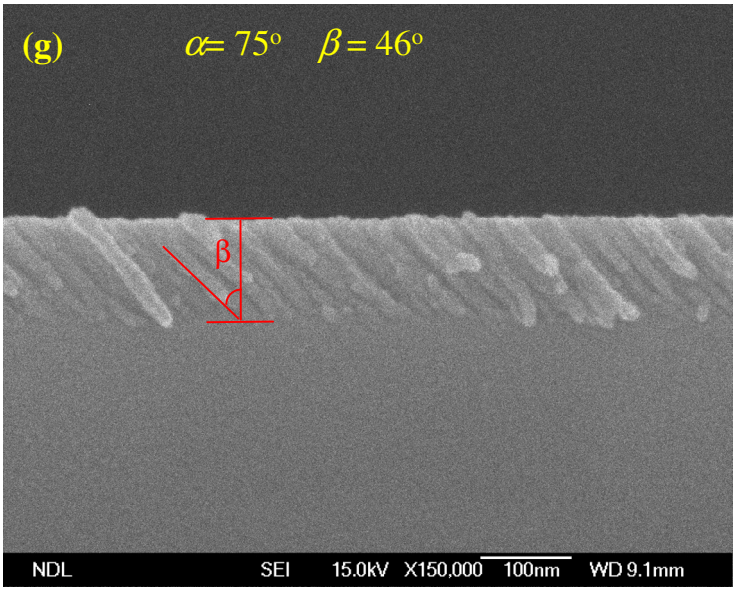
(g)
α= 75°
β = 46°
β
NDL
SEI
15.0kV X150,000
100nm
WD 9.1mm

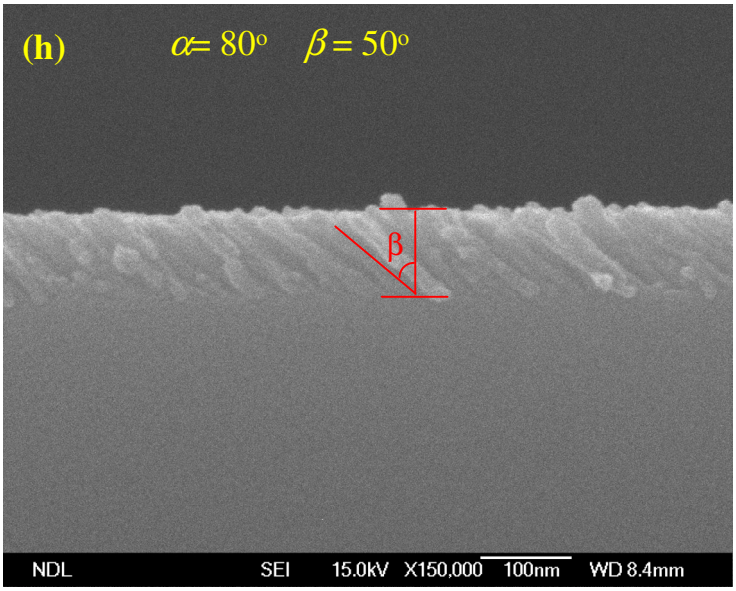
(h)
α= 80°
β = 50°
β
NDL
SEI
15.0kV X150,000
100nm
WD 8.4mm

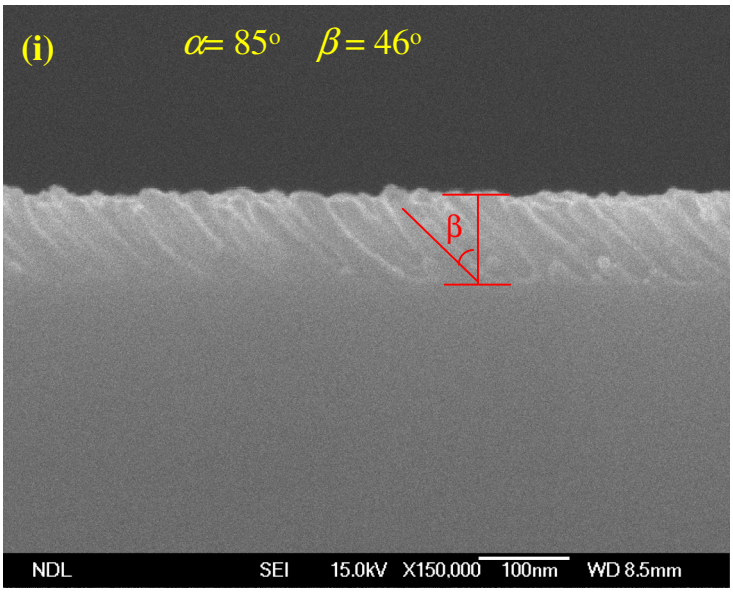

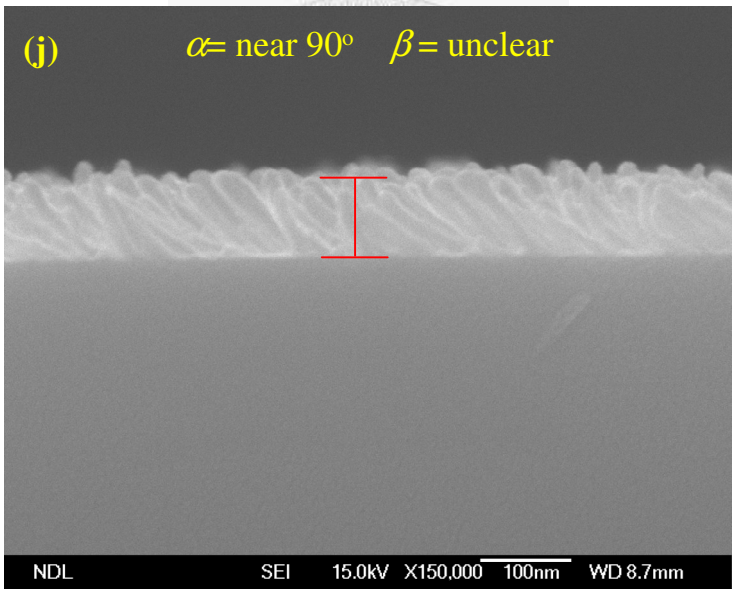

Fig. 3-3 TiO_2 nanoporous thin films on silicon substrate.

Deposition source	Incident flux angle	Deposition rate	Base pressure	Deposition pressure	Chamber temperature
Si	0^o, 50^o~90^o	0.3 nm/s	3×10^{-7} torr	1.6×10^{-6} ~ 7 $\times10^{-6}$ torr	23^oC ~ 30^oC

Table 3-3 Deposition parameters of Si nanoporous thin films on Si substrate.

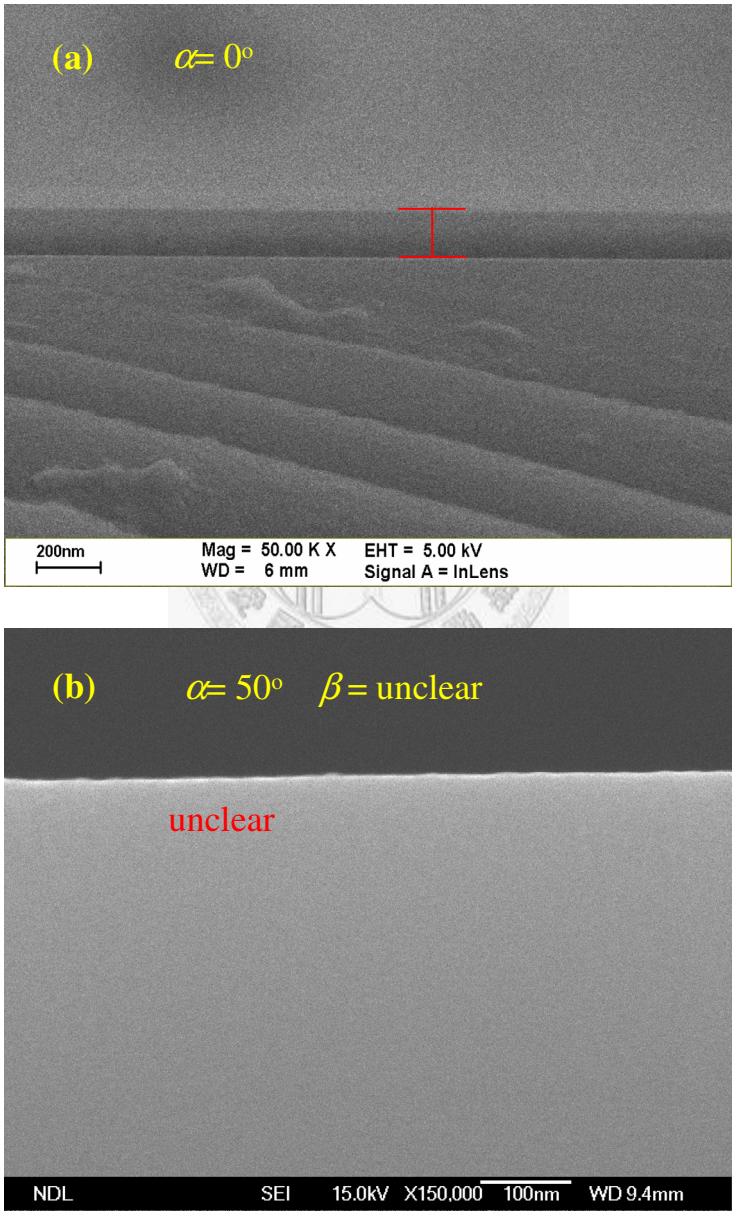

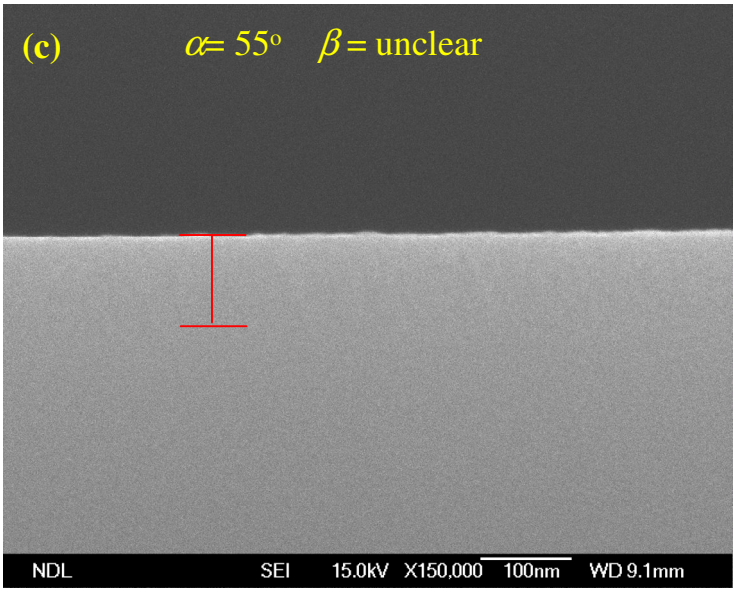
(c)
α= 55°
β = unclear
NDL
SEI
15.0kV X150,000
100nm
WD 9.1mm

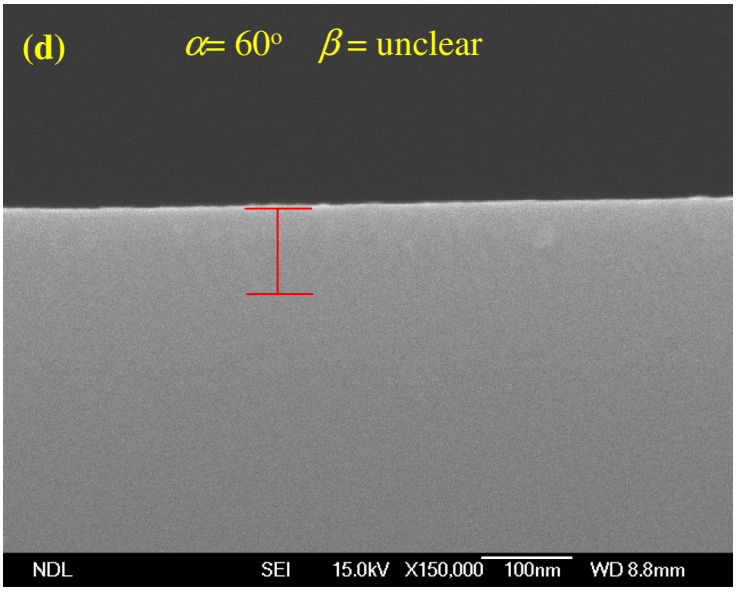
(d)
α= 60°
β = unclear
NDL
SEI
15.0kV X150,000
100nm
WD 8.8mm

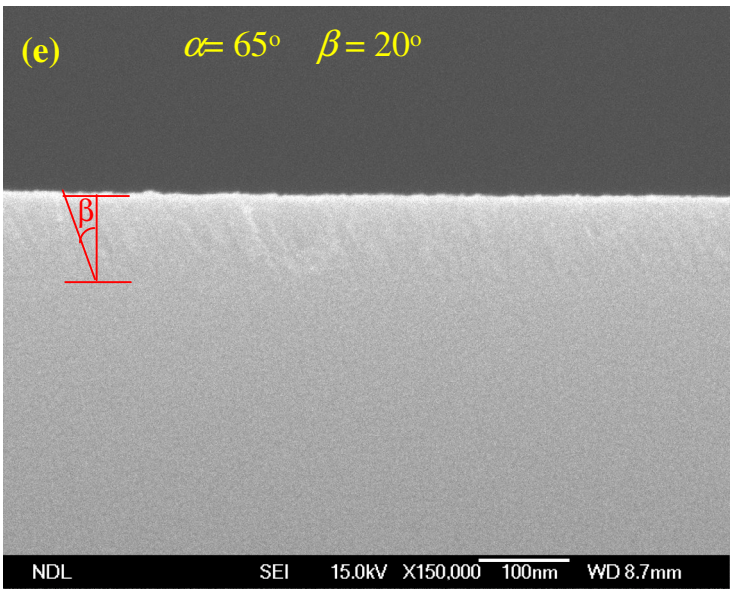
(e)
α= 65°
β = 20°
β
NDL
SEI
15.0kV X150,000
100nm
WD 8.7mm

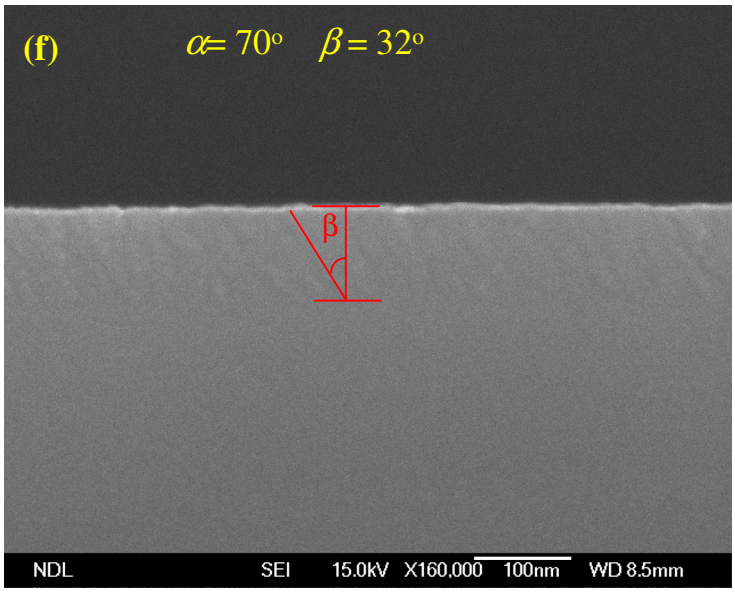
(f)
α= 70°
β = 32°
β
NDL
SEI
15.0kV X160,000
100nm
WD 8.5mm

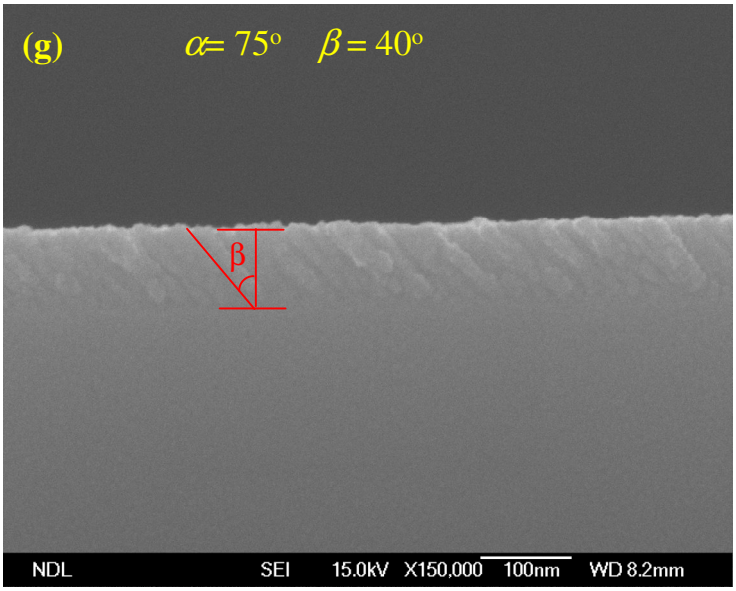
(g)
α= 75°
β = 40°
β
NDL
SEI
15.0kV X150,000
100nm
WD 8.2mm

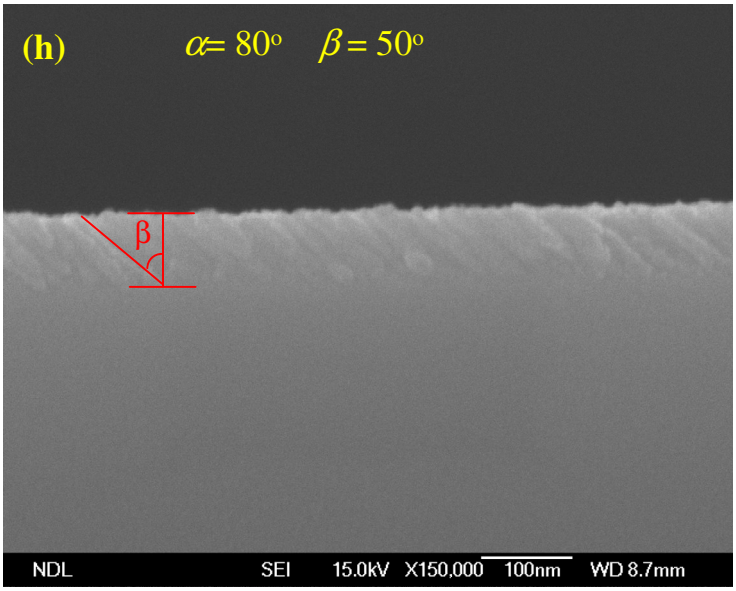
(h)
α= 80°
β = 50°
β
NDL
SEI
15.0kV X150,000
100nm
WD 8.7mm

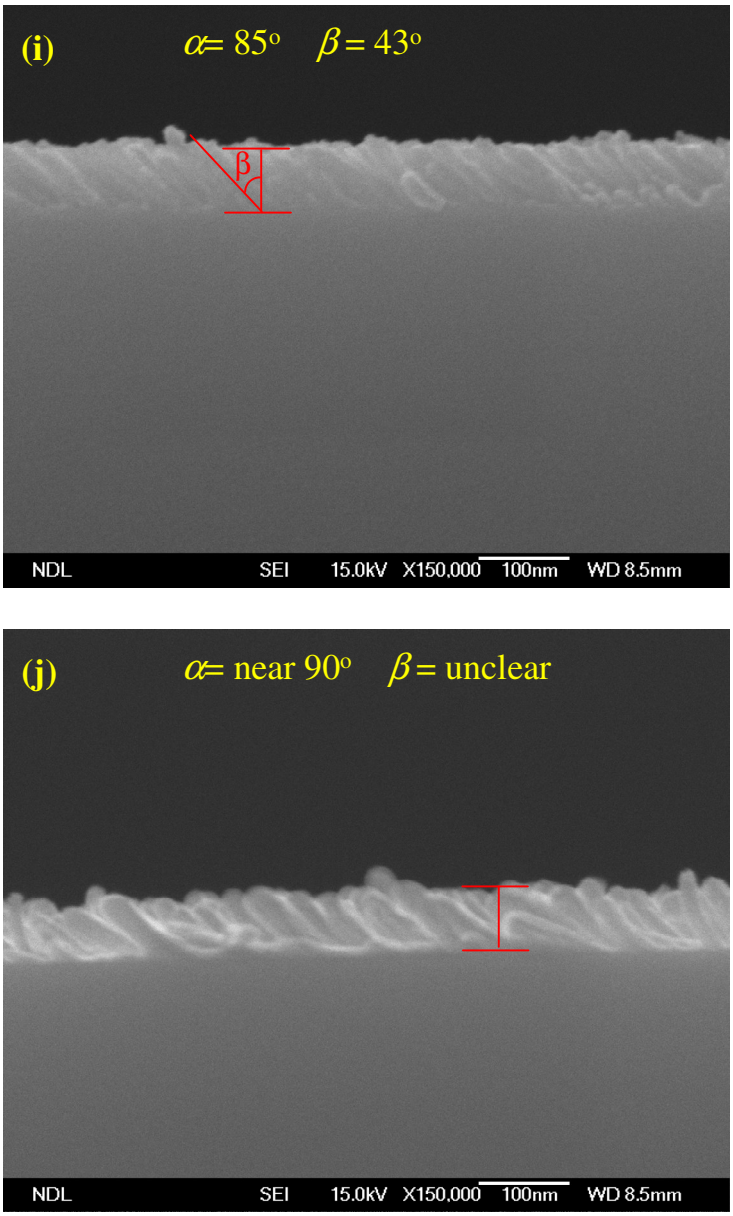

Fig. 3-4 Si nanoporous thin films on silicon substrate.

When thin films are deposited onto stationary substrates with the flux arriving at a non-normal angle ($\alpha \neq 0^{o}$), an inclined columnar microstructure (β) is produced. Excellent reviews of the effects of oblique-angle deposition technique were published

[9, 10]. As it has been mentioned previously, many parameters affect the relation between incident flux angle (α) and column angle (β). However, there is a fixed relationship between incident flux angle and column angle for "a given set of deposition conditions". The column angle (β) is uniquely determined by the choice of the deposition angle (α). The relationship is very complicated and not easy to be understood, despite numbers of research have been presented. The empirical "tangent rule" as shown in below [11] is proposed by geometrical analysis.

$$\tan(\beta) = (\frac{1}{2})\tan(\alpha) \tag{3-1}$$

It is a simple relationship based on near normal flux angle, but it gives very poor results for incident flux angle (α) greater than about 50^{o}. Another relationship given by Tait *et al.* [12] based on geometrical analysis is shown in below:

$$\beta = \alpha - \sin^{-1}\left[1 - \cos(\frac{\alpha}{2})\right] \tag{3-2}$$

This equation gives much reasonable results for highly oblique angles. Note that the geometrical analysis given by Tait *et al.* gives some qualitative predictions, but they do not account for varied material or deposition conditions. Some publications with different parameters by oblique-angle deposition were presented [13, 14].

Fig. 3-1, 3-2 and 3-3 show that the higher incident flux angle is the higher column angle, our oblique-angle deposition results are not very match with the Eq. 3-2, since the Eq. 3-2 is analyzed with specific deposition condition with Fe deposition source.

3-2 Experimental results of nanoporous thin film versus the incident flux angle during deposition

In this work refractive index, thickness and porosity will be discussed with different evaporation incident flux angles.

Principles of refractive index measurement

In this work the refractive indices were measured by white light interferometer, Filmetrics F20 (configuration is shown in Fig. 3-5) made by Filmetrics Incorporation.

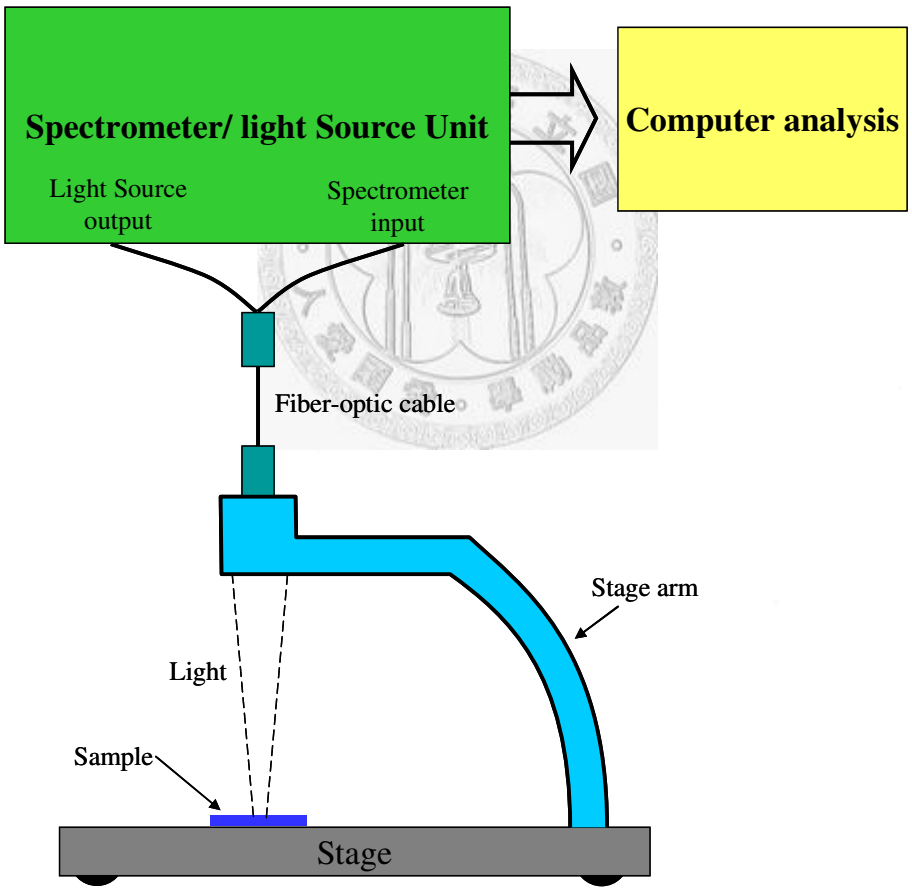

Fig. 3-5 Configuration of F20 stage. Optical properties are measured of normal incident light.

The thin film characteristics measured by the normal-incident reflection spectrum. Whether the reflections are in-phase or out-of-phase, it depends on the wavelength of the light as well as the thickness (reflections are in-phase when $\lambda = (2 \times n \times d)/i$, where λ is the wavelength, *n* is the refractive index, d is the film thickness, and i is an integer). Reflection spectrum of the measurement film is shown in Fig. 3-6. The result is characteristic intensity oscillations in the reflectance spectrum. In general, the thicker the film, the more oscillations are in a given wavelength range.

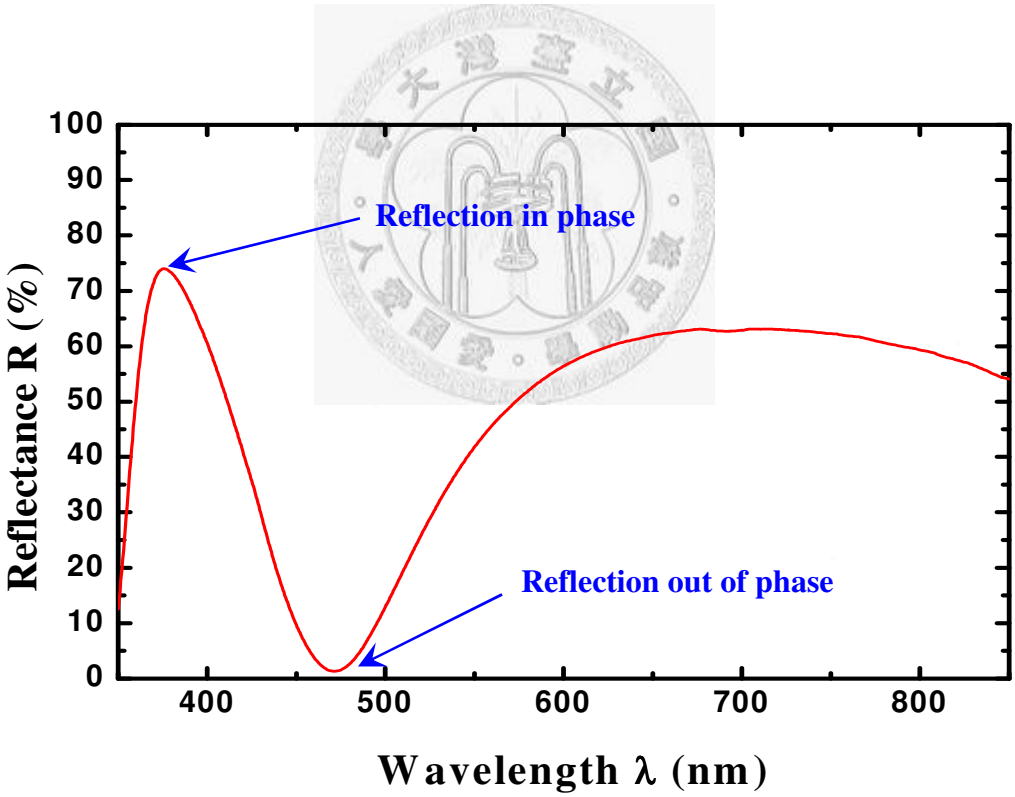

Fig. 3-6 Example of reflection spectrum. Optical properties are measured with the principle of interference of reflection normal incident light.

Optical thin film thickness (*d*), refractive index (n) and extinction coefficient (k) measurements require the acquisition and then analysis of an accurate reflection spectrum. To determine thin film properties, a reflection spectrum and calculation spectrum matches as closely as possible. F20 begins with an initial guess for what the reflectance spectrum should look like theoretically which is based on the user's input of a thin film structure for the sample. Since n and k vary as a function of wavelength, it is necessary to solve for them at every wavelength. For a unknown material, it is not possible to do this using a reflection spectrum only since at each wavelength only one know parameter is known and there are two more unknowns. However, n and k are not independent, but are related to each other via what is known as the Kramers-Kronig relation. If refractive index n was known at every wavelength, extinction coefficient k could be computed solely from "n". Since it is only possible to measure refractive index n over a finite wavelength range, extinction coefficient k cannot be computed directly from "n".

In reality, there is plenty of data present from a single reflection spectrum to determine both "n" and "k" simultaneously. Thus, if the equation for refractive index has three adjustable parameters, it is only necessary to adjust these three parameters in order to match the calculated and measured spectrum. Therefore, the measurement of

"n" and "k" has been reduced to choosing an appropriate model [15, 16] for "n" and "k" as a function of wavelength and then adjusting the parameters in the model to obtain a good fit to the measured data.

The configuration of all the fitting models for nanoporous thin film is shown in Fig. 3-7. And the most fitting results are confirmed by SEM to make sure our optical measurements are reliable. Cauchy model was demonstrated that it is an appropriate model for nanoporous thin film deposited by SiO_2, TiO_2 and Si deposition sources.

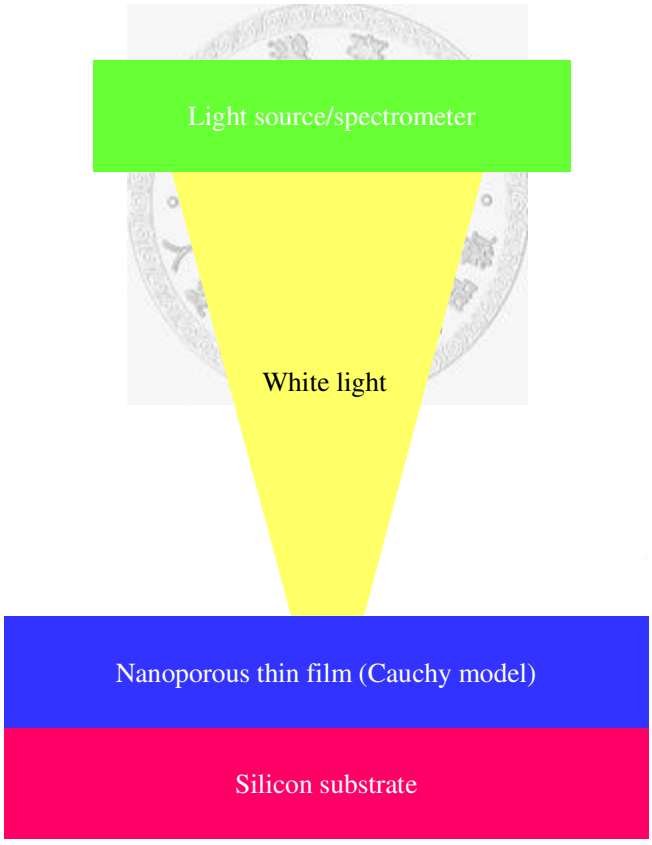

Fig. 3-7 Illustration of nanoporous thin film measurement. Cauchy model is suitable to depict the light through the transparent thin film.

Cauchy model is suitable for transparent layers (low-k material), SiO_2, TiO_2 and Si dense film/ nanoporous thin films, especially SiO_2, TiO_2 and Si nanoporous thin films (lower k of nanoporous thin film than dense film).

Measurement of low-extinction-coefficient thin film

Low-extinction-coefficient thin film can be measured by an accurate method. According to a single layer AR coating principle, which will be introduced in chapter 4, if the reflective minimum of reflection spectrum is fitted to the measurement spectrum, the fitting result is trusted. All of the measurements are fitted with the principle, namely, nanoporous thin films are deposited with suitable refractive indices and thickness.

There is a problem should be noted. For an accurate fitting result, a reflective minimum of reflection spectrum must be fitted. Note that the fitting results can be fitted accurately with only one reflective minimum in measurement region. It can be known from Eq. 2-2 and Fig. 2-6. The thickness of nanoporous thin film is not uniform when deposition is containing an incident oblique angle. Suitable thickness (only one reflective minimum of reflection spectrum) can alleviate this problem.

To solve this problem of not uniform thickness of nanoporous thin film, a nanoscale rotating sample holder is useful to solve [4].

Anisotropic nanoporous thin film

Optical properties, for example, refractive indices of nanoporous thin films are not constants, which are dependent on the azimuthal angle of incident light. This kind of thin film is anisotropic nanoporous thin film as show in Fig. 3-8 [6].

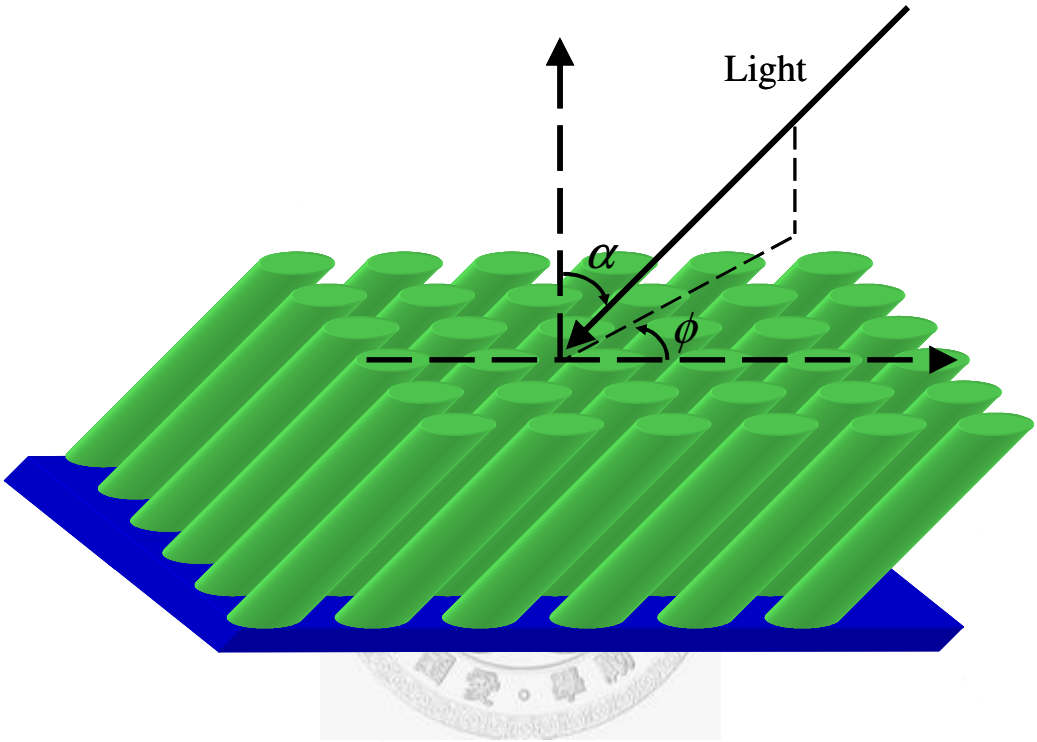

Fig. 3-8 Anisotropic nanoporous thin film fabricated by oblique angle deposition. Optical properties of anisotropic thin film are dependent on the azimuthal angle of incident light.

In our experiment, the optical properties are measured at normal incident light.

Incident flux angle vs. refractive index of nanoporous thin film

All the refractive indices of nanoporous thin films were measured by F20 on

as-deposited day and most of the values were confirmed by SEM. The following tables below are the relations between incident flux angles vs. refractive indices.

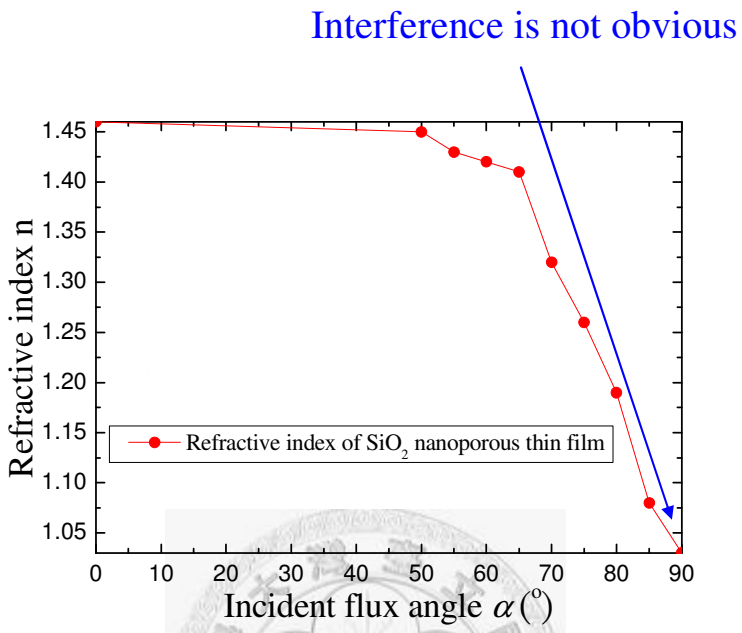

Fig. 3-9 Refractive indices of SiO_2 nanoporous thin films vs. incident flux angles during deposition process. The refractive indices of SiO_2 thin films are reduced from 1.46 to 1.08 at wavelength λ= 550 nm. The nanoporous thin film at incident flux angle near 90^o has no obvious interference phenomenon.

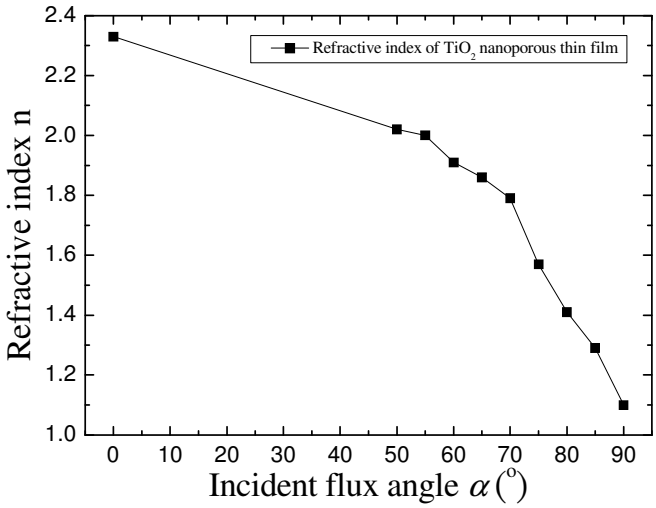

Fig. 3-10 Refractive indices of TiO_2 nanoporous thin films vs. incident flux angles during deposition process. The refractive indices of TiO_2 thin films are reduced from 2.3 to 1.1 at wavelength λ= 550 nm

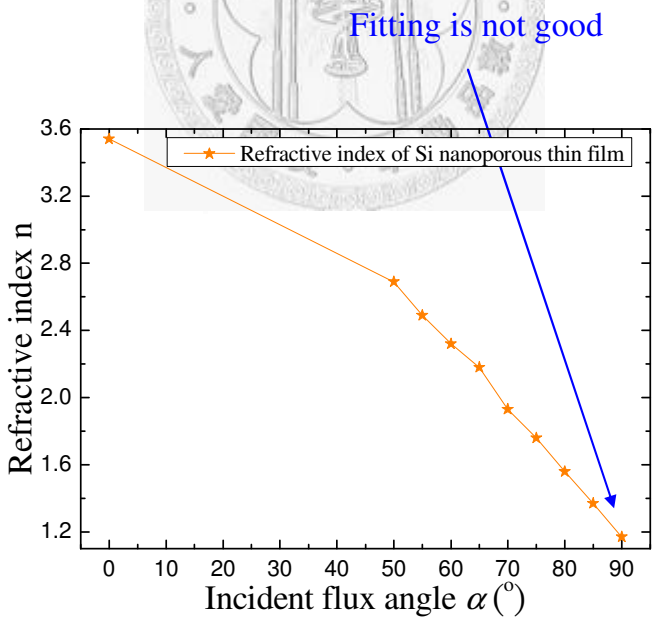

Fig. 3-11 Refractive indices of Si nanoporous thin films vs. incident flux angles during deposition process. The refractive indices of Si thin films are reduced from 3.35 to 1.2 at wavelength λ= 550 nm. The fitting of Si nanoporous thin film is

not good at incident flux angle near 90o probably due to nanoporous thin film disorders.

The fitting results of the nanoporous thin film deposited by SiO_2 and Si at incident flux angle near 90^o are not very well. So I marked the question sign in the table. For the SiO_2 nanoporous thin film at incident angle at near 90^o, I guess that it's due to the refractive index is too close to the refractive index of air, the interfere phenomenon is not obvious. Moreover, the interface between nanoporous thin film and air is not very clear and uniform, which may cause the poor fitting result.

Incident flux angle vs. thickness of nanoporous thin film

All the thickness of nanoporous thin films was measured by SEM except for the images of SEM photos were stretched evidently. The thickness values are replaced by the values measured by F20, and most thickness measured by F20 are matched with thickness measured by SEM. The following tables below are the relations between incident flux angles vs. thickness.

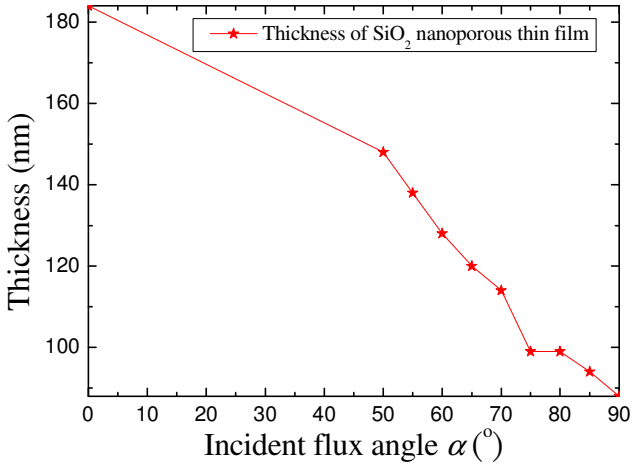

Fig. 3-12 Thickness of SiO_2 nanoporous thin films vs. incident flux angles during deposition process

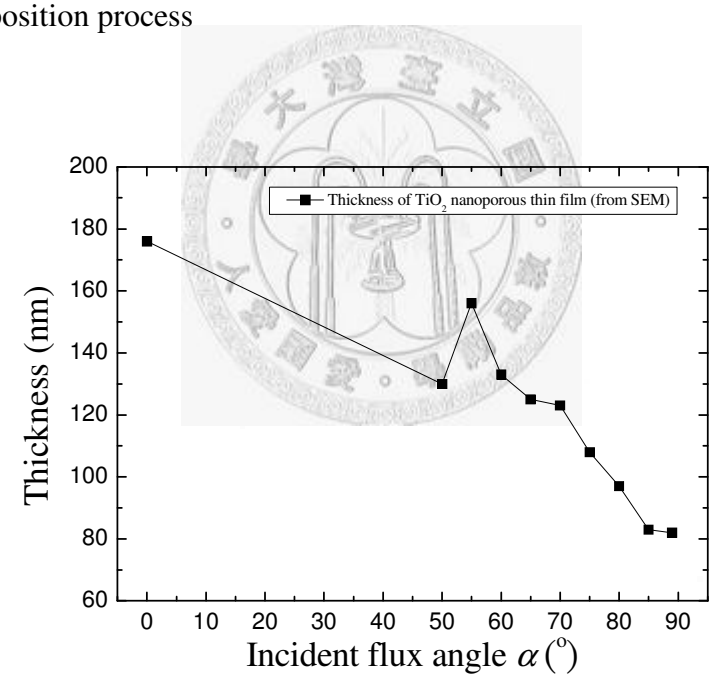

Fig. 3-13 Thickness of TiO_2 nanoporous thin films vs. incident flux angles during deposition process

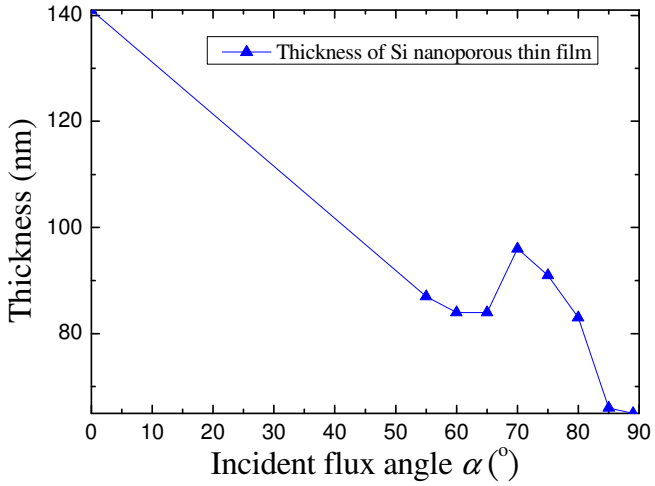

Fig. 3-14 Thickness of Si nanoporous thin films vs. incident flux angles during deposition process

Incident flux angle vs. porosity of nanoporous thin film

All the porosities were determined by the equation, which is rewrote of Eq.1-2, as shown in follow:

$$V_{air}\frac{n_{air}^{2}-n_{eff}^{2}}{n_{air}^{2}+2n_{eff}^{2}}+(1-V_{air})\frac{n_{m}^{2}-n_{eff}^{2}}{n_{m}^{2}+2n_{eff}^{2}}=0 \qquad (3\text{-}3)$$

Where V_{air} is the porosity of the nanoporous thin film, n_{air} is the refractive index of the air, n_{eff} is the refractive index of the nanoporous thin film and n_m is the refractive index of the thin film deposited at 0^o.

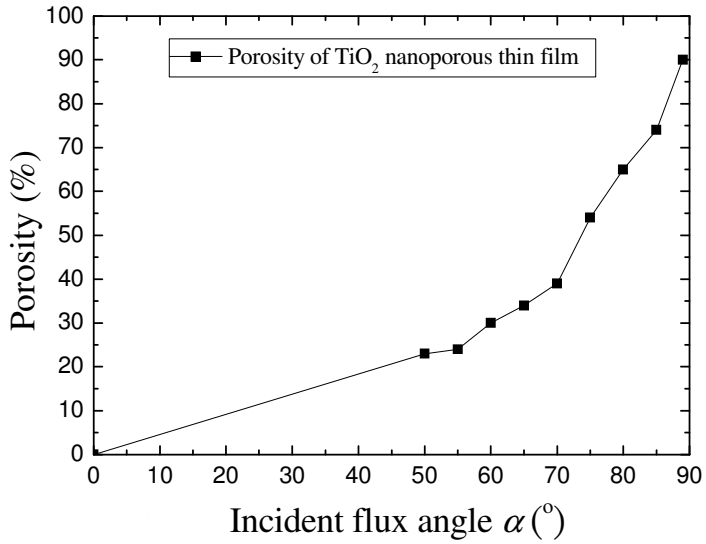

Fig. 3-15 Porosity of SiO_2 nanoporous thin films vs. incident flux angles during deposition process

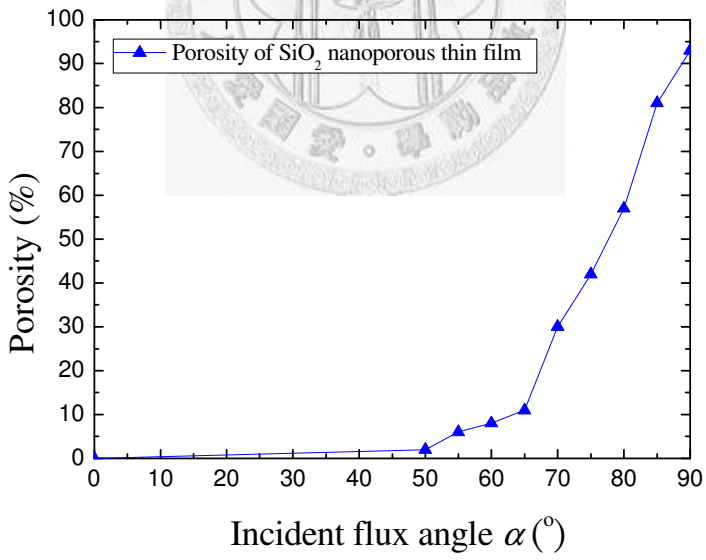

Fig. 3-16 Porosity of TiO_2 nanoporous thin films vs. incident flux angles during deposition process

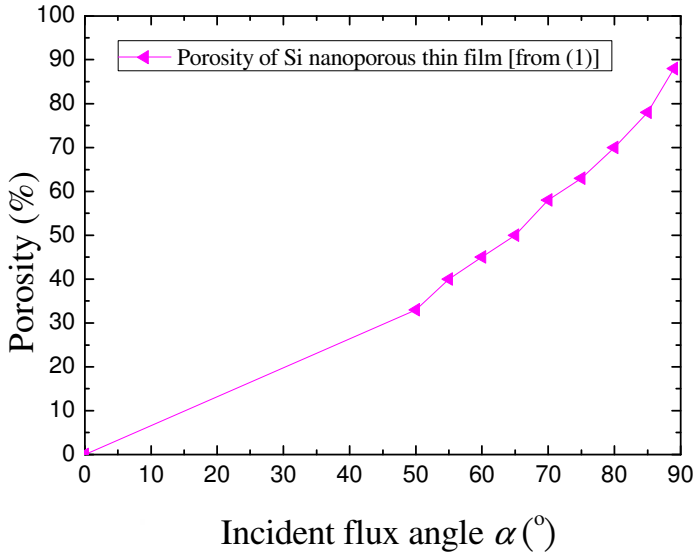

Fig. 3-17 Porosity of Si nanoporous thin films vs. incident flux angles during deposition process

Note that the porosity estimated by Bruggeman EMA equation has some deviation. EMA has some limits of validity [2]. Accurate measurement of nanoporous thin film can solve this problem [15].

3-3 Summary

Pertinent parameters of oblique-angle deposition include the deposition rate, the angular distribution of the incident vapor flux, the film and substrate temperature, the energies of the surface–substrate interface, and the partial pressure of residual gases in the deposition chamber. Our results show different trends between the three kinds of deposition sources SiO_2, TiO_2 and Si. The refractive index of nanoporous film can be

measured well by white light interferometer and Cauchy model is suitable for these kinds of low-k nanoporous thin films. It can be found that the refractive index decreases when the incident flux angle increases. But compare the Eq. 2-2 to my measurement result, it's not match with the equation due to the higher porosity in the thin film will accompany the higher thickness if the total incident flux is the same. The schematic is show in Fig. 3-8.

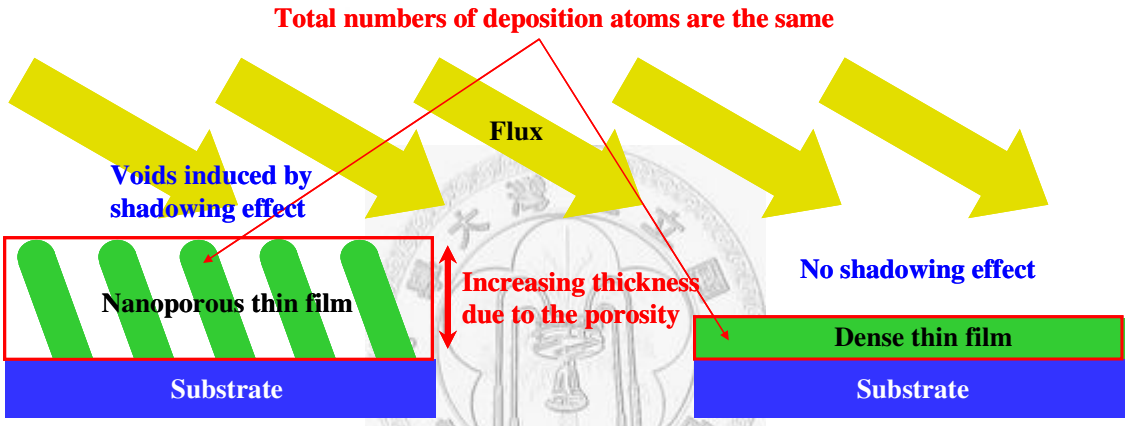

Fig. 3-18 Illustration for illustration of higher porosity accompanying higher thickness of nanoporous thin film than of thickness of dense thin film.

Also, highly oblique incident angle will extend the shadow region and increase the porosity of thin film, the refractive index measurement can demonstrates it. Although, the relation between incident flux angle (α) and column angle (β) is not match the Eq. 3-1 well, the principle of shadowing effect still exists.

The refractive index n= 1.08 of nanoporous thin film deposited by SiO_2 source is achieved. For the result, high reflection of DBR can also be fabricated [7] due to

ultra-low-refractive-index accompany with increasing Δn and very low reflection AR coating with the ultra-low-refractive-index nanoporous thin film. Also, the three kinds of deposition source can be used to fabricate the refractive indices of nanoporous thin films from n= 3.54 to n=1.08 by oblique-angle deposition. The tunable refractive index property can make higher performance of optical device, even some of the ideal optical devices made by only one material.

Chapter 4 Nanoporous thin film for Distributed Bragg Reflector (DBR) and Anti-Reflection (AR) coating applications

In this chapter, Distributed Bragg Reflector (DBR) and Anti-Reflection (AR) coating are fabricated by e-beam oblique-angle deposition. Besides, the designs of these kinds of optical device principles and some simulation results will also be introduced.

Angle-varied holder design

Venting the chamber not only degrades the qualities of thin films but also consumes the time. An angle-varied holder is needed.

In the e-beam chamber, the only jig rotation mechanical device can be controlled from the outside, since we design a mechanical device connecting to the jig rotator to cause angle-varied purpose. The angle-varied holder must contain these functions: many different angles for holder setup, repeatable angle rotation and outside-control from jig rotation. Mine design configuration of angle-varied holder is shown in Fig. 4-1 (a).

First, we put the springs into the spring holes which represent the different angles subtended by the incoming flux and the outward substrate normal. When the angle-varied holder is connecting to the spur gear connecting to the e-beam rotator, we

can use the jig rotation controller to let the angle holder rotate by the rotating rod drove by the connecting gears. The angle holder drove by the rotating rod from 90^{o} will drop on the upper spring because of the gravity, and this is the first angle we want to stop. And the rotating rod is still rotating. When the rotating rod touches the angle holder but the rotating rod is still running, the rotating rod will press the angle holder to press the spring. The flexible spring will change its shape to let the angle holder pass through itself. Then the angle holder will drop on the second spring, the second holder we want to stop. The Fig. 4-2 (b) is the illustration of the process. Using the angle-varied holder, we can fabricate some optical devices with many different angles by oblique-angle deposition technique at a time.

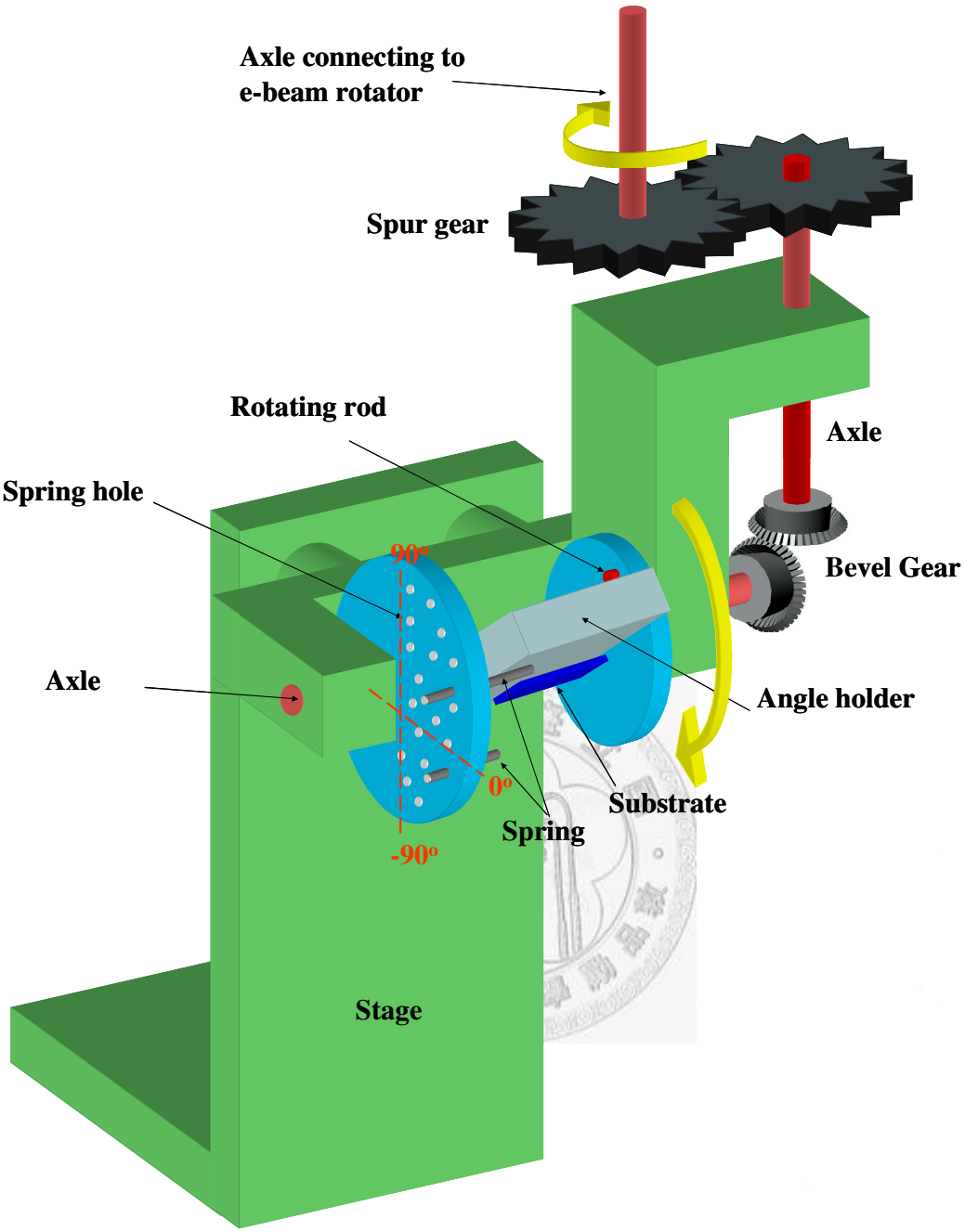
Axle connecting to
e-beam rotator
Spur gear
Rotating rod
Axle
Spring hole
Bevel Gear
90°
Axle
Angle holder
0°
Substrate
Spring
-90°
Stage

(a)

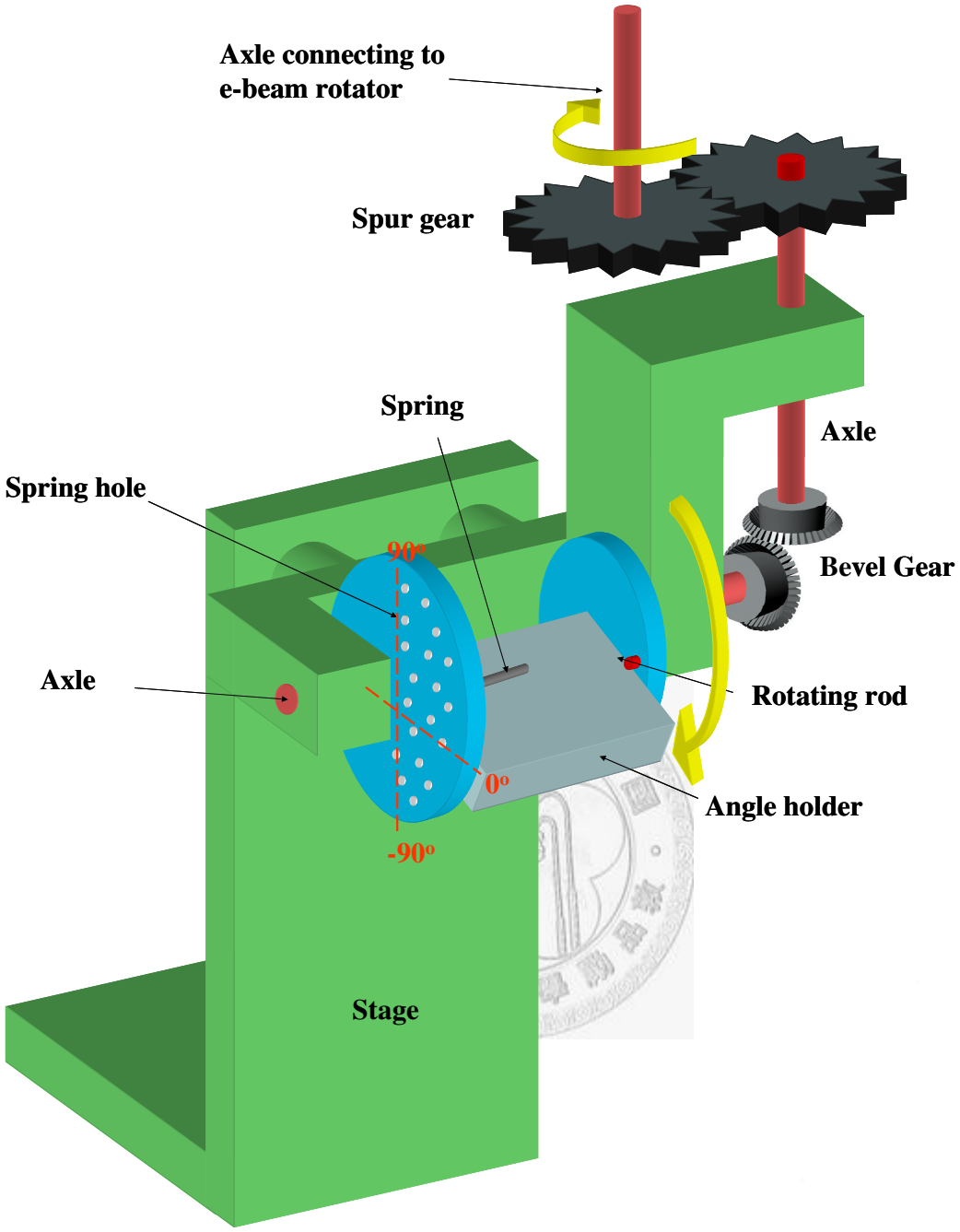

(b)

Fig. 4-1 Illustration of angle-varied holder.

(a) and (b) show an angle-changing process. Using the angle-varied holder, we can fabricate some optical devices with many different angles by oblique–angle deposition technique at a time.

4-1 Nanoporous thin film for Distributed Bragg reflector (DBR)

4-1-1 Introduction to Distributed Bragg reflector (DBR)

A Distributed Bragg reflector (DBR) is a high quality reflector which can be used in optical fibers and some optical devices like Light Emitting Diode (LED) to enhance light extraction efficiency. It's a structure formed from multiple layers of alternating materials with varying refractive indices. Each layer boundary causes a partial reflection of an optical wave. A periodic structure that consists of an alternating series of a quarter-wavelength thick high-index and low-index material with a refractive index of n_{high} and n_{low}, respectively combine constructive interference and act as a high-quality reflector as shown in Fig.4-2. The following figures are the properties of a single pair DBR:

The reflectance of a single interface of a single pair DBR:

$$R = \left[\frac{\Delta n}{n_{high} + n_{low}} \right]^2 \tag{4-1}$$

The spectral width of a single pair DBR stop band:

$$\Delta\lambda_{stop} = \frac{2\lambda\Delta n}{n_{eff}} \tag{4-2}$$

The maximum angle of incidence at which high reflectivity is maintained:

$$\theta_c \approx \frac{n_{low}}{n_0}\sqrt{\frac{2}{n_0}\frac{2\Delta n}{n_{low}+n_{high}}} \tag{4-3}$$

These optical properties are described for a single pair DBR. Note that for a double pair or several pair DBR, these equations are not suitable to describe optical properties of DBR. Optical properties of multiple pair DBR can be depicted by "scattering matrix formalism".

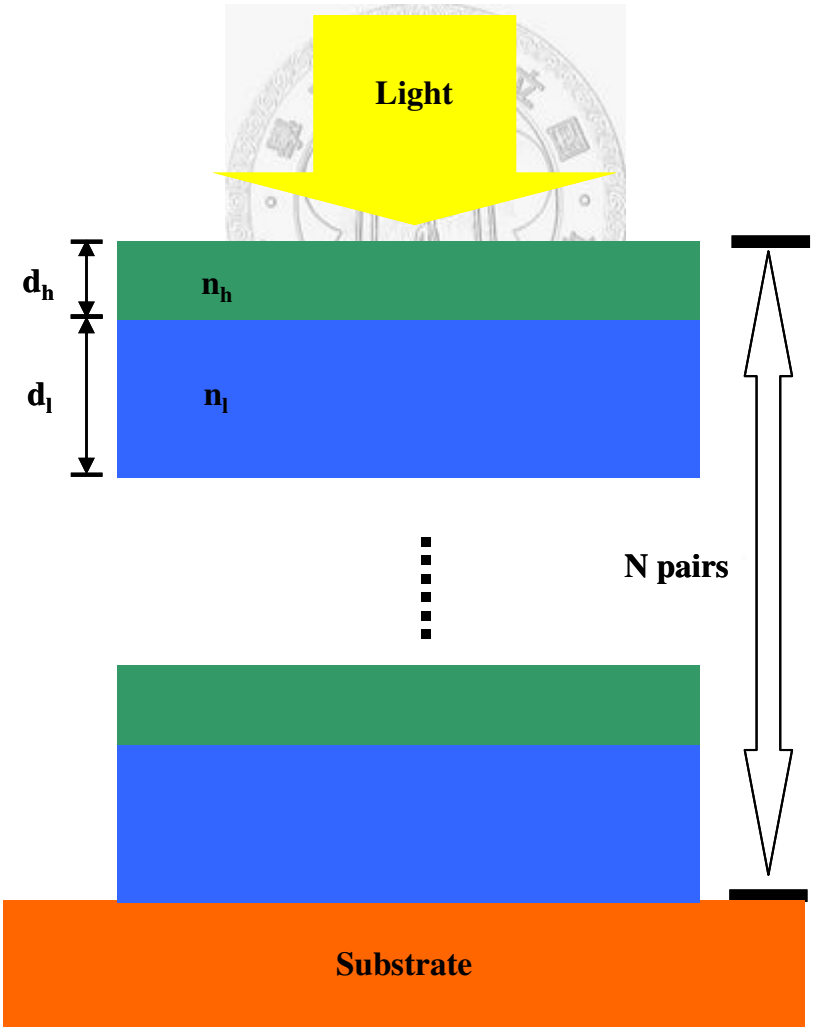

(a)

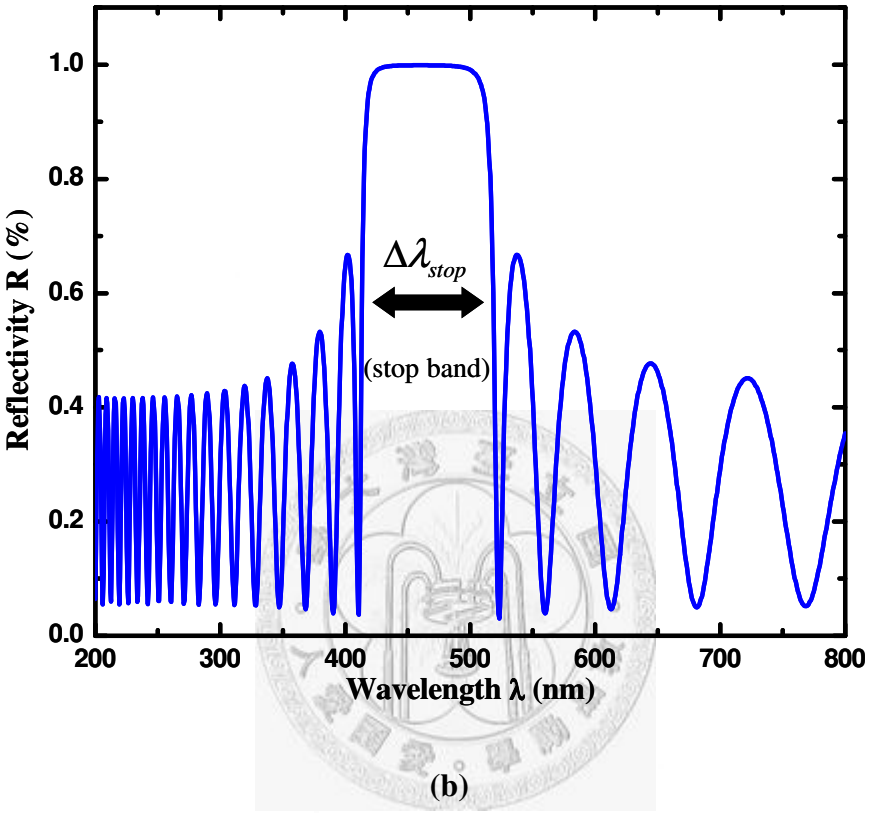

Fig. 4-2 (a) Configuration of Distributed Bragg reflector (DBR).

(b) The illustration of reflectivity spectrum of DBR.

These equations above show that the refractive index contrast (Δn) is a key quantity for DBR. Increasing the index contrast would allow one to improve every single figure of quality given above and thus make better DBRs. More importantly, not only the higher reflectance of DBR can be obtained but also better spectral width of stop band

and maximum allowed incident angle can be obtained. Namely, we can get better DBRs as long as we can make lower or higher refractive index material. Conventionally, DBR can be deposited with different materials, but we can just use single material to successfully make DBR by oblique-angle deposition technique.

4-1-2 Fabrication and measurements of DBR

First, the nanoporous thin film has been deposited to fabricate low-n thin film on the silicon substrate. Lower incident flux angle makes the refractive index of thin film higher. Lower incident flux angle on the nanoporous with higher incident flux angle makes the continuous deposition atoms fill into the gaps of the nanoporous thin film so that DBR is needed by such a process. Some solutions were found to solve this problem [15, 18]. The deposition process is shown in Fig. 4-3.

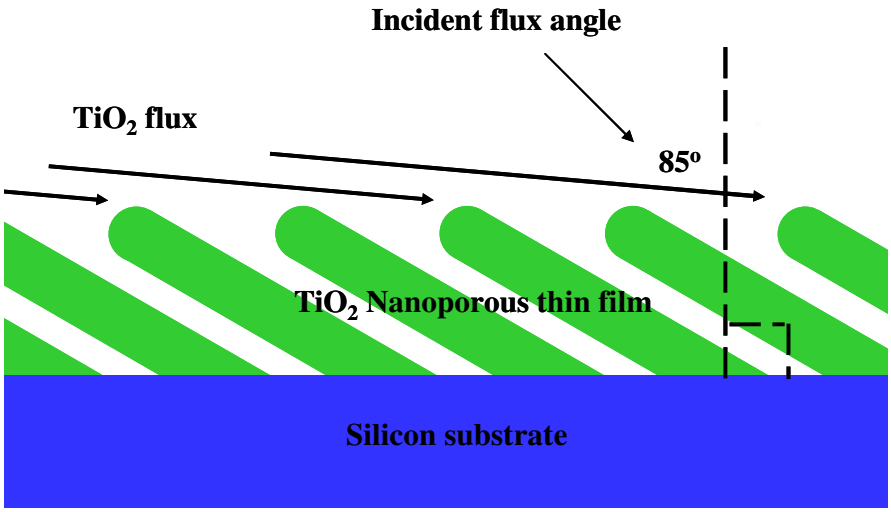

(a)

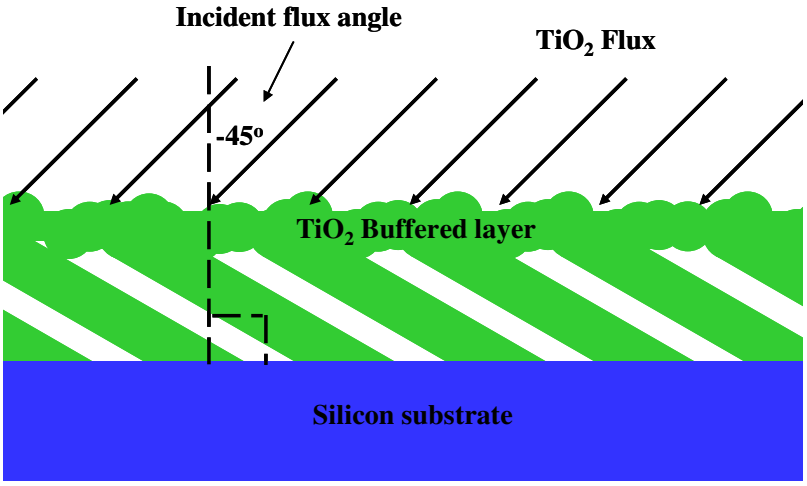

(b)

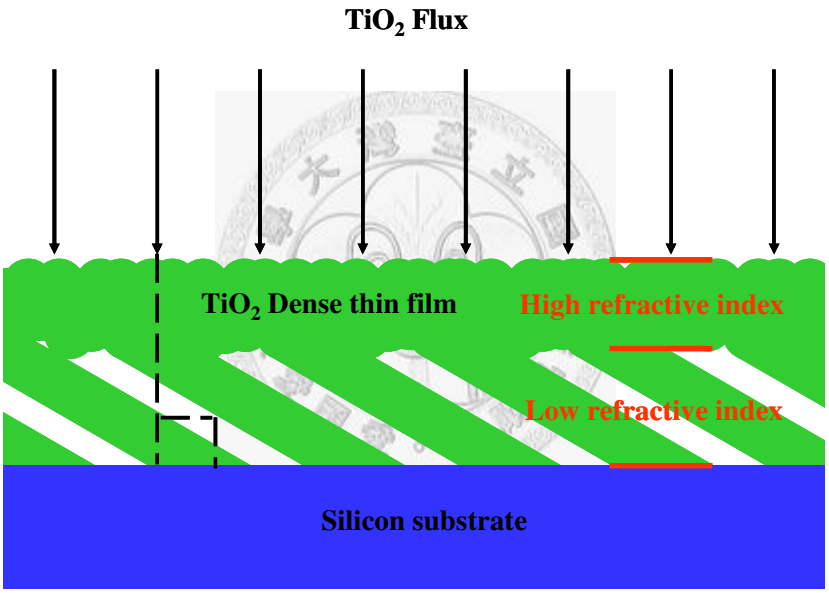

(c)

Fig. 4-3 Illustration of single pair DBR with only TiO_2 materiel.

(a) Deposition of low-refractive-index TiO_2 nanoporous thin film by incident flux angle 85^o.

(b) The buffered layer deposited by negative angle, 45^o, to prevent the normal incident flux filling the gaps.

(c) The dense film is deposited by normal incident flux on the buffered layer to complete the DBR.

The experiment parameters of single pair DBR are shown in Table 4-1. And the parameters of double pair DBR are trying as same as the parameters of single pair DBR.

Deposition source	Incident flux angle	Deposition rate	Base pressure	Deposition pressure	Chamber temperature
TiO_2	85^o	0.1 nm/s	1.6×10^{-6} torr	9.4×10^{-6} ~ 6×10^{-6} torr	25^oC ~ 54^oC

(a) Nanoporous thin film parameters

Deposition source	Incident flux angle	Deposition rate	Base pressure	Deposition pressure	Chamber temperature
TiO_2	-45^o	0.1 nm/s	1.6×10^{-6} torr	6×10^{-6} ~ 6×10^{-6} torr	54^oC ~ 55^oC

(b) Buffered layer parameters

Deposition source	Incident flux angle	Deposition rate	Base pressure	Deposition pressure	Chamber temperature
TiO_2	0^o	0.1 nm/s	1.6×10^{-6} torr	6.1×10^{-5} ~ 4.9×10^{-6} torr	55^oC ~ 56^oC

(c) Dense thin film parameters

Table 4-1 Deposition parameters of single pair DBR.

Note the deposition parameters of double pair DBR are the same as single pair DBR.

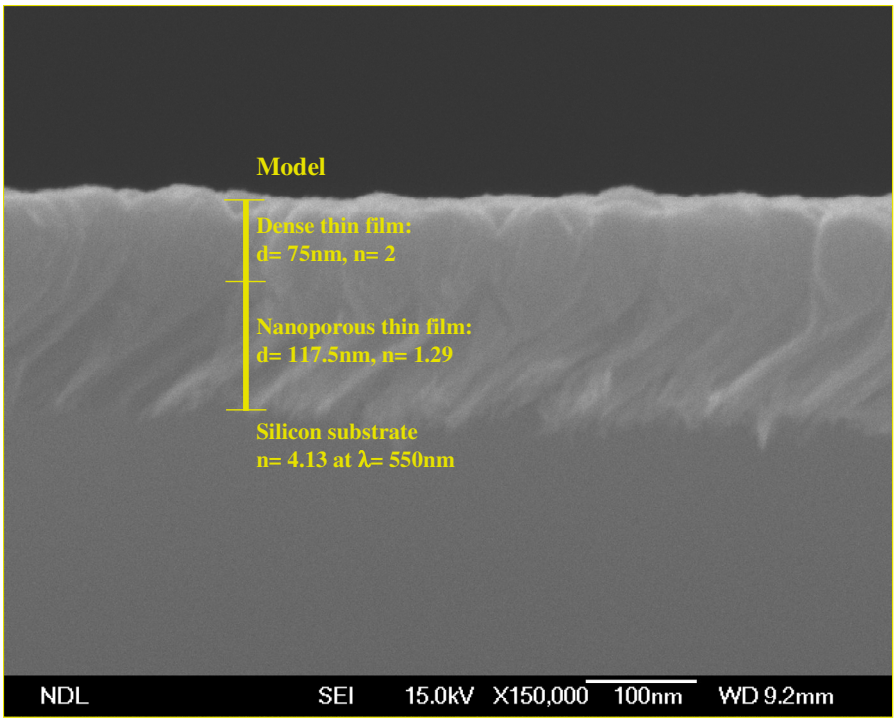

(a)

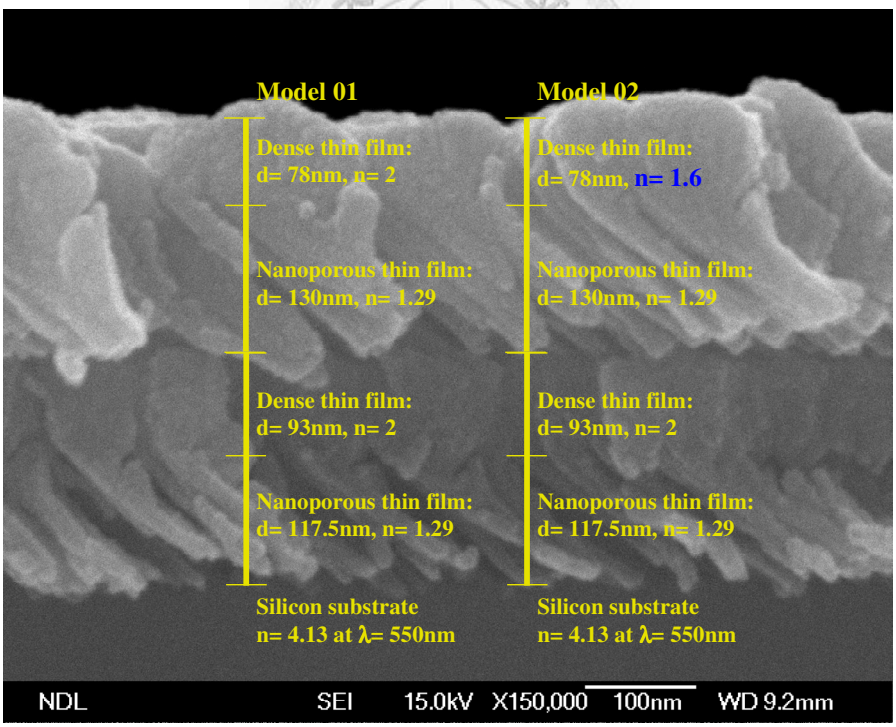

(b)

Fig. 4-4 (a) Crosse-section SEM photo of single pair DBR deposited by TiO_2 source.

(b) Crosse-section SEM photo of double pair DBR deposited by TiO_2 source.

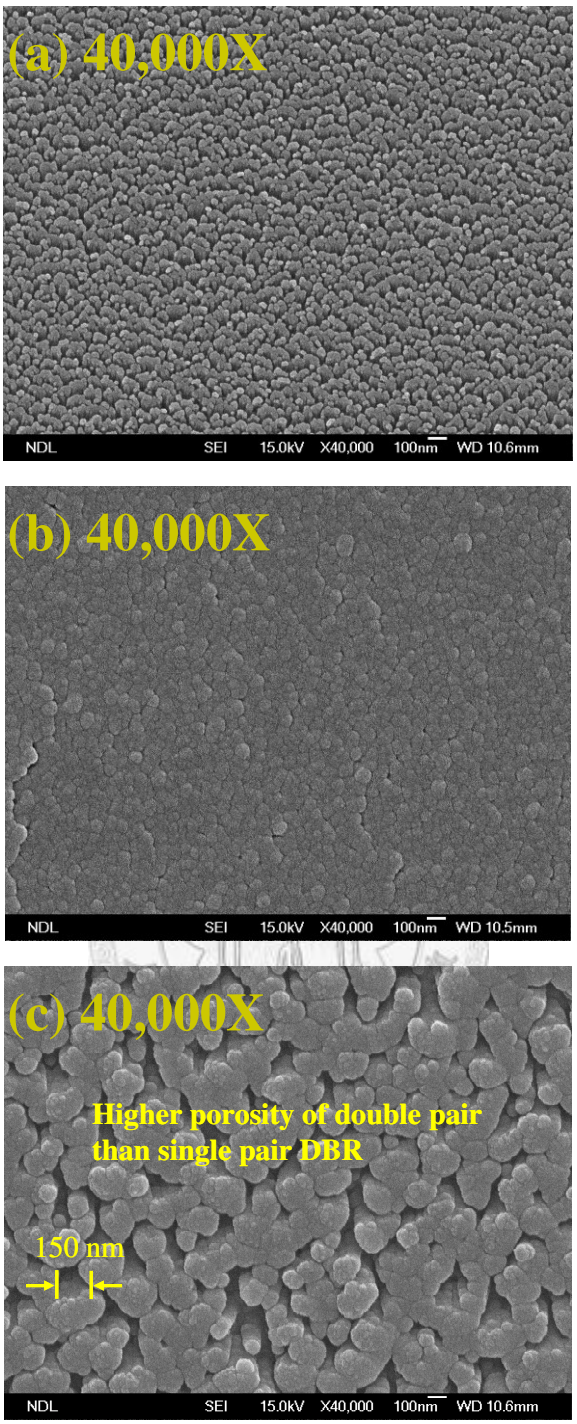

Fig. 4-5 (a) Top-view SEM photo of nanoporous thin film deposited by TiO_2 source at incident flux angle 85^{o}.

(b) Top-view SEM photo of single pair DBR deposited by TiO_2 source.

(c) Top-view SEM photo of double pair DBR deposited by TiO_2 source.

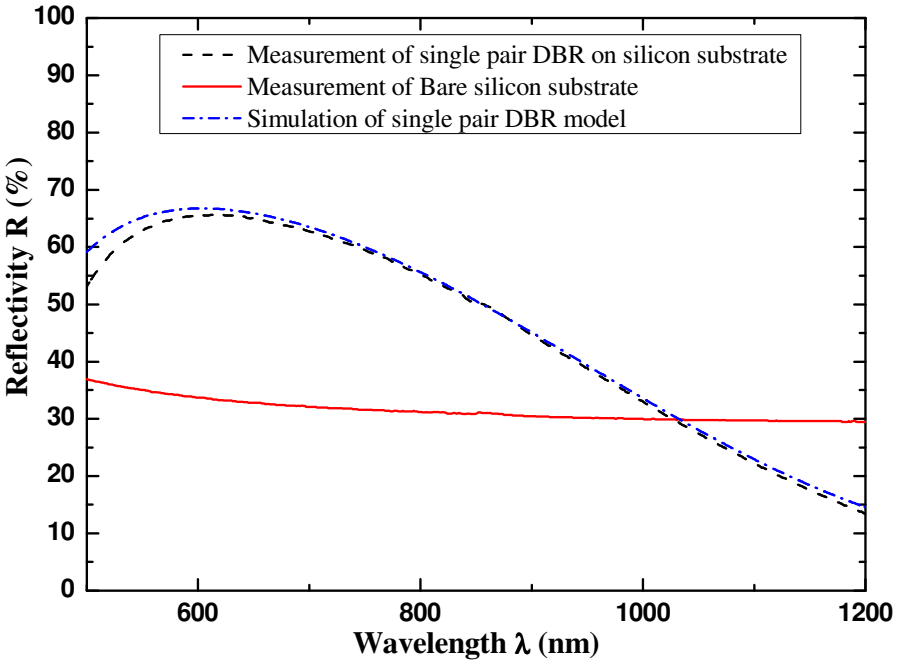

(a)

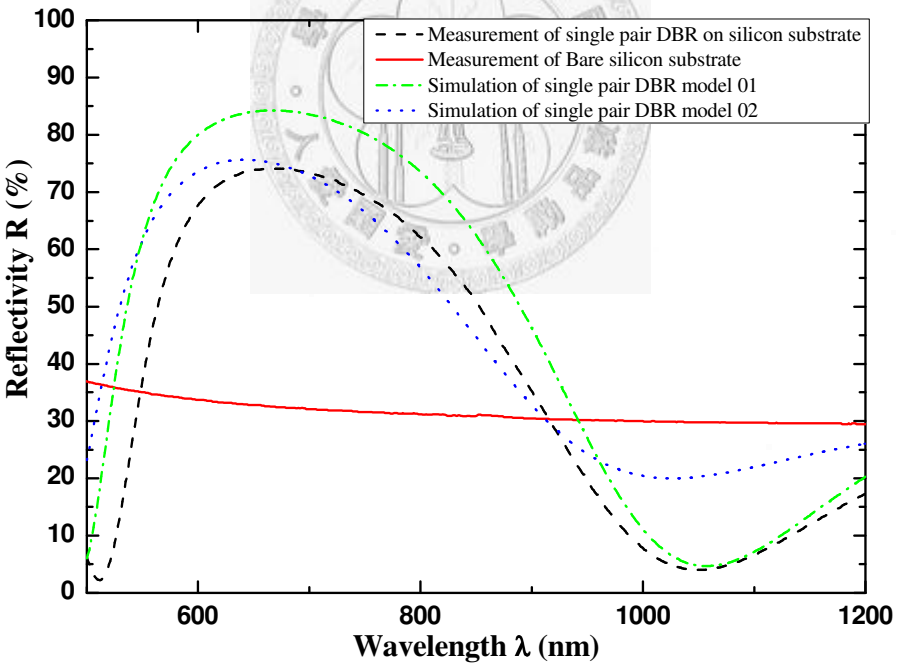

(b)

Fig. 4-6 (a) Normal incident spectrum of single pair DBR deposited by TiO_2 source.

(b) Normal incident spectrum of double pair DBR deposited by TiO_2 source.

4-1-3 Discussion

DBR can be fabricated by Oblique-angle deposition by with only TiO_2 deposition source. The reflectivity of single pair DBR and double pair DBR are 65% and 74% at center wavelength, respectively.

The simulation result of single pair model can most match the spectrometer measurement result. But note the double pair measurement result, the dense film on the second nanoporous layer is not the same as the dense film on the first nanoporous layer. To investigate the top view SEM photos, it can be found that the bundles of the second dense film become larger as well as the voids of the second dense film. The simulation and measurement results also provide some information, namely, the refractive index of the dense thin film decreases obviously.

To solve this problem, heating the substrate during deposition process of dense film probably helps deposit denser film. This will be in my future work.

4-2 Nanoporous thin film for Anti-Reflection (AR) coating

The refractive indices choice is a primary problem of Anti-reflection coating, suitable refractive indices are desirable. The limitation problem of materials is hard to result due to thermal, electro and optical properties are matched. Besides, not all the refractive index values of materials exist in the real world. It causes inferior qualities of

conventional anti-reflection coating. In this work, some anti-reflection coatings on two different substrates will be fabricated to achieve anti-reflection effect.

4-2-1 Single layer AR coating on glass substrate

The simplest interference AR coating consists of a single quarter-wave layer of transparent material whose refractive index is the square root of the refractive index of the substrate. Zero reflectance at the center wavelength and decreased reflectance for wavelengths in a bow-shape band around the center are given theoretically. The reflectivity of incident normal light from air to the front side of the substrate is given in follow:

$$R = \left(\frac{n_0 - n_s}{n_0 + n_s} \right)^2 \tag{4-4}$$

Where the n_0 is the refractive index of the air, n_s is the refractive index of the substrate. For transparent substrate, the total reflectivity of both sides is

$$R_T = \frac{2R}{1+R} \tag{4-5}$$

And the conditions of single layer AR coating is shown in follow:

$$d = \frac{\lambda_0}{4 \cdot n_1} \tag{4-6}$$

$$n_1 = \sqrt{n_0 n_s} \tag{4-7}$$

Where the d is the thickness of the coating layer and n_1 is the refractive index this layer.

The illustration of single layer AR coating is shown in Fig. 4-7.

The refractive index of glass slider is about 1.46. An optimum single layer AR coating would have to be made of a material with an index equal to about 1.23. Unfortunately, there is no material with such an index for this kind of AR coating. Conventionally, the closest and easy-use material is magnesium fluoride, MgF_2 (with an index of 1.38). On glass slider substrate, MgF_2 gives a reflectivity of about 1% on front side and total reflectivity is about 2% on both sides.

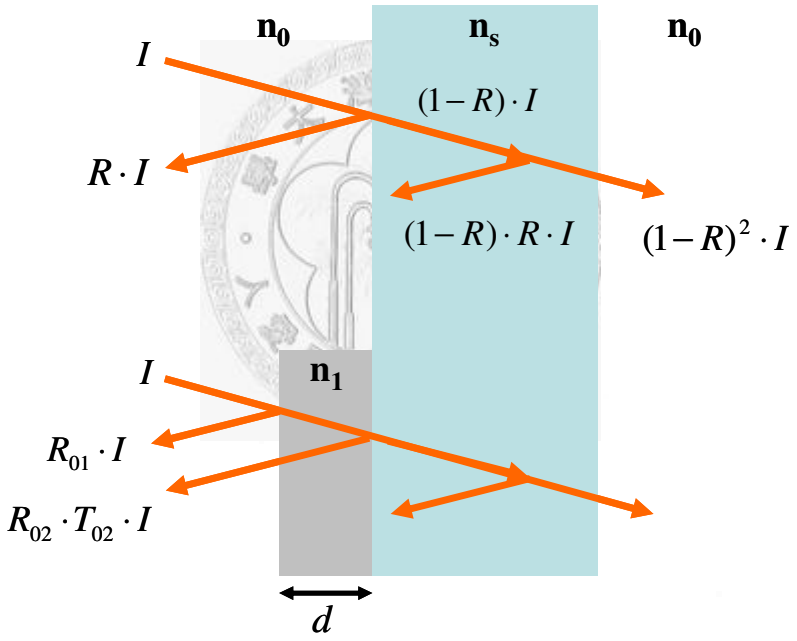

Fig. 4-7 Illustration of single layer Anti-Reflection (AR) coating. The value of n_1 determines the intensity of $R_{01}I$ and $R_{02}T_{02}I$, the value of d determines the phase of $R_{02}T_{02}I$.

In chapter 3, it has been found that the relationships between refractive indices and incident flux angles of SiO_2 deposition source. The experiment parameters of single layer AR coating on glass slider substrate are shown in Table 4-2. The thickness and refractive index of the nanoporous thin film on glass slider substrate are not definitely sure due to it's difficult to measure these parameters by white-light interferometer. But, actually, the reflectivity spectrum and the principle of single layer AR coating can be used to suppose the probable values. Fig. 4-8 (a) and (b) are the reflectivity and transmission spectrum, respectively.

Deposition source	Incident flux angle	Deposition rate	Base pressure	Deposition pressure	Chamber temperature
SiO_2	75^o	0.3 nm/s	1.7×10^{-6} torr	5×10^{-5} ~ 5.2×10^{-6} torr	22^oC ~ 24^oC

Table 4-2 Experiment parameters of single layer AR coating on glass slider substrate.

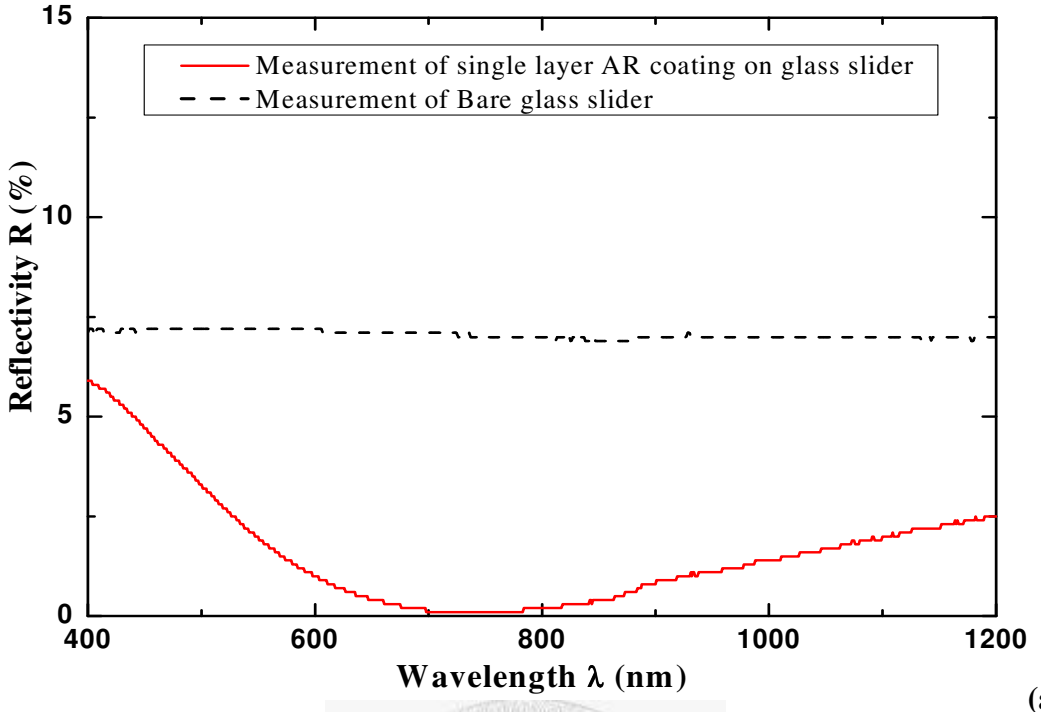

(a)

(a)

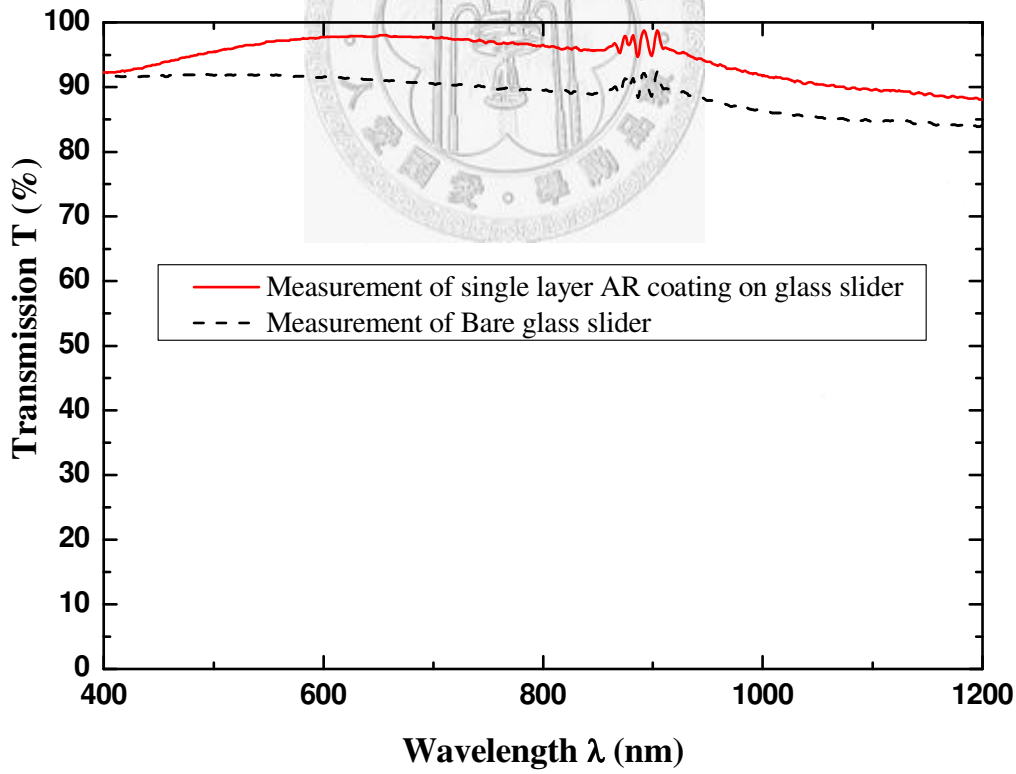

(b)

Fig. 4-8 Spectrums of single layer AR coating on glass slider.

It can be easily known that the single layer AR coating on both sides let the reflectivity of the glass slider eliminate at the center wavelength and diminish around the center. The reflectivity result is better than the single layer AR coating with MgF_2 material, the reflectivity of the center wavelength of MgF_2 using is about 4% theoretically. The single layer AR coating with SiO_2 nanoporous thin film gives the reflectivity of the center wavelength just 0.1%.

4-2-2 Gradient-index AR coating of quintic profile design

For high performance of AR coating, single layer AR coating is not sufficient. There is only low reflectivity at the center wavelength and the reflectivity increase dramatically with high incident angle of light. Some gradient-index AR coatings are designed for such desires [18- 22].

A design of AR coating is a consideration of optical distance instead of physical distance. To understand the gradient-index AR coating layers as shown in Fig. 4-9. The relation between optical x and physical distance z is shown in below:

$$z = \int_0^x \frac{dx'}{n(x')} \tag{4-8}$$

Here, we adopt a quintic AR coating design [18] for our nanoporous thin film. The quintic equation is shown in below:

$$n(x)=n_{\min}+(n_{\max}-n_{\min})(10x^3-15x^4+6x^5) \quad (x=0\sim 1) \tag{4-9}$$

The equation means the refractive index increase gradually from incident medium with low refractive index to the substrate with high refractive index and follows the equation. If the light passes through the quintic-index profile AR coating layers, the anti-reflection effect will be better than the linear-index and cubic-index profiles [3]. Besides, the reflection effect to angles performs much better than the linear-index and cubic-index too.

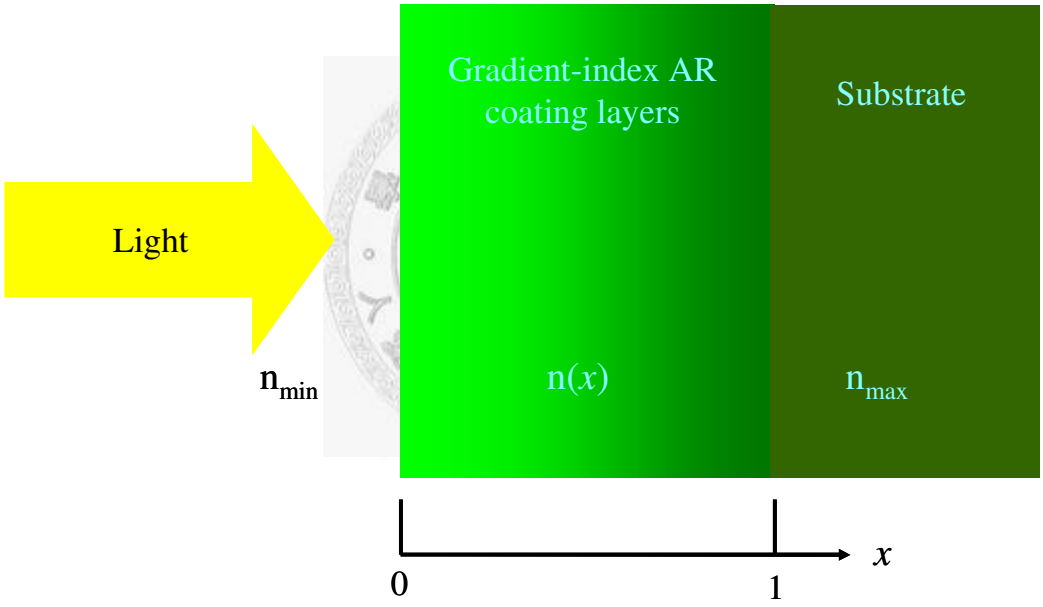

Fig. 4-9 Illustration of optical path from air to substrate. The design of AR coating is a consideration of optical distance.

From Eq. 4-9, the diagram of refractive index vs. optical distance x can been plotted as shown in Fig. 4-10. The AR coating refractive indices and thickness can be derived from Eq. 4-8. But the quintic profile is a sinusoidal-like curve it's very hard to deposit such a quintic profile AR coating layer. This quintic-index profile can be modified by a

simple way [23, 24]. There are two rules of modified principle:

- The refractive index is obtained by sampling the original profile at the center of a layer and equal layer spacing (Δx).
- The thickness of each layer is obtained by performing the integration of Eq. (4-8), with limits $-x/2$ to $x/2$, centering at the sample point.

Following the two steps, the 7-layer modified layers can be obtained.

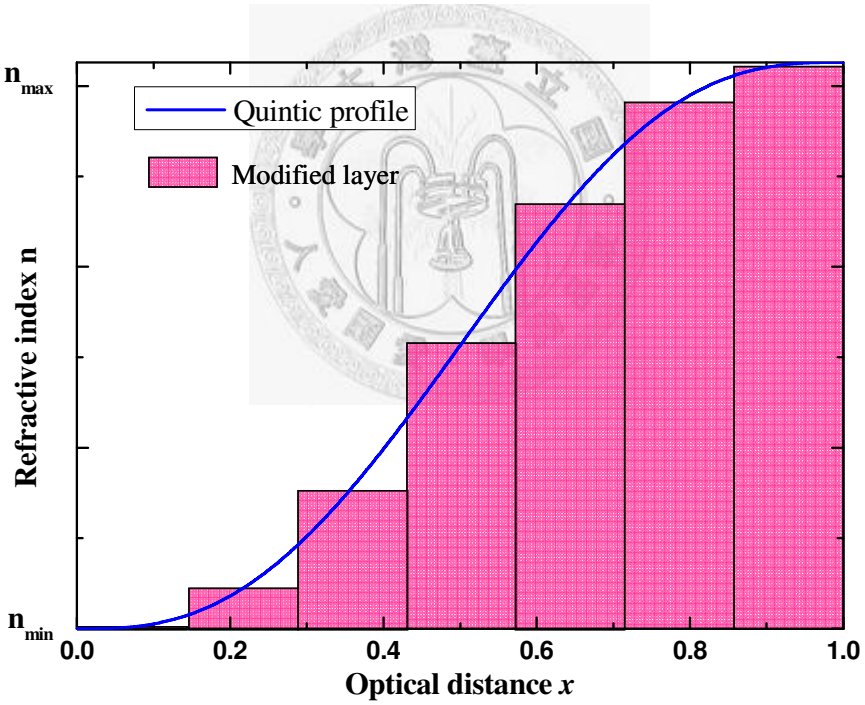

Fig. 4-10 Modified quintic profile of optical distance vs. refractive index.

This 7-layer modified AR coating layers have the similar effect with quintic profile AR coating layers.

4-2-3 Fabrication and measurement of modified 4-layer AR coating

We followed the modified rules to design 4-layer AR coating layers with quintic-index profile. Some refractive indices of layers like n= 1.01 and n= 4.12 etc are not easy to achieve. Abandon of layers are unavoidable. If the AR coating design with some abandon layers also has the high anti-reflection quality, it will also be accepted.

	Air	Layer	Layer 01	Layer 02	Layer 03	Layer 04	Layer	Layer	Silicon substrate
Ideal refractive index n (550 nm)	1	1.01	1.22	1.77	2.57	3.36	3.91	4.12	4.13
Coating refractive index n (550 nm)			1.22	1.78	higher than 2.57	3.3			
Thickness (nm)			103	72	50	38			
Incident flux angle			85^{o}	-70^{o}	40^{o}	0^{o}			
Deposition rate			0.1 nm/s	0.1 nm/s	0.3 nm/s	0.3 nm/s			
Chamber temperature (^{o}C)			45~63	42~55	42	75			
Deposition pressure (torr)			2.4×10^{-6}	7×10^{-7}	1.7×10^{-6}	2.2×10^{-6}			
Deposition source			TiO_2	TiO_2	Si	Si			

Table 4-3 4-layer modified quintic-index AR coating deposition parameters.

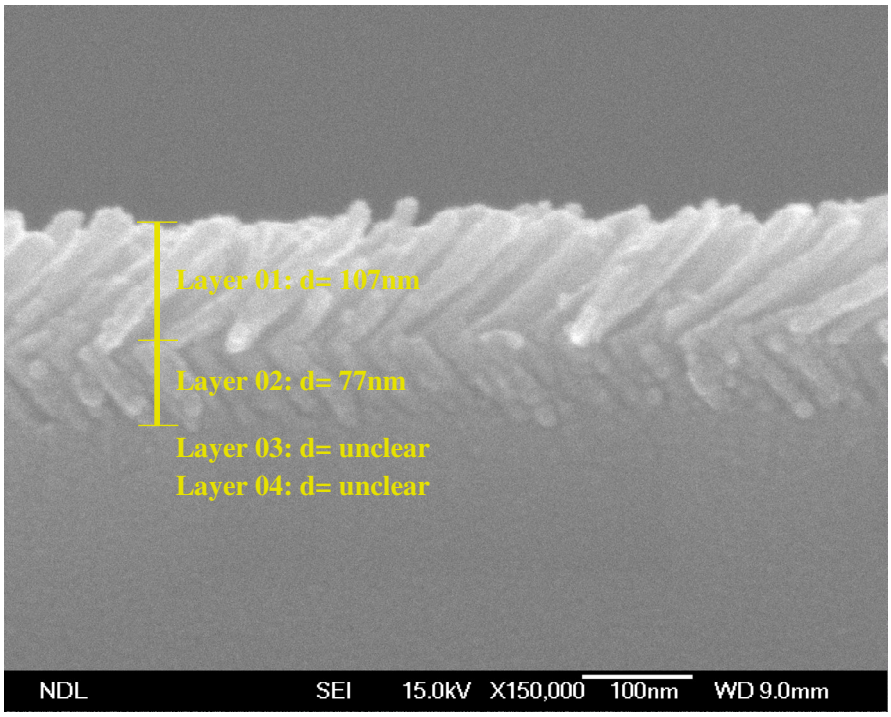

Fig. 4-11 Cross-section SEM photo of 4-layer modified quintic-index AR coating.

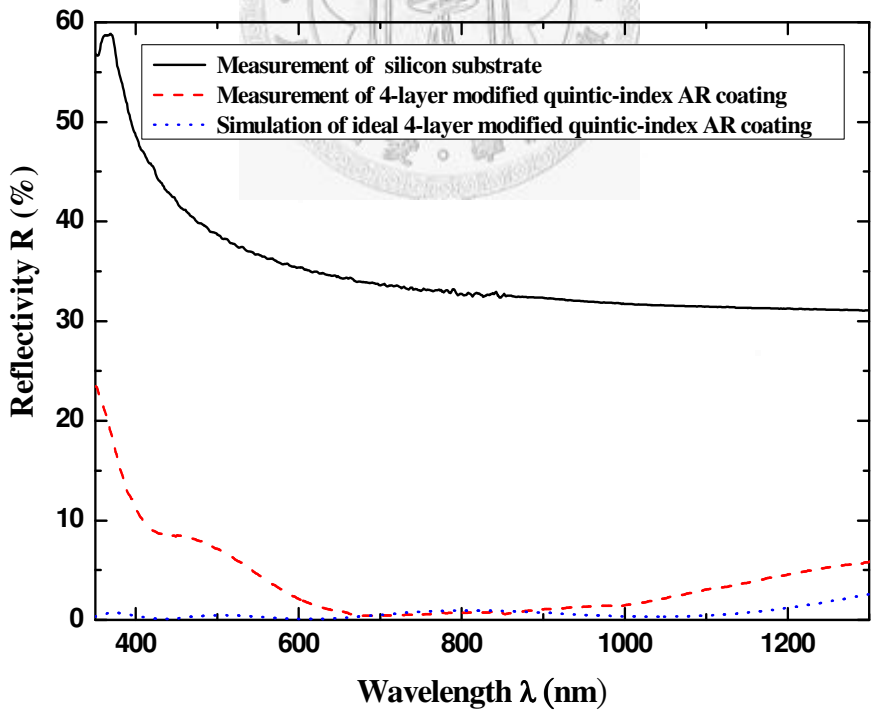

Fig. 4-12 Reflection measurement and simulation of 4-layer modified quintic-index AR coating on silicon substrate.

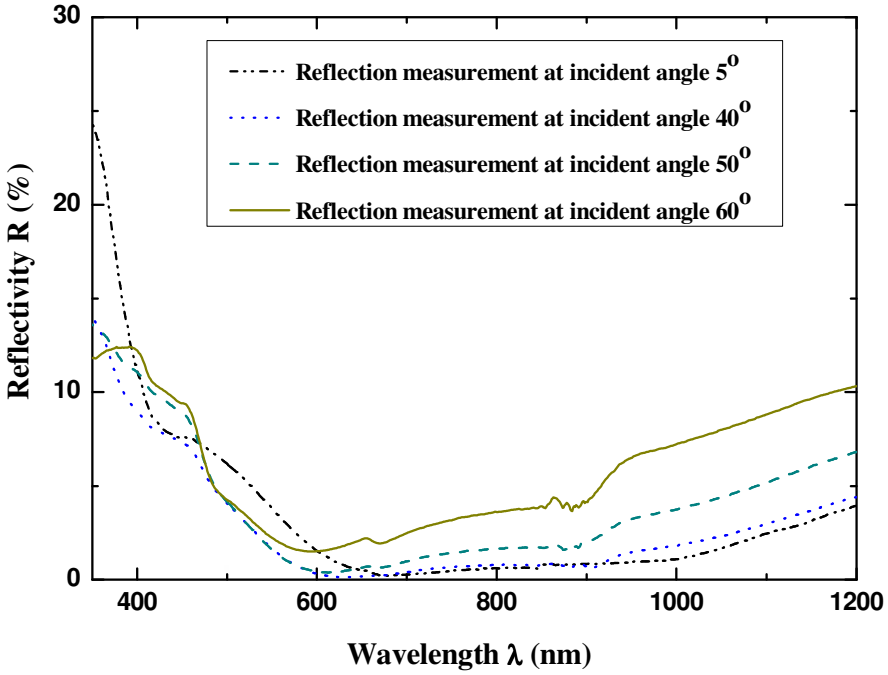

Fig. 4-13 Reflection measurements vs. incident angles of 4-layer modified quintic-index AR coating on silicon substrate.

The simulation spectrum is under the condition of silicon substrate without dispersion effect, the refractive index of silicon substrate at every wavelength is the same as 4.13. In reality silicon substrate has high dispersion the wavelength less than 550 nm. It will cause the measurement result will not match well at all the wavelength range.

The spectrum measurement was on as-deposited day. The reflectivity is diminish from R= 33% to R= 0.7% at wavelength 800 nm. It has low reflectivity (R< 10%) over 900 nm wide.

4-2-4 Discussion

The nanoporous thin film for optical device is a useful tool. Unlike any other AR coating on substrate, oblique-angle deposition technique can easily design for AR coating at desired wavelength range. A good quality AR coating needs the precise thickness and accurate refractive index of nanoporous thin film. To avoid the continuous incident flux to fill the gaps of nanoporous thin film, the higher incident flux angle than the angle of the last deposition nanoporous thin film is successful [3]. The ultra-low-refractive-index thin film also helps the design of AR coating successfully.

4-3 Degradation of nanoporous silicon thin film

Oxidation phenomenon of porous silicon film was discussed before [25- 27]. The silicon nanoporous thin film has high porosity so that it's an essential degradation for optical device. The degradation of silicon nanoporous thin film is due to the surface connecting to the air, moreover, wet environment will accelerate the oxidation rate. The attack of oxygen and water is possible against the Si-Si bond. The oxidation at ca. 330K proceeds at a slow rate in a dry atmosphere, whereas the rate is accelerated in wet air. Oxygen attacks a Si-SiH_x bond and is introduced between the Si atoms in the course of back-bond oxidation.

The refractive indices reduction of silicon nanoporous thin films

We measured the silicon nanoporous thin films on as-deposited day, four days later, eight days later and twelve days later. The samples are reserved in the room temperature with normal humidity.

Incident flux angle	40^o	45^o	50^o	55^o	60^o	65^o
Refractive index	2.84	2.73	2.69	2.49	2.32	2.18
Incident flux angle	70^o	75^o	80^o	85^o	near 90^o	
Refractive index	1.93	1.76	1.56	1.37	1.17 (?)	

Table 4-4 Refractive indices of silicon nanoporous thin film on as-deposited day.

Incident flux angle	40^o	45^o	50^o	55^o	60^o	65^o
Refractive index	2.66	2.68	2.49	2.32	2.16	2.02
Incident flux angle	70^o	75^o	80^o	85^o	near 90^o	
Refractive index	1.87	1.71	1.50	1.36	1.12 (?)	

Table 4-5 Refractive indices of silicon nanoporous thin film on four days later.

Incident flux angle	40°	45°	50°	55°	60°	65°
Refractive index	2.67	2.57	2.56	2.37	2.19	1.99
Incident flux angle	70°	75°	80°	85°	near 90°	
Refractive index	1.86	1.66	1.48	1.29	1.11 (?)	

Table 4-6 Refractive indices of silicon nanoporous thin film on eight days later.

The refractive indices of silicon nanoporous thin film on twelve days later are most the same as eight days later. The fitting result of silicon nanoporous thin film at incident flux angle 90° is not good either.

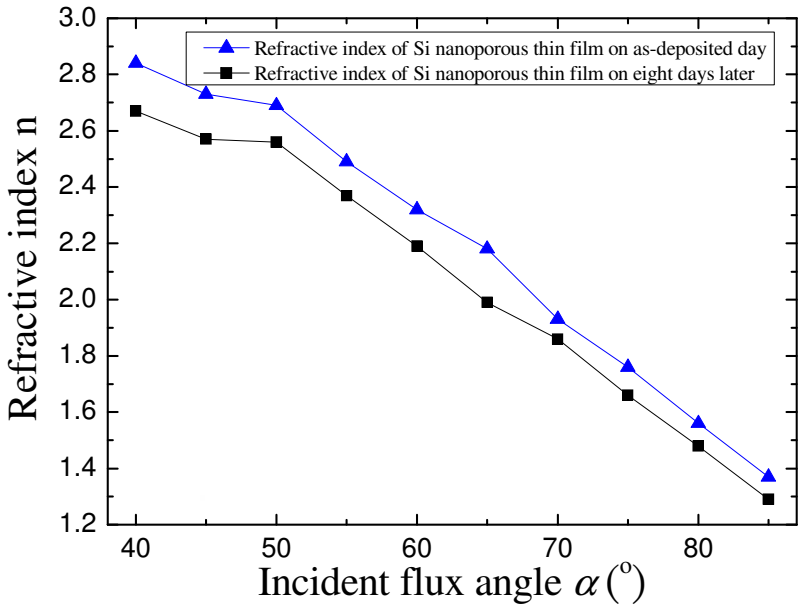

Fig. 4-14 Eight days later reduction of refractive index of silicon nanoporous thin film vs. deposition flux angle α.

The reduction of refractive index has a decreasing trend with high incident flux angle except for the incident angle 65°. The density of nanoporous thin film can be derived from Bruggeman effective medium approximation. The oxidation degree is proportional to the surface connecting to the air. It can be supposed that the total surface of silicon nanoporous thin film connecting to the air is under deposition condition at incident flux angle 40° compared to these angles from 40° to 90°.

The effect of optical coatings with silicon nanoporous thin film

For optical coatings, the refractive index of each layer can not be changed for the original high performance design. When optical coating is using silicon nanoporous thin film, the degradation problem is unavoidable. The following figure is a spectrum of AR coating on silicon substrate. About a week later, the degradation of reflection is revealing.

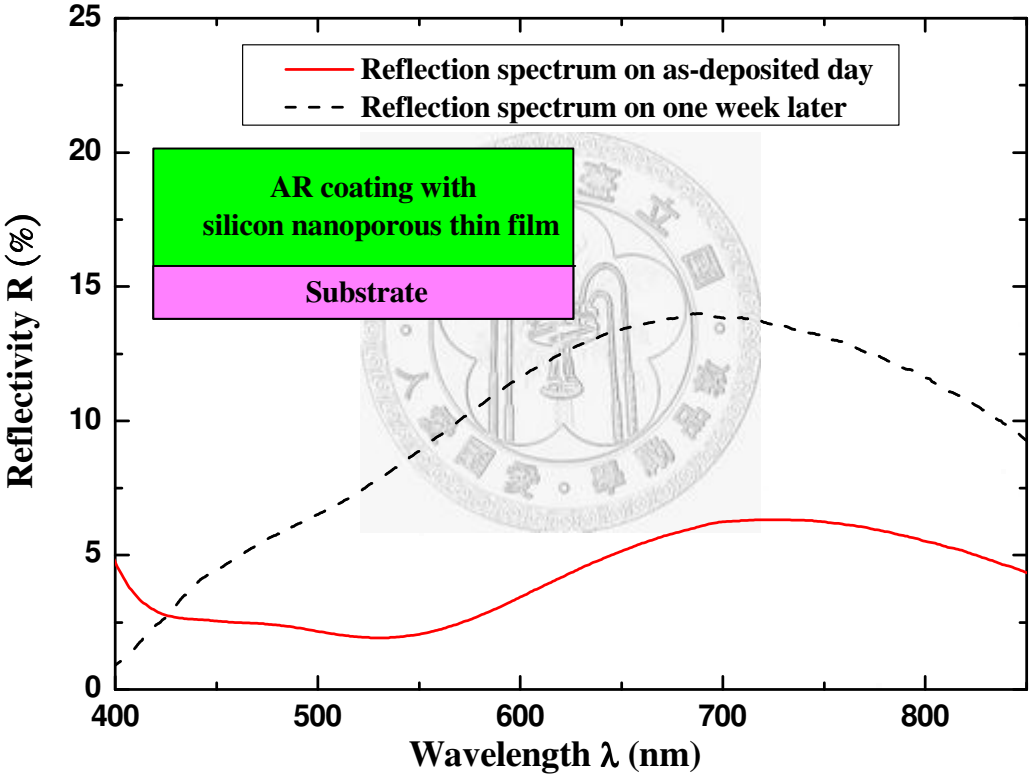

Fig.4-15 Illustration of degradation phenomenon. The Si nanoporous thin film used AR coating has a reflectivity change problem.

If we want to use porous silicon for optical devices, oxidation mechanism is must to be understood. Silicon passivated by hydrogen is relatively resistant to oxidation [28]. However porous silicon has very large surface area and the oxidation cannot be

neglected even under mild conditions.

An easy way to maintain the quality of AR coating is predicting the degradation degree. Namely, if we want to deposit a silicon nanoporous thin film with refractive index= 2.57, we will deposit the nanoporous thin film under higher refractive index condition. The following reflection spectrum shows an easy way to maintain the reflection quality.

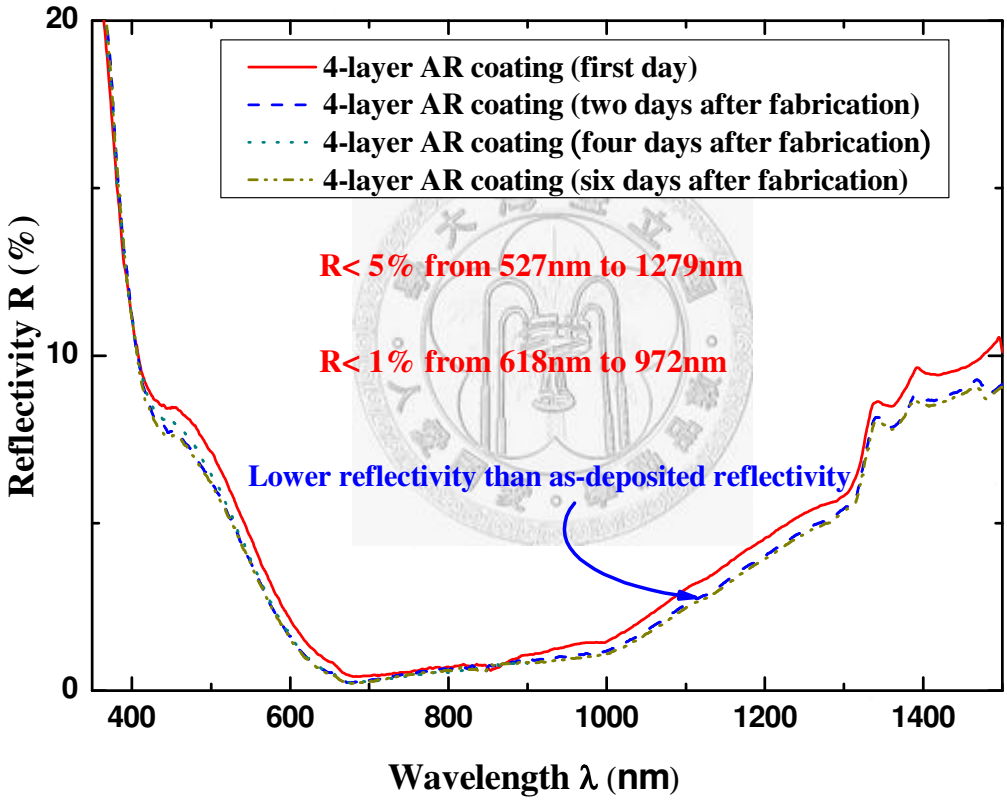

Fig. 4-16 Reflection spectrum of AR coating under deposition parameters of table 4-3.

Suitable refractive index of Si nanoporous thin film can modify the degradation problem.

The layer 03 deposition parameters of table 4-3 is design for little higher refractive index to offset the degradation phenomenon. It is believed that the reflection of Fig. 4-16 is different from Fig. 4-15 due to a design for preventing the effect from degradation in advance.

4-4 summary

Nanoporous thin films used for optical device like DBR and anti-reflection coating are achieved. For DBR, deposition of only one material can be instead of conventional two different materials deposition alternatively. Even the high reflective and high conductive properties can be fabricated at the same time [29]. For AR coating, the tunable refractive index property is used for single layer AR coating and gradient-index AR coating successfully. The nanoporous thin films with tunable refractive indices can be coated in ideal AR coating design like the refractive index n= 1.23 to optimize the single layer AR coating on glass slider substrate. But the nanoporous thin film deposited on nanoporous thin film may meet the situation of not well control of thickness or refractive index. To solve the problem, more research for this is needed.

Chapter 5 Conclusions and future work

5-1 Conclusions

The refractive index is one of the most important properties for optical devices. Varied refractive index can also change the properties of optical devices. E-beam oblique-angle deposition is a technology for fabricating the ultra-low-refractive-index nanoporous thin films. In this work, the nanoporous thin films deposited by SiO_2, TiO_2 and Si deposition sources are analyzed by white light interferometer, spectrometer and SEM. The reduction of refractive index is due to the nanoporous structure, and the nanoporous structure is due to the shadowing effect during oblique-angle deposition. The lowest refractive index of nanoporous thin film fabricated with SiO_2 deposition source at incident deposition angle 85^o is as low as 1.08. And the refractive index of nanoporous thin film can be achieved arbitrarily at different incident deposition angles if the values is over the range from n= 1.08 to n= 2.84

The single and double pair DBRs on silicon substrate deposited by only TiO_2 deposition source were successfully fabricated at different incident deposition angles and enhancing the reflectivity above 74%. The single layer AR coating on glass substrate is fabricated with SiO_2 source at incident deposition angle 75^o, and the reflectivity at central wavelength of single layer AR coating on glass slider substrate is

eliminated from R= 7% to R=0.1% at the center wavelength. The gradient-index modified 4-layer AR coating is fabricated with TiO_2, TiO_2, Si and Si sources at incident deposition angle 0^o, 40^o, -70^o and 85^o on silicon substrate, respectively, which also diminish the reflectivity R< 5% from 527 nm to 1279 nm and reflectivity R< 1% from 618 nm to 972 nm. It provides a broad band anti-reflection region. The precise thickness and refractive index control is the most important process for optical devices used with nanoporous thin films.

Oxidation phenomenon of silicon nanoporous thin film was discussed before. The reduction of refractive index measurement results provides a view of differences of total surfaces with different incident deposition angles. Moreover, the effect of degradation of silicon nanoporous thin film for optical AR coating is demonstrated and we provide a way to solve this kind of problem.

5-2 Future work

Dense film on nanoporous thin film has some unpredictable results like the refractive index of the dense film, the filling factor of the dense film and the better way to deposit the dense film on nanoporous thin film to make the refractive index of the dense film higher. If the problems be solved, more optical devices can easier to be complete by oblique-angle deposition.

In the UV region, high reflection DBR is not easy to fabricate due to the material is not very suitable. Oblique-angle deposition provides a possible way to fabricate high performance DBR due to the possibility of high refractive index contrast.

References

[1] K. H. H. Peter, T. D. Stephen, H. F. Richard, and T. Nir. "All-polymer optoelectronic devices" *Science* **285,** 233 (1999)

[2] G. A. Niklasson, C. G. Granqvist, and O. Hunderi "Effective medium models for the optical properties of inhomogeneous materials" *Appl. Opti.* **44,** 26 (1981)

[3] J.-Q. Xi, Martin F. Schubert, Jong Kyu Kim, E. Fred Schubert, Minfeng Chen, Shawn-Yu Lin, W. Liu and J. A. Smart "Optical thin-film materials with low refractive index for broadband elimination of Fresnel reflection" *Nature Photonics* **1,** 176 (2007)

[4] K. Robbie, L. J. Friedrich, S. K. Dew, T. Smy, and M. J. Brett, J. "Fabrication of thin films with highly porous microstructures" *Vac. Sci. Technol. A* **13,** 1032 (1995)

[5] D. Vick, J. J. Friedrich, S. K. Dew, M. J. Brett, K. Robbie, M. Seto, and T.Smy " Self-shadowing and surface diffusion effects in obliquely deposited thin flms" *Thin Solid Films* **339,** 88 (1999)

[6] G.B. Smith "Theory of angular selective transmittance in oblique columnar thin films containing metal and voids" *Opt. Commun.* **71,** 279 (1989)

[7] E. F. Schubert, J. K. Kim, and J.-Q. Xi "Low-refractive-index materials: A new class of optical thin-film materials" *Phys. Stat. Sol. (b)* **244,** 3002 (2007)

[8] Physical vapor deposition is available at http://www.ee.byu.edu/

[9] L Abelmann, C Lodder "Oblique evaporation and surface diffusion" *Thin Solid Films* **305,** 1 (1997)

[10] H. van Kranenburg and C. Lodder "Tailoring growth and local composition by oblique-incidence deposition: a review and new experimental data" *Mater. Sci. Eng., R.* **11,** 295 (1994)

[11] J. M. Nieuwenhuizen and H. B. Haanstra "Microfractography of thin films" *Philips Tech. Rev.* **27,** 87 (1966)

[12] R. N. Tait, T. Smy, and M. J. Brett "Modelling and characterization of columnar growth in evaporated films" *Thin Solid Films* **226,** 196 (1993)

[13] K. Robbie, J. C. Sit, and M. J. Brett "Advanced techniques for glancing angle deposition" *J. Vac. Sci. Technol. B* **16,** 1115 (1998)

[14] Kevin Robbie, Gisia Beydaghyan, Tim Brown, Cory Dean, Jonathan Adams, and Cristina Buzea "Ultrahigh vacuum glancing angle deposition system for thin films with controlled three-dimensional nanoscale structure" *Rev. Sci. Instrum.* **75,** 1089 (2004)

[15] K. Robbie and M. J. Brett "Sculptured thin films and glancing angle deposition: Growth mechanics and applications" *J. Vac. Sci. Technol. A* **15,** 1460 (1997)

[16] Jong Kyu Kim, Thomas Gessmann, E. Fred Schubert, J.-Q. Xi, Hong Luo, Jaehee

Cho, Cheolsoo Sone, and Yongjo Park "GaInN light-emitting diode with conductive omnidirectional reflector having a low-refractive-index indium-tin oxide layer" *Appl. Phys. Lett.* **88,** 013501 (2006)

[17] J.-Q. Xi, Jong Kyu Kim, E. F. Schubert, Dexian Ye, T.-M. Lu, and Shawn-Yu Lin "Very low-refractive-index optical thin films consisting of an array of SiO2 nanorods" *Opti. Lett.* **31,** 601 (2006)

[18] W. H. Southwell "Gradent-index antireflection coatings" *Opt. Lett.* **8,** 584 (1983)

[19] E. Spiller, I. Haller, R. Feder, J. E. E. Baglin, and W. N. Hammer "Graded-index AR surfaces produce by ion implantation on plastic materials," *Appl. Opt.* **19,** 3022 (1980)

[20] P. Yeh and S. Sari "Optical properties of stratified media with exponentially graded refractive index" *Appl. Opt.* **22,** 4142 (1983)

[21] P. G. Verly, J. A. Dobrowolski, and R. R. Willey, "Fouriertransform method for the design of wideband antirefretion coatings" *Appl. Opt.* **31,** 3836 (1992)

[22] E. B. Grann, M. G. Moharam, and D. A. Pommet "Optimal design for antireflective tapered two-dimensional subwavelength grating structures" *J. Opt. Soc. Am. A* **12,** 333 (1995)

[23] Minfeng Chen, Hung-chun Chang, Allan S. P. Chang, Shawn-Yu Lin, J.-Q. Xi and E. F. Schubert "Design of optical path for wide-angle gradient-index antireflection

coatings" *Appl. Opti.* **46,** 6533 (2007)

[24] Jong Kyu Kim, Sameer Chhajed, Martin F. Schubert, E. Fred Schubert, Arthur J. Fischer, Mary H. Crawford, Jaehee Cho, Hyunsoo Kim, and Cheolsoo Sone "Light-extraction enhancement of GaInN light-emitting diodes by graded-refractive-index indium tin Oxide anti-reflection contact" *Adv. Mater.* **0000,** 1 (2007)

[25] Y.H. Ogata, T. Tsuboi, T. Sakka and S. Naito "Oxidation of porous silicon in dry and wet environments under mild temperature conditions" *Journal of Porous Materials* **7,** 63 (2000)

[26] R. Herino, G. Bomchil, K. Barla, and C. Bertrand "Porosity and pore size distributions of porous silicon layers" *J. Electrochem. Soc.* **134,** 1994 (1987)

[27] Yukio Ogata, Hiroyuki Niki, Tetsuo Sakka, and Matae Iwasaki "Oxidation of porous silicon under water vapor environment" *J. Electrochem. Soc.* **142,** 1595 (1995)

[28] E. Yablonovitch, D.L. Allara et al. "Unusually low surface-recombination velocity on silicon and germanium surfaces" *Phys. Rev. Lett.* **57,** 249 (1986)

[29] Martin F. Schubert, J.-Q. Xi, Jong Kyu Kim, and E. Fred Schubert "Distributed Bragg reflector consisting of high- and low-refractive-index thin film layers made of the same material" *Appl. Phys. Lett.* **90,** 141115 (2007)

[30] M. Khardani, M. Bouaïcha, and B. Bessaïs "Bruggeman effective medium approach for modelling optical properties of porous silicon: comparison with experiment" *phys. stat. sol.* **4**, 1986 (2007)

[31] W. H. Southwell "Gradient-index antireflection coatings" *Opt. Lett.* **8**, 584 (1983)

[32] J. Zhao and Martin A. Green "Optimized antireflection coatings" *IEEE Trans. on Electron Devices* **38,** 1925 (1991)

[33] William H. Southwell "Coating design using very thin high- and low-index layers" *Appl. Opti.* **24**, 457 (1985)

[34] E. Spiller, 1. Hailer, R. Feder, J. E. E. Baglin, and W. N. Hammer "Graded-index AR surfaces produced by ion implantation on plastic materials" *Appl. Opt.* **19**, 3022 (1980)

[35] E Fred Schubert, Jong Kyu Kim, Hong Luo and J-Q Xi "Solid-state lighting—a benevolent technology" *Rep. Prog. Phys.* **69**, 3069 (2006)